A Finite Element Study of the DNA Hybridization Kinetics on the Surface of Microfluidic Devices

by

Jean-Roland Pascault

A thesis
Submitted to the faculty
of the

WORCESTER POLYTECHNIC INSTITUTE

In partial fulfillment of the requirements for the degree of
Master of Science
In
Chemical Engineering
April 2007

_____

Dr. Hong Susan Zhou, Assistant Professor

_____

Dr. David DiBiasio, Associate Professor, Department Head

ABSTRACT

DNA arrays, capable of detecting specific DNA sequences from a sample have become widely used. They rely on DNA heterogeneous hybridization, which is the binding between a single strand of DNA immobilized on a surface (probe) and its complementary strand present in the bulk (target). In order to improve the hybridization time in DNA arrays, it is crucial to understand the kinetics of DNA hybridization. The study of the Damkohler number that compares the DNA supply by diffusion to the DNA consumption by reaction (hybridization) shows that in many cases we can expect DNA hybridization to be a diffusion limited process. This is verified by a finite element study, where a whole microfluidic chamber (bulk and reacting surface) is simulated. In these cases, the formation of a depletion zone above the sensing zone is observed. The reaction rate is much lower than in the ideal case where the reaction would be reaction rate limited. A better DNA transport could be a solution to overcome the diffusion barrier. Therefore, the influence of convection on DNA hybridization was studied. Finite element simulation shows that even a small DNA velocity (10 μm/s) can greatly enhance the overall reaction rate and help preventing the formation of a depletion zone. These observations are valid when one kind of probe reacts with one kind of target. In reality, non specific hybridization can happen between a probe and a non complementary target. We show that in some cases, non specific hybridization can slow down the kinetics and reduce the fraction of specifically hybridized probes at equilibrium. The fraction of non specific hybrids can reach a maximum before decreasing and reaching equilibrium, suggesting

that a longer hybridization time would lead to a better specificity. The addition of convective transport does not affect the equilibrium, but allows to reach it faster and with a better ratio between specific and non specific hybrids during the process. Therefore, convective transport of DNA appears to be beneficial. Another possibility is to act on the DNA itself to focus it near the sensing zone. Our study of the different electrokinetic forces leads us to derive the expression of the dielectrophoretic force in a field resulting from the combination of a DC field and an AC field. This could be a novel way to act on polarizable particles like DNA.

ACKNOWLEDGEMENTS

I would like to thank my advisor Dr. Hong Susan Zhou for the confidence she placed in me and for her patience.

I would like to thank the faculty, staff, my labmates and all the graduate students in the department of chemical engineering.

Finally, special thanks to my family and friends for their precious and continuous support.

TABLE OF CONTENTS

INDEX OF FIGURES

INDEX OF TABLES

Chapter 1. Introduction

DNA arrays are playing an important role in the growing field of molecular diagnostics. They are now widely used in bioanalytical chemistry with applications in gene identification, genetic expression analysis and DNA sequencing. This part quickly presents their working principle, their technology, the current issues and perspectives.

Working principle of DNA arrays:

DNA arrays consist of single strands of DNA whose sequences are known, immobilized on the surface of the chip, called "probes". When a sample containing unknown single strands of DNA ("targets") is applied to the chip, DNA duplexes are formed between the probes and their complementary strands if it is present. This event is called hybridization and can be detected, thus indicating the presence of the target in the sample (see figure 1).

Figure 1: Working principle of a DNA array

1) application of the sample   2) hybridization   3) Washing, detection
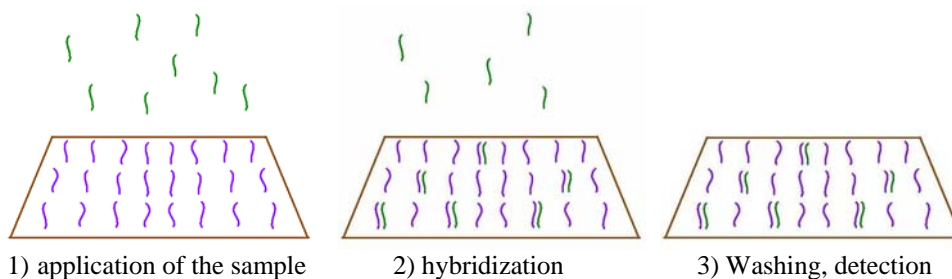
<u>Different types of DNA arrays:</u>

There are different types of DNA arrays, all relying on DNA hybridization but built using different technologies and thus presenting different characteristics. Information can be found in reviews[1, 2] and on the websites of different DNA arrays manufacturers, like Affymetrix[3].

A first type of DNA array is the macroarrays. They exhibit a lower probe density, and typically use radioactive labels to detect the hybrids. This is the most ancient and less sophisticated technique to build a DNA array.

The second type of arrays is the microarrays. They use a glass or plastic slide as a matrix and generally a fluorescent dye labeling detection of the hybrids. The probe density is much larger in these arrays than on the macroarrays. The probes are spotted robotically on the matrix.

The third type of arrays is the high density oligonucleotide arrays. This is the latest type of arrays and generally corresponds to what people have in mind when they use words such as "gene chip" or "DNA chip". They can be obtained by physical delivery techniques, such as inkjet or microjet deposition technology. In that case, the probes are not chemically bound to the surface. Another process called photolithography can be used to construct the probes on the array surface by making oligonucleotides one base at

a time. This way, the probes are chemically attached to the surface and the highest probe density is achieved: up to 60,000 probes can be present on the chip. Only Affymetrix produces these arrays.

The last type of DNA arrays is the microelectronic array technology developed by Nanogen. They consist of sets of electrodes covered by a thin layer of agarose coupled with an affinity moiety, permitting biotin-avidin immobilization of probes. Each electrode is 80 μm in diameter and is capable of generating a current, which opens the possibility to use electrokinetics to control the hybridization.

From this brief overview of the DNA array technology, we can already notice that important parameters such as the probe concentration can vary a lot in different types of arrays. This is going to have an impact on the kinetics, which is discussed in this work. The microfabrication technology is quickly improving, making it possible to implement electrokinetics in the DNA arrays. A novel way to use electrokinetics to act on particles is presented in this thesis.

.

Current issues and perspectives:

DNA are now widely used, but mainly in laboratories and hospitals. Indeed, they require sophisticated readout equipment, sample preparation and analysis can take a long time

(several hours). Researchers are working towards more portable devices that could be used on the field or near the patient. To achieve this goal, the obstacles cited before have to be overcome. This thesis focuses on one of them: the enhancement of the DNA hybridization rate.

Chapter 2. Literature Review

The literature review is an important part of this overall thesis. Indeed, the literature provides some contradictory approaches and results, and some studies have been done based on wrong assumptions. Here, the purpose is to identify and clarify some key points, in order to obtain a solid basis to study the hybridization kinetics.

2.1 Reaction kinetics in affinity assays

2.1.1 Factors affecting the kinetics and the equilibrium

Before starting to model the DNA hybridization kinetics, it is important to look at the different factors affecting it. In this review, the different factors are categorized in terms of scale. Indeed, it is very complicated to combine different scales in one model, which is the role of the "multi-scale modeling". In this thesis the focus is on the macroscale only, but the factors that have an influence at a smaller scale should be regarded. In some cases we can neglect them; however they can not always be completely ignored. This will set some limits to the work presented here that we have to be aware of.

At a molecular scale and mesoscale

The effect of high probe density

High probe density may be desired to enhance signals in some devices. If the probes are close, they can interact with each other, which leads to effects (a) and (b) described below.

   (a) Interaction between probes and brush effects

Often, targets are much longer than the probes. For example, in the Affymetrix Gene-Chip *Escherichia Coli* antisense genome array, the immobilized probes have a length of 25 base pairs, whereas the targets have a length comprised between 50 and 200 base pairs[4]. As the probes are hybridized with long targets, the surface becomes crowded with the unhybridized tails of the targets. This crowding can give rise to a polymer brush, which results in slower hybridization as explained in recent studies by Halperin et al.[5]. Halperin et al. provide criteria do determine if there is interaction between the probes or a brush effect.

The parameters involved are:

- n : number of bases in the probe

- N : number of bases in the target

- a : monomer size (6Å for DNA)

- Σ_0 : probe density

According to Halperin et al.[5], considering single-stranded as a swollen coil characterized by its Flory radius[6], an isolated unhybridized probe occupies a hemisphere of radius $r_F \approx n^{3/5}a$ whereas a terminally hybridized target occupies a hemisphere of radius $R_F \approx (N-n)^{3/5}a$. The criteria they found are:

- unhybridized probes do not interact when $r_F^2 < \Sigma_0$

- there is no brush regime when $R_F^2 < \Sigma_0$

They lead to three regimes:

- a Langmuir regime when $\Sigma_0 > R_F^2 > r_F^2$

- brush effects without interactions when $r_F^2 < \Sigma_0 < R_F^2$

- brush effects and probe-probe interactions when $\Sigma_0 < r_F^2 < R_F^2$

All these regimes occur in the different types of DNA arrays.

(b) Location of the complementary sequence on the probe

It has been shown experimentally that the location of the complementary sequence on the probe has an influence on the hybridization kinetics[7]. If the complementary sequence is at the lower part of the probe, hybridization will occur more slowly.

The effect of the conformation of DNA attached to a surface

The conformation of DNA attached on a surface can be affected by electric fields. This is particularly important since electrokinetics (application of electric fields) is investigated as a way to actuate fluid, particles and molecules in microfluidic platforms. Several effects have been reported.

(a) DNA Stretching

It is well known that in the presence of an electrical field, long fibers tend to align along an electric field line. DNA is no exception, and its orientation and stretching was studied from the 90's by Washizu and coworkers[8]. As the interest in DNA microarrays increased, more researchers observed the behavior of DNA strands attached to surfaces[9]. The conclusion of these studies can be summarized as followed: in DC and AC fields, DNA (immobilized or free in solution) tends to align with the electrical field. When DNA is attached to a surface, it stretches in the direction of the electrical field.

To the best of our knowledge, the influence of this electrokinetically induced DNA stretching on the hybridization kinetics has not been studied. However, since the conformation of the probes and "crowding effects" play a role in the kinetics, it is very likely that DNA stretching will also have an influence. We could even anticipate that DNA stretching could have a favorable effect by unfolding the DNA strands and making

17

the initial formation of a binding nucleus easier. This remains a hypothesis that has not been verified yet.

(b) Influence of an electrical field on the DNA hybrids

A legitimate question arises when considering the application of electrical fields in presence of DNA hybrids. Is the stress caused by the electrical field going to denature the DNA hybrids? Many studies have been conducted about the "mechanics" of DNA. According to the literature[10], an external force of 150 pN is required to melt double-stranded DNA. Lower forces are required to unbind smaller hybrids, typical values being 20 to 40 pN. These forces can be compared to the force exerted by an electric field on a strand of DNA attached on a surface. In an electrical field of 10^6 V.m^{-1}, the external force is around 0.2 pN[11], which is 1 to 2 orders of magnitude lower than the required force to unmelt the DNA hybrids, even if they are short. We can conclude that the use of electrokinetics is not incompatible with DNA arrays.

The effect of a label

In many arrays, the targets are labeled with a fluorescent dye, or a radioactive label. It has been shown that a fluorescent dye can have some effect on the binding[12]. However, it is reasonable to think that a fluorescent label or a radioactive label will not drastically change the motion of DNA or change its electrical properties. These assumptions are

probably not possible if DNA is labeled with nanoparticles (as investigated by some researchers in "lab on a chip" systems) whose size is bigger than the DNA molecule.

The effect of a velocity field

A fluid velocity field can have a disturbing action on the hybridization kinetics. It should be noticed, because fluid flow is sometimes being used to enhance the overall kinetics. Vanderhoeven et al. have experimentally observed that increasing the fluid velocity in a rotating microchamber enhances the kinetics, but that this effect was no longer observed when the velocity was too high[13]. They even reported that a discontinuous rotation including some stop periods was more efficient than a continuous rotation. They replaced the stop periods by a period where the chamber was slightly oscillating, which led to a slower hybridization rate. According to the authors, it suggests that the velocity field can hinder the hybridization process by affecting one of the successive steps involved in the hybridization process (collision between probe and target strand; formation of a binding nucleus involving three consecutive matching base pairs and the subsequent zippering reaction).

At a macroscale

Non specific adsorption of the targets on the surface

It has been observed that DNA can adsorb on the surface of the array, where there is no probe[14-20]. It is important because it could lead to a reaction mechanism where the targets adsorb non-specifically on the surface, and then diffuse on the surface towards the probes. This phenomena has been modeled in the case of an array with well spaced probes[21, 22] by adding a non specific adsorption step and a 2D diffusion coefficient of DNA on the surface . However, this 2D diffusion is less likely to occur on high density microarrays and not easy to model (see section 2.1.2)

Target and probe concentration

Obviously, like most chemical reactions, the hybridization rate depends on the concentration of the different species involved. The surface concentration of the probe and the bulk concentration of the target will be key elements in modeling the reaction rate. This is the purpose of section 2.1.2.

The diffusion coefficient of DNA in solution depends on the length of the strand. The longer the DNA strands, the lower the diffusion coefficient. Some researchers have enhanced the hybridization kinetics by convective transport of DNA, which supposes that in some cases, the DNA hybridization is a diffusion limited reaction. This is obviously a crucial question that is discussed in details in section 2.1.3.

2.1.2 Kinetic models

The literature shows that two main attempts have been done to develop comprehensive models of the hybridization kinetics between immobilized probes and free targets. The earlier model was published in 1995 by Chan et al.[21], the later model was developed in 2003 by Erickson et al[22].

Chan et al.[21]

The model developed by Chan et al. uses two hybridization mechanisms: direct hybridization from the bulk to the immobilized probes (direct hybridization) or non specific adsorption of the target on the surface followed by two dimensional diffusion towards the probes (indirect hybridization). Several assumptions are made. The DNA

hybridization is supposed to be irreversible (no hybrid dissociation). The number of available probes is constant throughout the hybridization and is independent of the reaction rate. This assumption is valid initially, so the whole model only predicts the initial (maximal) rate of hybridization. In addition, the authors write that "the evidence that there is an intrinsic reaction limitation" makes them assume that hybridization is reaction rate limited. However, it is not evident at all that the reaction is intrinsically reaction limited; this is the subject of section 2.1.3.

Erickson et al.[22]

Their model also uses two hybridization mechanisms, as illustrated in figure 1:

- mechanism 1: formation of DNA hybrids (H) by direct hybridization between the targets in the bulk (T_{bulk}) and the immobilized probes (P) with a forward rate constant $k_{f,1}$ and a reverse rate constant $k_{r,1}$.

- mechanism 2: non specific adsorption of the target on the surface (T_{surf}) with a forward rate constant k_a and a reverse rate constant k_d followed by two dimensional diffusion towards the probes with a diffusion coefficient D_2 and hybridization with a forward rate constant $k_{f,2}$ and a reverse rate constant $k_{r,2}$.

These two mechanisms are described by the following equations:

$T_{bulk} + P \Leftrightarrow H$ (direct hybridization)

$T_{bulk} \Leftrightarrow T_{surf}$ (non specific adsorption)

$T_{surf} + P \Leftrightarrow H$ (indirect hybridization)
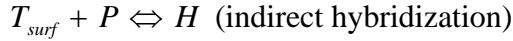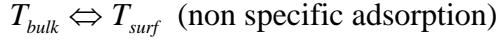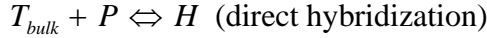
These elementary steps (non specific adsorption/ desorption followed by binding/dissociation, or direct binding/direct dissociation from the bulk) are described with first order kinetics, leading to the following rates of formation of hybrids H :

$$\frac{\partial [T_{surf}]}{\partial t} = D_2 \nabla^2 [T_{surf}] + k_a [T_{bulk}]\left([T_{surf}]_{\max} - [T_{surf}]\right) - k_d [T_{surf}] - k_{f,2} [T_{surf}]\left([T_{surf}]_{\max} - [H]\right) + k_{r,2}[H]$$

$$\frac{\partial [H]}{\partial t} = k_{f,1} [T_{bulk}]\left([P]_{\max} - [H]\right) - k_{r,1} [H] + k_{f,2} [T_{surf}]\left([T_{surf}]_{\max} - [H]\right) - k_{r,2} [H]$$

The order could be adjusted to obtain a better fit with experimental data, but first order kinetics is enough to model the hybridization.

The model assumes that the probes are well spaced and do not interact with each other. Thus, the rate constant $k_{f,1}$ can be estimated using relationships found in the literature, such as the Wetmur and Davidson relationship[23]. If the assumption of the well spaced probes is not valid, then the calculated $k_{f,1}$ is overestimated. As the target adsorb non specifically on the surface, the crowding will decrease the value of the 2D diffusion coefficient D_2. Ideally, the model should take account of this phenomenon and include a varying 2D diffusion coefficient.

2.1.3 Diffusion limitation and reaction rate limitation

It is crucial to know when DNA hybridization is reaction rate limited or diffusion limited. Unfortunately, the literature provides a lot of contradictory works. Some authors claim that DNA hybridization is reaction rate limited, whereas some researchers try to create some convection to enhance the kinetics by overcoming a diffusion barrier, which is contradictory. Obviously a sound study was needed, which Pappaert et al. recently did[24, 25].

They considered a spot in a DNA array, with the following parameters:

- a is the radius of the probe spot

- C is the volumetric concentration of target DNA in solution

- d is the height of the liquid layer

- D_{mol} is the molecular diffusion coefficient

- H_{max} is the molar surface concentration of free binding sites on probe spot at t=0

- k_{off} is the kinetic backward reaction rate constant

- k_{on} is the kinetic forward reaction rate constant

The problem is described by three equations:

- Diffusion mass balance:

$$\frac{\partial C}{\partial t} = D_{mol} \left[\frac{\partial^2 C}{\partial r^2} + \frac{1}{r}\frac{\partial C}{\partial r} + \frac{\partial^2 C}{\partial y^2} \right]$$

- The net amount of target molecules diffusing towards the spot surface is equal to the amount of hybrids pairs formed during the time interval:

$$D_{mol}\frac{\partial C}{\partial y} = \frac{\partial H}{\partial t}$$

- Hybridization:

$$\frac{\partial H}{\partial t} = k_{on}\, C\,\left(H_{max} - H\right) - k_{off}\, H$$

The following dimensionless variables are introduced:

$$y' = \frac{y}{d},\, r' = \frac{r}{a},\, C' = \frac{C}{C_0},\, h = \frac{H}{H_{max}} \text{ and } t' = t\frac{D_{mol}}{d^2}$$

The previous equations take the following form:

- Diffusion mass balance:

$$\frac{\partial C'}{\partial t'} = \left[\frac{1}{\alpha^2}\left(\frac{\partial^2 C'}{\partial r'^2} + \frac{1}{r'}\frac{\partial C'}{\partial r'} \right) + \frac{\partial^2 C'}{\partial y'^2} \right]$$

- The net amount of target molecules diffusing towards the spot surface is equal to the amount of hybrids pairs formed during the time interval:

$$\frac{\partial C'}{\partial y'} = \frac{1}{C'_0} \frac{\partial h}{\partial t'}$$

- Hybridization:

$$\frac{\partial h}{\partial t'} = \frac{Da\ C'_0}{\kappa_A} \left[\kappa_A\ C'(1-h) - h \right]$$

These three equations depend only on four dimensionless parameters, including the well known Damkohler number Da :

$$Da = \frac{k_{on}\ H_{max}\ d}{D_{mol}} = \frac{ma.ximal\ forward\ reaction\ rate}{ma.ximal\ normal\ diffusion\ rate}$$

$$\kappa_A = \frac{k_{on}\ C_0}{k_{off}} = \frac{ma.ximal\ forward\ reaction\ rate}{ma.ximal\ backward\ reaction\ rate}$$

$$C'_0 = C_0 \frac{d}{H_{max}} = \frac{number\ of\ ta.rgets\ present\ above\ spot\ at\ r=0}{number\ of\ binding\ sites\ in\ spot\ at\ t=0}$$

$$\alpha = \frac{a}{d} = \frac{spot\ radius}{liquid\ layer\ height}$$

They discussed the influence of each of these dimensionless numbers. According to them, the occurrence of diffusion-limited or kinetically limited hybridization conditions can be fully interpreted in terms of the balance between the demand for probe by the spots and the supply of probe from the solution. This balance between demand and supply is most

26

apparent in the Damkohler number Da. If Da is larger than a given critical value, the system will be diffusion-limited. The value of this critical Da-number depends on secondary conditions represented by the three other dimensionless numbers. However, an order of magnitude can be given[24]:

- when $Da > 10$, the process is clearly diffusion-limited

- when $Da < 0.1$, the process is clearly reaction-limited

If κ_A is high, it means that the probe demand is large and the critical Da-number will be lower: the system will be more prone to become diffusion-limited. The same argumentation can be made with α : if it is high, the system will be more prone to become diffusion-limited. A small C_0' means that a limited number of target DNA is present above the probe spot, and the system will be more prone to become diffusion-limited.

2.1.4 Non-specific hybridization

Non-specific hybridization (also called "non-specific binding" or "cross-hybridization" in the literature) is the low affinity binding that can occur between a probe and a target that does not have the exact complementary sequence. On a DNA array, non-specific hybrids will lead to an undesirable false signal.

Experimental studies:

The main experimental studies are reported in a review by Levicky et al.[26], and it appears that some observations are contradictory. No discussion is given to explain this discrepancy. I have wondered if the experimental studies reported below were done under conditions that prevent effects related to the diffusion of the DNA targets. All the studies used flow conditions or some stirring, therefore there should not be important diffusion effects and the rate constants measured can be used in a kinetic model, like those presented in 2.1.2.

Using 25mer end-tethered probes and 25mer targets, and a probe density of $3 \cdot 10^{12}$ probes cm^{-2}, Peterson et al.[27] found that the presence of mismatches slowed down the approach to equilibrium. However, at a lower probe coverage of $1.5 \cdot 10^{12}$ probes cm^{-2}, they observed that the hybridization rate was similar for matched and mismatched targets, although the fraction of hybridized probes at equilibrium was different. The experiments were conducted separately for non specific and specific hybridization (only one species in the sample). The authors concluded that surface concentration is a key factor in governing the influence of mismatches, and explained the lower observed rates at a higher probe coverage by crowding effects. Forman et al.[28] report something similar, as they observed that a central mismatch in a 20mers probe-target pair did not influence the kinetics. These studies tend to prove that non specific and specific hybridization have the same forward rate constant, which explains why the reaction rates are similar.

However, some researchers observed different trends. Okahata et al. studied hybridization of 20mers at a probe coverage of $1.2 \cdot 10^{13}$ probes cm^{-2}, finding that the forward rate constant of non specific hybridization was lower than the forward rate constant of specific hybridization. They also observed that the reverse rate constant of non specific hybrization was higher than the reverse rate constant of specific hybridization.

In contrast to the other studies, Dai et al.[29] performed experiments with samples containing a mixture of target sequences (matched and mismatched targets). They observed that mismatched targets achieved equilibrium faster than matched targets, which is in agreement with the observations by Okahata et al.[30]

Finally, a study by Bishop et al.[31] was published at the beginning of 2007. This is an experimental validation of a model that they published one year before[32], presented in the next paragraph. An equimolar mixture of matched and mismatched target was presented to the probes. Two phases were observed. First, the perfect and incorrect hybrids are formed. Then, the concentration of incorrect hybrids decreases as the concentration of perfect hybrids continues to increase and reaches equilibrium.

Theoretical studies and models:

Two studies, both very recent, have been published.

(a) Study by Zhang et al.[33] (2005)

Zhang et al.[33] used the following approach to model the hybridization when matched and mismatched hybridization occur. They did not consider diffusion effects and treated the DNA array like a perfectly stirred reactor. They considered one type of target present in the bulk, noted C, and two types of immobilized probes A and B. The perfect hybrids AC are the result of the binding of A and C; the incorrect hybrids BC are the result of the binding of B and C.

Formation of perfect-match hybrids:

$$\frac{\partial [CA]}{\partial t} = k_{f1}[C][A] - k_{r1}[CA]$$

Formation of incorrect hybrids:

$$\frac{\partial [CB]}{\partial t} = k_{f2}[C][B] - k_{r2}[CB]$$

They considered that the rate constants of the forward binding reaction k_{f1} and k_{f2} have the same value. The difference between perfect hybridization and incorrect hybridization

appears in the dissociation constant. k_{r2} was given a higher value than k_{r1}: the cases

$\dfrac{k_{r2}}{k_{r1}} = 10$ and $\dfrac{k_{r2}}{k_{r1}} = 100$ were studied.

For equimolar amounts of A and B, and when C is not in excess, their calculations show that at equilibrium, C does not partition between its perfect match partner and the mismatch partner in a ratio proportional to the dissociation constant ratio. According to the authors, once a molecule C has hybridized with a mismatched probe B, it becomes virtually impossible to get most of it to find its correct partner A. In general, one of their conclusions is that the relative abundance of the pairs is not what one would expect from their dissociation constants.

(b) Bishop et al.[32] (2006)

Bishop et al. used a model similar to the one developed by Zhang et al. Perfect and incorrect hybridization have the same forward rate constant, and differ by their dissociation constant. In contrast to Zhang et al., Bishop et al. used a finite element software package (Femlab) that simulates the hybridization reaction and the DNA diffusive transport in the DNA array. In their computer simulations, one type of immobilized probe was considered, and two types of targets were included: a matched target and a mismatched target. Thus, the match and the mismatched targets are in "competition" for the same probes. They observed that hybridization proceeds in two phases: in an early phase, where the amount of bound targets is much lower than the

amount of probes available, both matched and mismatched species bind to the sensing surface independently. In the second phase, when the amount of the bound hybrids is comparable to the amount of free probes, the matched species gradually displaces mismatched species from the surface due to their higher stability. Concretely, the concentration of incorrect hybrids increases in the first phase, then decreases during the second phase. These predictions were confirmed experimentally by the authors[31].

2.2 The thermodynamics of binding reactions

In the field of DNA arrays, the equilibrium is described by hybridization isotherms that relate the equilibrium fraction of hybridized probes θ_{eq} to the concentration of DNA in the solution C. The simplest and most common hybridization isotherm is the Langmuir isotherm: $\dfrac{\theta_{eq}}{1-\theta_{eq}} = C\,K_{eq}$, where K_{eq} is the equilibrium constant, which is independent of θ_{eq}.

Several conditions have to be verified to apply this model[34]:

- the DNA concentration C in solution should not be affected by hybridization (small spot condition)

- there should be only one type of probes on the spot (identical in length and sequence)

- each probe should hybridize with a single target (perfectly selective probe, or single component hybridization solution)

- a target can not hybridize another target in solution

- a target hybridizes with one probe only (no hybridization with two adjacent probes)

- no interaction between probes (hybridized or not hybridized)

When the Langmuir model is applicable, the equilibrium constant is usually evaluated by

$$K_{eq} = \exp\left(-\frac{\Delta G^0}{RT}\right),$$ where ΔG^0 is the free energy, R is the gas constant and T the temperature.

Very often, the concept of "melting temperature" is used. The melting temperature is defined as the temperature at which half of the probes are hybridized, and is a function of the DNA concentration in solution.

Unfortunately, all the conditions to apply the Langmuir isotherms are not always fulfilled. Non specific hybridization can occur (see section 2.1.4), and probes can interact with each other (see section 2.6.1), which will modify the Langmuir isotherms[5, 35].

2.3 Fluid actuation

In this thesis, we anticipate (section 2.6.2) and show (chapter 3) that DNA hybridization can be a diffusion limited process. Therefore, it is important to know the main methods used to enhance transport in microfluidic devices. Fluid flow can be used to achieve two different goals: pumping and mixing. Because the flow is laminar at a microfluidic scale (the reason is given further in this section), mixing is difficult and requires more effort than simply pumping. In the first part, the flow obtained by mechanical and electrokinetic pumping is described. In the second part, strategies used to create mixing are reviewed.

Pumping

Mechanical and electrokinetic pumping are the two main methods that can be used to create some convective transport in a DNA array. Other pumping methods (electrohydrodynamic and magnetohydrodynamic) exist, but seem more complicated to be implemented in DNA arrays.

Mechanical pumping

A mechanical pump is a system that requires a mechanical actuator that provides mechanical work to the fluid. However, the description of these actuators in microfluidics is out of the scope of this thesis. More information can be found in two recent reviews[36, 37]. Here, the focus is on the characteristic of the obtained flow. The volumetric flow rate obtained with these pumps typically lies between 10 µL/min and several mL/min.

Knowing the size of a typical chip[24] (2 x 5 cm, and a height of 100 μm), we can deduce that the fluid velocity v in the chamber will be between 10 μm/s and a few millimeters per second. The regime (turbulent or laminar) can be deduced by calculating the Reynolds number. A rectangular cross section (w = 2 cm and h = 100 μm) leads to a hydraulic diameter $D_h = \dfrac{4hw}{2(h+w)} = 2 \cdot 10^{-4} \, m$, and the physical properties of water are: density $\rho = 1000 \, kg/m^3$, viscosity $\mu = 0.001 \, Pa \cdot s$. The Reynolds number $\mathrm{Re} = \dfrac{\rho v D_h}{\mu} = 0.2$ is very low, which is a well known characteristic of microfluidics flows and means that the flow is laminar. Therefore, the velocity profile will be parabolic, equal to zero at the walls (non slip condition) and maximal at the center.

Electrokinetic pumping

Let us consider a microfluidic chamber. In most cases, a surface charge exists. It comes from the wall property or the adsorption of charges species in the fluid. When the chamber is filled with an electrolyte, the ions with a charge opposite to the charge of the surface will be attracted and form a double layer. When an electrical field is applied, it interacts with this double layer and moves the charges as well as the fluid. The induced flow is called electroosmotic flow. The velocity profile is different from a pressure driven flow: it is flat, instead of being parabolic. The velocity v is constant in the whole chamber and proportional to the field strength E:

$$\vec{v} = \mu_{EO}\ \vec{E}$$

Where μ_{EO} is the electroosmotic mobility, which depends on the surface of the wall and on the electrolyte.

Mixing

In this work, what we call "mixing" is the creation of complex flow patterns (vortices, fluid recirculation…). Several methods are available to create such flow patterns[38], but they have not been used to enhance the kinetics of DNA hybridization.

Passive mixing

Passive mixing is the deformation of the flow obtained using geometry effects. It is possible to add obstacles[39], or pattern the surface of the chamber with grooves[40] to modify the flow. It is also possible to completely modify the three dimensional shape of the microchannel by giving it a zig-zag shape[41] or more complicated shapes[42].

AC electroosmosis

AC electroosmosis is similar to the electroosmosis described a little bit earlier in this section ("electrokinetic pumping"). The interaction between the double layer and an AC field can induce a flow. The AC electroosmotic flow can present vortices, which has been

used to act on microparticles. However, it has not been used to enhance a surface reaction. AC electroosmosis is dominant over AC electrothermal flow at frequencies lower than 100 kHz[43].

AC electrothermal flow

When an AC electrical field is applied in a microfluidic device, Joule heating is going to occur, which leads to temperature gradients in the fluid. The dielectric constant of the fluid and its conductivity are functions of the temperature, therefore these properties will also present gradients, which creates a body force on the fluid. AC electrothermal flow is dominant over AC electroosmosis at frequencies higher than 100 kHz[43]. The analytical expression of the body force on the fluid is well known. Sigurdson et al. have performed simulations where the electrothermal flow was used to enhance the kinetics of the binding between immobilized antigen and free antibodies[44].

2.4 Particle actuation

In this thesis, we anticipate (section 2.6.2) and show (chapter 3) that DNA hybridization can be a diffusion limited process. To enhance DNA transport, fluid flow can be used and has been reviewed in section 2.3. It is also possible to directly act on the DNA molecules in the bulk. The purpose of this part is to describe the different forces that can act on DNA.

Electrophoresis

Electrophoresis is the motion of a charged particle induced by the Coulomb force in an electrical field. In a liquid medium, a steady state velocity is quickly reached by the particle. This velocity is proportional to the electrical field:

$$\vec{v} = \mu_{EP} \ \vec{E}$$

Where μ_{EP} is the elctrophoretic mobility.

Electrophoresis is widely applied to DNA since its backbone is negatively charged. The mobility of DNA depends on the length of the strand and on the medium. Typically, in a microfluidic device, electrophoresis will occur at the same time as eletroosmosis (see section 2.3 "electrokinetic mumping"). In that case, the DNA velocity will be:

$$\vec{v} = \mu_{App} \ \vec{E}$$

Where $\mu_{App} = \mu_{EO} + \mu_{EP}$ is the apparent mobility. If the electrical field is uniform, the resulting DNA velocity profile will be flat (constant velocity in the chamber). This is why a constant velocity was given to DNA in chapters 3 and 4 when convection was artificially added in the chamber.

Dielectrophoresis

Dielectrophoresis[43] is the force that arises when a polarizable particle (susceptible to gain a dipole moment induced by an external electrical field) is placed in a non uniform electrical field. This field can be a DC field or an AC field. In the case of an AC field, the dielectrophoretic force will depend on the frequency of the field.

DNA is polarizable and thus can undergo dielectrophoresis, but the polarization mechanism is not well known. DC dielectrophoresis and AC dielectrophoresis have been observed by different researchers[45-47]. However, these observations are not very consistent with each other. The frequency at which dielectrophoresis occurs can vary a lot in different observations. Although most of the research groups have observed positive dielctrophoresis (DNA is moved towards the region where the potential is high), one has observed negative dielectrophoresis[47]. These descrepancies could come from the fact that DNA is a very complex molecule. It is charged, long (not spherical like a microparticle) and its polarizability depends on the ions present in the medium, which make it very difficult (so far impossible) to predict and quantify its behavior.

<u>Other methods</u>

Travelling wave dielectrophoresis is a sophisticated way to use the dielectrophoretic force. It allows to move a particle in the same direction as a traveling electrical wave, typically created by a series of electrodes with phase shifted signals. The simple observation of the dielectrophoretic force on DNA is already not simple, so it is not surprising that there is no literature reporting the actuation of DNA by traveling wave dielectrophoresis.

Another improvement of the dielectrophoresis has been studied. Researchers have investigated the superposition of two dielectrophoretic signals with different frequencies[48-51]. These studies remain mainly theoretical, and would probably be applied to particle with a more simple behavior than DNA.

2.5 Enhancement of DNA hybridization kinetics

Researchers are looking for ways to enhance DNA array kinetics. Several methods have been investigated to create some flow or agitation in the array, under the assumption (sometimes implicit) that hybridization is mass transport limited. Surface acoustic waves[52] and cavitation microstreaming[53] were used to induce agitation at a microscale and facilitate DNA transport. The signal obtained was five to six times better than without agitation. Another solution to create convection is to use a shear-driven flow system[54] or a rotating chamber[13]. Das et al.[55] have used the model of DNA hybridization developed by Erickson[22] and coupled it with electroosmotic transport. They find that the hybridization rate is enhanced, but do not discuss it further or mention diffusion effects. Another way to enhance the kinetics without creating mixing is to focus DNA near the sensing zone. This is the approach followed by the Nanogen[56] company and described in research papers[57]. DNA is focused near the sensing zone by applying a positive potential. In order to enhance the hybridization specificity and prevent the detection of non specific hybrids, the hybridization step is followed by a washing step supposed to preferentially remove the non specific hybrids. The theoretical study by Zhang et al.[33] suggests that this step can be optimized (not too short, not too long) to achieve a better selectivity.

2.6 Values of important parameters in DNA arrays

The previous sections have shown that parameters such as the chamber height, the rate constant, the concentration of the involved species and their diffusion coefficient affect the reaction rate and the kinetic regime of the hybridization. Therefore, it is crucial to have a precise idea of the values of these parameters in DNA arrays.

Probes:

The length of the immobilized single stranded DNA probes is relatively short. They typically present between 10 and 60 nucleobases[3, 5, 34] (adenine, cytosine, guanine, and thymine). In the literature, the notation "bp" is used: "the DNA probes have a length between 10 and 60 bp".

Their surface concentration on one spot of a DNA microarray (the "high density arrays" presented in chapter 1) varies between $1.2 \cdot 10^{10}$ and $4 \cdot 10^{13}$ probes cm^{-2}, which corresponds to a range between $2 \cdot 10^{-10}$ and $6.6 \cdot 10^{-8}$ moles m^{-2}.

Targets:

The length of the DNA targets lies between 50 and 350 bp. They are generally much longer than the probes[3, 5, 34]. Their diffusion coefficient depends on various parameters,

the main factor being their length. The DNA coefficient of DNA strands increases with the length of the strands. A table found in a paper by Chan et al.[21] is reported below.

Table 1: Transport parameters of DNA in free solution

Base pairs (#)	Diffusion coefficient (10^{-12} m$^2\cdot$s^{-1})	Reference
6	188	Garcia de la Torre et al.[58]
30	90	Garcia de la Torre et al.[58]
160	6.91	Ferrari et al.[59]
2686	3.8	Gosnell et al.[60]
4373	2.7	Gosnell et al.[60]
5996	2.2	Gosnell et al.[60]
10,600	1.69	Liu et al.[61]
21,692	1.1	Liu et al.[61]
40,461	0.9	Strasburger et al.[62]

From this table and the length of DNA targets, we can conclude that the diffusion coefficient in DNA arrays spans two orders of magnitude, between 10^{-12} m$^2\cdot$s^{-1} and 10^{-10} m$^2\cdot$s^{-1}.

The target concentration in samples to analyze can vary a lot. It spans three to five orders of magnitude according to a review by Gadgil et al[63]. The concentration used in calibrations experiments by Affymetrix is varied between 0.25 pM and 1024 pM[63]. Typically, concentrations ranging from 1 pM to several hundred pM are seen in DNA arrays.

Rate constants:

The forward rate constant (corresponding to the binding) depends on the DNA sequence involved, the ionic strength of the medium, the temperature but not to the point that it would drastically change the order of magnitude. Based on experimental observations reported in the literature[22, 30, 64, 65], we can safely say that the order of magnitude of the forward rate constant is 10^5 L·mol^{-1}·s^{-1} to 10^6 L·mol^{-1}·s^{-1}.

The reverse rate constant (corresponding to hybrid dissociation) also depends on the DNA sequence involved, the ionic force of the medium and the temperature. The typical range for the reverse rate constant[30, 32] is 10^{-5} s^{-1} to 10^{-3} s^{-1}. The reverse rate constant is the main difference between the perfect hybridization and the non-specific hybridization, and can be one to two orders of magnitude higher for non-specific hybridization compared to perfect hybridization[30, 32, 33].

Channel height:

The typical channel height in microfluidic devices ranges from 50 μm to several hundred micrometers.

Sensing zone dimension:

Pappaert et al.[24] and Bishop et al.[32] performed simulations with target spots that have a diameter of 200 μm. Gadgil et al.[63] used a spot diameter of 100 μm.

2.7 Discussion and proposed work

2.7.1 Brush effects and probe-probe interaction in DNA arrays

Section 2.1.1 shows that in high density arrays, probes can interact (probe-probe interaction) and hybridized probes can interact (brush effect). The occurrence of interaction depends on three parameters: the probe length, the target length, and the probe surface concentration. In a given array, the probe surface concentration is fixed whereas the probe length and target length vary. Therefore, in tables 2.1 to 2.6, a probe surface concentration was fixed while the probe length and target length were varied over the typical values they take in DNA arrays (see section 2.6). The criteria given by Halperin et al.[5] were used to determine what kind of interaction takes place. These criteria have been detailed in section 2.1.1.

From tables 2 and 3, we can see that at lower probe concentration (10^{-10} mol·m^{-2} and 10^{-9} mol·m^{-2}) there is no brush effect nor probe-probe interaction. When the probe coverage is 10^{-8} mol·m^{-2} (table 4), brush effects start to occur for targets presenting a length higher than 180 base pairs. As the probe coverage is increased to is $3 \cdot 10^{-8}$ mol·m^{-2} (table 5), the brush effects are observed for shorter targets (around 100 base pairs). If the probe coverage is slightly increased to $5 \cdot 10^{-8}$ mol·m^{-2} (table 6), probe-probe interaction starts to occur in the array for probes longer than 50 base pairs, and in almost all cases, the brush effect will happen. Eventually, for a coverage of 10^{-7} mol·m^{-2} (table 7), there is always a brush effect, and probe-probe interaction is very likely to occur.

From this preliminary study, we can conclude that the assumptions of well-spaced probes, not interacting with each other is invalid for a probe surface concentration higher that 10^{-8} mol·m^{-2}. This will have an impact on the kinetic model used, as discussed in section 2.6.3.

Table 2: Probe-Probe Interaction (Probe surface concentration = 10^{-10} mol·m^{-2})

Target length (# bp)	Probe length (# bp)					
	10	20	30	40	50	60
50						
60						
70						
80						
90						
100						
110						
120						
130						
140						
150						
160						
170						
180						
190						
200			**NO INTERACTION**			
210						
220						
230						
240						
250						
260						
270						
280						
290						
300						
310						
320						
330						
340						
350						

Table 3: Probe-Probe Interaction (Probe surface concentration = 10^{-9} mol·m^{-2})

Target length (# bp)	Probe length (# bp)					
	10	20	30	40	50	60
50						
60						
70						
80						
90						
100						
110						
120						
130						
140						
150						
160						
170						
180						
190						
200			**NO INTERACTION**			
210						
220						
230						
240						
250						
260						
270						
280						
290						
300						
310						
320						
330						
340						
350						

Table 4: Probe-Probe Interaction (Probe surface concentration = 10^{-8} mol·m^{-2})

Target length (# bp)	Probe length (# bp)					
	10	20	30	40	50	60
50						
60						
70						
80						
90						
100						
110						
120			NO INTERACTION			
130						
140						
150						
160						
170						
180						
190						
200						
210						
220						
230						
240						
250						
260						
270			BRUSH EFFECTS			
280						
290						
300						
310						
320						
330						
340						
350						
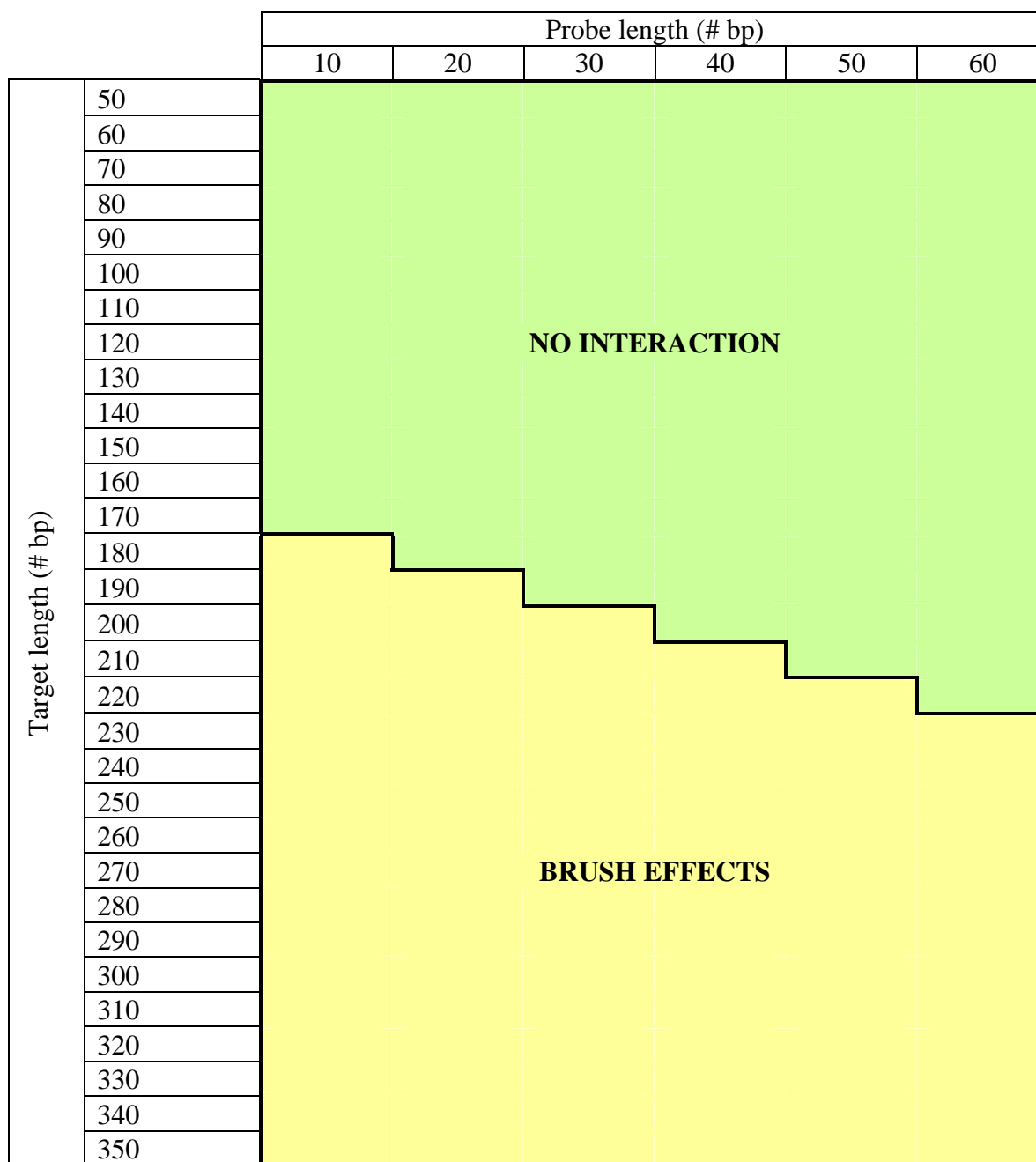
Table 5: Probe-Probe Interaction (Probe surface concentration = $3 \cdot 10^{-8}$ mol·m^{-2})

		Probe length (# bp)					
		10	20	30	40	50	60
Target length (# bp)	50						
	60			NO INTERACTION			
	70						
	80						
	90						
	100						
	110						
	120						
	130						
	140						
	150						
	160						
	170						
	180						
	190						
	200						
	210			BRUSH EFFECTS			
	220						
	230						
	240						
	250						
	260						
	270						
	280						
	290						
	300						
	310						
	320						
	330						
	340						
	350						

Table 6: Probe-Probe Interaction (Probe surface concentration $= 5 \cdot 10^{-8}$ mol·m^{-2})

	Probe length (# bp)					
	10	20	30	40	50	60

Target length (# bp): 50, 60, 70, 80, 90, 100, 110, 120, 130, 140, 150, 160, 170, 180, 190, 200, 210, 220, 230, 240, 250, 260, 270, 280, 290, 300, 310, 320, 330, 340, 350

NO INTERACTION

BRUSH EFFECTS

PROBE-PROBE INTERACTION

&

BRUSH EFFECTS

Table 7: Probe-Probe Interaction (Probe surface concentration = 10^{-7} mol·m^{-2})

	Probe length (# bp)					
	10	20	30	40	50	60
50						
60						
70						
80						
90						
100						
110						
120						
130						
140						
150						
160						
170		BRUSH EFFECTS		PROBE-PROBE INTERACTION & BRUSH EFFECTS		
180						
190						
200						
210						
220						
230						
240						
250						
260						
270						
280						
290						
300						
310						
320						
330						
340						
350						

Target length (# bp)

2.7.2 Kinetic regime in DNA arrays

Section 2.1.3 shows that the Damkohler number is the main criterion to determine if hybridization is diffusion limited or reaction-rate limited. In addition, section 2.6 provides the values of important parameters in DNA arrays, which allows us to calculate the Damkohler number in DNA arrays, and thus predict the kinetic regime of hybridization.

The Damkohler number is defined by:

$$Da = \frac{k_f \, P_{max} \, h}{D} = \frac{ma.ximal \ forward \ reaction \ rate}{ma.ximal \ normal \ diffusion \ rate}$$

Where:

- h is the height of the liquid layer

- D is the molecular diffusion coefficient

- P_{max} is the molar surface concentration of free binding sites on probe spot at t=0

- k_f is the kinetic forward reaction rate constant

Among these four parameters, two are constant for a given DNA array: the liquid layer height h and the probe surface concentration P_{max}. In contrast, the size of the DNA targets and their diffusion coefficient D as well as the kinetic forward rate constant k_f will vary in one given array. Thus, a system with a given channel height h and probe

concentration P_{max} will present different Damkohler numbers due to the non uniformity of

the kinetic forward rate constant k_f (that can take values comprised between 10^2 and 10^3

$m^3 \cdot mol^{-1} \cdot s^{-1}$) and of the diffusion coefficient D (that can take values comprised between

10^{-12} $m^2 \cdot s^{-1}$ and 10^{-10} $m^2 \cdot s^{-1}$) over the chip. In order to illustrate this and have an idea of

the expected kinetic regime in DNA arrays, the Damkohler number has been calculated

under different array conditions. The results are reported in tables 8, 9, 10 and 11. Each

table corresponds to a different value of the probe surface concentration. The channel

height was kept to a reasonable value of 100 μm, but could vary between 50 and several

hundred micrometers.

Table 8: Damkohler number in DNA array (Probe surface concentration: 10^{-10} $mol \cdot m^{-2}$; Channel height: 100 μm)

		Target diffusion coefficient ($m^2 \cdot s^{-1}$)		
		10^{-12}	10^{-11}	10^{-10}
k_f	10^2	1	0.1	0.01
($m^3 \cdot mol^{-1} \cdot s^{-1}$)	10^3	10	1	0.1

Table 9: Damkohler number in DNA array (Probe surface concentration: 10^{-9} $mol \cdot m^{-2}$; Channel height: 100 μm)

		Target diffusion coefficient ($m^2 \cdot s^{-1}$)		
		10^{-12}	10^{-11}	10^{-10}
k_f	10^2	10	1	0.1
($m^3 \cdot mol^{-1} \cdot s^{-1}$)	10^3	100	10	1

Table 10: Damkohler number in DNA array (Probe surface concentration: 10^{-8} $mol \cdot m^{-2}$; Channel height: 100 μm)

		Target diffusion coefficient ($m^2 \cdot s^{-1}$)		
		10^{-12}	10^{-11}	10^{-10}
k_f	10^2	100	10	1
($m^3 \cdot mol^{-1} \cdot s^{-1}$)	10^3	1000	100	10

Table 11: Damkohler number in DNA array (Probe surface concentration: 10^{-7} mol·m^{-2}; Channel height: 100 μm)

		Target diffusion coefficient (m^2·s^{-1})		
		10^{-12}	10^{-11}	10^{-10}
k_f	10^2	1000	100	10
(m^3·mol^{-1}·s^{-1})	10^3	10000	1000	100

Tables 8 and 9 correspond to the lower values of the probe surface concentration. We observe that in these systems, the Damkohler number can take low values (lower than one) and high values (higher than 10), which means that reaction rate limitation and diffusion limitation can occur. Clearly, for higher values of the probe surface concentration (tables 10 and 11), the Damkohler number takes very high values, going up to several thousand. It means that these systems will present a strong diffusion limitation.

From this preliminary study, we can conclude that using realistic parameters, it is expected that hybridization will be diffusion limited in DNA arrays. It directly contradicts the assumptions made by some others who used the fact that DNA hybridization is reaction limited[21]. Some authors did not take account of the large variation of some parameters (the diffusion coefficient, the surface concentration), leading them to calculate a low value of the Damkohler number; they concluded that hybridization is reaction limited and that enhancing the DNA transport by convection is not a useful approach to enhance the kinetics[44]. This preliminary study is in agreement with experimental observations[13]. Indeed, several research groups have enhanced the kinetics of DNA hybridization by using convective transport, which means that diffusion effects were overcome.

2.7.3 Choice of a kinetic model

In section 2.1.2, the two main kinetic models of DNA heterogeneous hybridization were described. In section 2.1.4, we reviewed how non specific hybridization was modeled in theoretical studies.

A model like the one published by Chan et al.[21] is too simplistic, because it assumes that hybridization is an irreversible process. It does not allow to compare specific and non specific kinetics, for the main difference between them is the value of the dissociation rate constant.

The model developed by Erickson et al.[22] is much more comprehensive. It considers that hybridization is a reversible process and takes account of two hybridization mechanisms: "direct hybridization" from the bulk and "indirect hybridization" (adsorption of target on the surface, followed by two dimensional diffusion towards the probes and reaction). However, the indirect hybridization is difficult to model. It requires the knowledge of parameters such as the two dimensional diffusion coefficient, the adsorption and desorption rate constants. Unfortunately, these parameters are not known, and could even vary with time as the surface becomes crowded. Anyway, this mechanism is expected to be much less important than the direct hybridization from the bulk. In addition, one of the main goals of this thesis is to show that DNA hybridization is very likely to be a diffusion limited process, and that ignoring this would lead to a dramatic overestimation of the kinetics. Therefore, in this work, we neglect the "indirect hybridization".

There is only one main way to model non specific hybridization. The same model was used by Bishop et al.[32] and Zhang et al.[33], we decide to use it as well.

Finally, specific and non specific hybridization are modeled as followed.

(a) Specific hybridization:

The immobilized probes (P) and the targets (T) form hybrids (H), with a forward rate constant k_f and a reverse rate constant k_r:

$$P + T \Leftrightarrow H$$
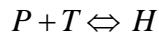
The rate of formation of hybrids can be written:

$$\frac{\partial [H]}{\partial t} = k_f [P][T] - k_r [H]$$

Where $[P] = [P]_{max} - [H]$, $[P]_{max}$ being the maximum (initial) number of free probes on the surface.

(b) Non specific hybridization:

Let us consider two reactions:

- the specific hybridization, where immobilized probes (P) and targets (T_1) form hybrids (H_1), with a forward rate constant k_f and a reverse rate constant k_{r1}.

- the non specific hybridization, where the same immobilized probes (P) and non specific targets (T_2) form non specific hybrids (H_2), with the same forward rate constant k_f and a reverse rate constant k_{r2}.

The corresponding reactions are:

$$P + T_1 \Leftrightarrow H_1$$

$$P + T_2 \Leftrightarrow H_2$$
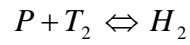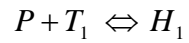
The rate of formation of hybrids can be written:

$$\frac{\partial [H_1]}{\partial t} = k_f [P][T_1] - k_{r1} [H_1]$$

$$\frac{\partial [H_2]}{\partial t} = k_f [P][T_2] - k_{r2} [H_2]$$

The interaction, the "competition" between T_1 and T_2 for the free probes $[P]$ can be seen in the term:

$$[P] = [P]_{max} - [H_1] - [H_2]$$

Chapter 3. Study of the hybridization kinetics

3.1 General approach

In this work, we study the hybridization kinetics under the conditions seen in DNA arrays. To achieve this goal, we simulate the DNA hybridization with a finite element softaware package (Comsol Multiphysics) at the scale of one sensing zone. Simulating a whole DNA array, with thousands of sensing zones is out of scope. In addition, only the hybridization step is studied here. Other steps, like the washing step, could be studied using the same computational tool.

More precisely, in a first part (section 3.3) we study the single species hybridization, which means that non specific hybridization is not taken in account. The software allows us to quantify hybridization and visualize the concentration profiles in the chamber.

In a second part (section 3.4), some convective transport is added to overcome the diffusion barrier showed in the first part.

In the last part (section 3.5), the influence of non specific hybridization is discussed.

3.2 Methodology: simulating with Comsol Multiphysics

Numerical simulations were performed with Comsol Multiphysics, a finite element software package. The same two dimensional microfluidic chamber was used in all simulations. The corresponding geometry is illustrated on figure 1. The chamber is 1 mm

long. The height was kept at a constant value of 100 μm and presents one sensing zone (covered with probes) in the middle of the bottom wall, whose length is 200 μm.

Figure 2: Chamber geometry
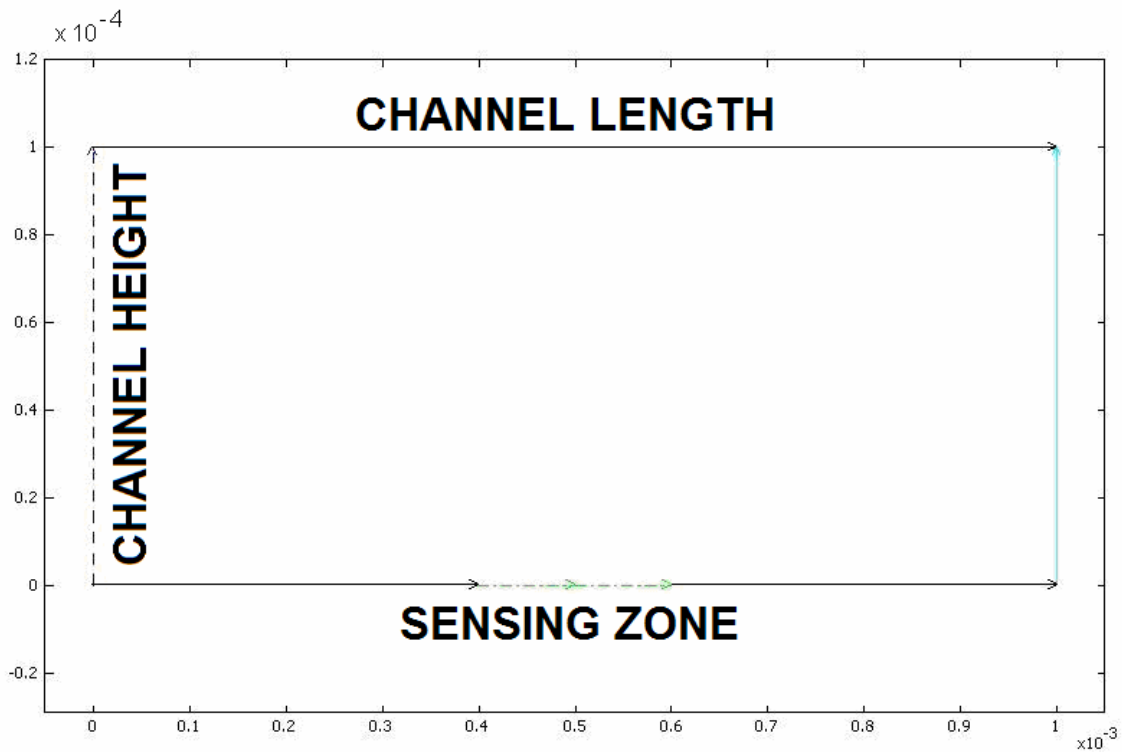
The convection/diffusion package was used to simulate the DNA transport in the channel. To simulate the reaction in absence of electrokinetical transport, the DNA concentration at the inlet and outlet of the chamber was fixed, thus providing some continuous supply in the chamber, only by diffusion. In the simulations where convective transport was included, DNA was supplied from the left wall with a constant inlet concentration, and was allowed to exit the channel through the right wall. We imposed a horizontal, uniform DNA velocity profile defined by its velocity v. It corresponds to the profile that would be obtained if a horizontal electrical field was applied in the chamber, pushing DNA by a

combination of electrophoresis and electroosmotic flow. Two values of the velocity were used ($v = 10 \, \mu m/s$ and $v = 100 \, \mu m/s$).

In all simulations, an "insulation" boundary condition was chosen for the non reactive surfaces at the top and the bottom of the channel. On the sensing zone, the surface reaction was modeled by defining the appropriate flux as a boundary condition. DNA hybridization was simulated for a period of 2880 minutes (2 days). Hybridization does not occur uniformly on the sensing zone. Therefore, in this work, the concentration or fraction of hybridized probes is an average taken over the sensing zone.

3.3 Single species hybridization

By definition, in absence of diffusion limitation, the target concentration is constant in the bulk. In "chemical engineering language", the DNA array behaves like a "perfectly stirred tank reactor". In addition, if the number of targets in the DNA array is much higher than the number of probes it can hybridize, we can assume that the target concentration will remain almost constant and equal to its initial value. Under these two assumptions, it is possible to find the analytical expression of the number of hybridized probes in function of time.

The immobilized probes (P) and the targets (T) form hybrids (H), with a forward rate constant k_f and a reverse rate constant k_r:

$$P + T \Leftrightarrow H$$

The rate of formation of H can be written:

$$\frac{\partial [H]}{\partial t} = k_f [P][T] - k_r [H]$$

Where $[P] = [P]_{max} - [H]$, $[P]_{max}$ being the maximum (initial) number of free probes on the surface.

Since the targets are in excess and there is no diffusion effect, their concentration remains equal to the initial value $[T]_0$. The rate of formation of H becomes:

$$\left(\frac{\partial [H]}{\partial t} \right)_{ideal} = k_f \left([P]_{max} - [H] \right) [T]_0 - k_r [H]$$

Assuming that there is no hybrid initially, the analytical solution of this differential equation is:

$$[H]_{ideal} = \frac{[T]_0 [P]_{max}}{[T]_0 + \dfrac{k_r}{k_f}} \left[1 - \exp\left(-\frac{t}{\tau} \right) \right]$$

Where $\tau = \dfrac{1}{k_f [T]_0 + k_r}$

This expression is an "upper bound", and corresponds to the fastest rate at which hybridization can occur. Diffusion effects and the occurrence of non-specific hybridization can potentially slow down the kinetics.

In addition, the equilibrium can be deduced from this expression. When time goes to

infinity, the fraction of hybridized probes will tend to $\dfrac{[T]_0}{[T]_0 + \dfrac{k_r}{k_f}}$, which is only a

function of k_f and k_r , and of the target concentration $[T]_0$.

The geometrical parameters (channel height "h" and the length of the sensing zone "a")

were kept constant ($h = 100\,\mu m$ and $a = 200\,\mu m$). These two last parameters could take

different values in different DNA arrays, but they will be almost constant in a given

device. Other parameters, like the rate constants and the diffusion coefficient of the DNA

targets will display different values in one given system. In addition, the probe surface

concentration and target concentration span a wider range of values than the channel

height and the size of the sensing zones, and play a direct role in the kinetics. Therefore,

it was chosen to vary the kinetic rate constants k_f and k_r, the diffusion coefficient D,

the target concentration $[T]_0$ and probe concentration $[P]_{max}$, which already leads to a

high number of combinations that can be observed in DNA arrays. In the simulations, the

association rate constant k_f was given the values 10^5 L·mol^{-1}·s^{-1} and 10^6 L·mol^{-1}·s^{-1}. For

the dissociation rate constant k_r, the values 10^{-5} s^{-1} to 10^{-3} s^{-1} were studied. Three values

covering three orders of magnitude were considered for the diffusion coefficient D : 10^{-12}

m^2·s^{-1}, 10^{-11} m^2·s^{-1} and 10^{-10} m^2·s^{-1}. The target concentration $[T]_0$ was allowed to take two

values: 1 pM and 100 pM. Four values covering four orders of magnitude were used for

the probe concentration $[P]_{max}$: 10^{-10} moles m^{-2}, 10^{-9} moles m^{-2}, 10^{-8} moles m^{-2} and 10^{-7}

moles m^{-2}. Overall, these parameters can form 96 combinations. These combinations can be divided into eight groups that present the same values for k_f, k_r, and $[T]_0$, but different values for D and $[P]_{max}$. In one group, all the combinations can be compared to the same "ideal case" detailed in earlier in this section, since the fraction of hybridized probes only depends on k_f, k_r, and $[T]_0$. Thus, the results are presented in eight tables (tables 12 to 19). In each table, the fraction of hybridized probes at equilibrium

$$f_{eq} = \frac{[H]_{eq}}{[P]_{max}} = \frac{[T]_0}{[T]_0 + \dfrac{k_r}{k_f}}$$ is the same, and the rate of formation of hybrids should tend

to the rate calculated in the ideal case as the reaction becomes less diffusion limited. The time necessary for the fraction of hybridized probes $f(t) = \dfrac{[H]}{[P]_{max}}$ to reach $0.5\, f_{eq}$ and $0.9\, f_{eq}$ is given in the tables. For the ideal case, these times are calculated analytically

since the analytical expression $\dfrac{[H]_{ideal}}{[P]_{max}} = \dfrac{[T]_0}{[T]_0 + \dfrac{k_r}{k_f}} \left[1 - \exp\left(-\dfrac{t}{\tau}\right) \right]$ is known. In all

other cases, the times are deduced from the hybridization curves obtained by finite element simulation, which take account of the diffusional effects. The Damkohler number Da was also calculated. Indeed, as detailed in section 2.1.3, according to Pappaert et al.[24, 25], the Damkohler number provides the main criterion to predict if DNA hybridization is either diffusion or reaction rate limited. This dimensionless number is defines as followed:

$$Da = \frac{k_a\, C_{H,max}\, h}{D} = \frac{\max imal\ forward\ reaction\ rate}{\max imal\ normal\ diffusion\ rate}$$

66

When this number takes high values (typically higher than 1), hybridization becomes a diffusion limited process. When Da is low, the reaction is more reaction rate limited.

Table 12: Hybridization time ($k_f = 10^2$ L·mol^{-1}·s^{-1}; $k_r = 10^{-5}$ s^{-1}; $[P]_{max}$ =100 pM)

$[P]_{max}$ moles·m^{-2}	D m^2·s^{-1}	Da No unit	t @ f = 0.5 f$_{eq}$ minutes	t @ f = 0.9 f$_{eq}$ minutes
Ideal case			578	1919
10^{-10}	10^{-10}	0.01	680	2140
10^{-10}	10^{-11}	0.1	850	2710
10^{-9}	10^{-10}		880	2650
10^{-10}	10^{-12}		> 2 days	
10^{-9}	10^{-11}	1	2860	> 2 days
10^{-8}	10^{-10}		> 2 days	
10^{-9}	10^{-12}			
10^{-8}	10^{-11}	10	> 2 days	> 2 days
10^{-7}	10^{-10}			
10^{-8}	10^{-12}	100	> 2 days	> 2 days
10^{-7}	10^{-11}			
10^{-7}	10^{-12}	1000	> 2 days	> 2 days

The time to reach $f = 0.5 f_{eq}$ and $f = 0.9 f_{eq}$ is given. It increases with the Damkohler number Da.

In all cases, no convection was added, and $k_f = 10^2$ L·mol^{-1}·s^{-1}; $k_r = 10^{-5}$ s^{-1}; $[T]_0$ =100 pM.

Table 13: Hybridization time ($k_f = 10^2$ L·mol^{-1}·s^{-1}; $k_r = 10^{-3}$ s^{-1}; $[P]_{max}$ =100 pM)

[P]$_{max}$ moles·m^{-2}	D m^2·s^{-1}	Da No unit	t @ f = 0.5 f$_{eq}$ minutes	t @ f = 0.9 f$_{eq}$ minutes
Ideal case			11	38
10^{-10}	10^{-10}	0.01	12	60
10^{-10}	10^{-11}	0.1	13	70
10^{-9}	10^{-10}		15	93
10^{-10}	10^{-12}		17	89
10^{-9}	10^{-11}	1	28	297
10^{-8}	10^{-10}		65	258
10^{-9}	10^{-12}		102	2710
10^{-8}	10^{-11}	10	527	2106
10^{-7}	10^{-10}		610	2010
10^{-8}	10^{-12}	100	> 2 days	> 2 days
10^{-7}	10^{-11}			
10^{-7}	10^{-12}	1000	> 2 days	> 2 days

The time to reach $f = 0.5\,f_{eq}$ and $f = 0.9\,f_{eq}$ is given. It increases with the Damkohler number Da.

In all cases, no convection was added, and $k_f = 10^2$ L·mol^{-1}·s^{-1}; $k_r = 10^{-3}$ s^{-1}; $[T]_0$ =100 pM.

Table 14: Hybridization time ($k_f = 10^2$ L·mol^{-1}·s^{-1}; $k_r = 10^{-5}$ s^{-1}; $[T]_0 = 1$ pM)

$[P]_{max}$ moles·m^{-2}	D m^2·s^{-1}	Da No unit	t @ f = 0.5 f$_{eq}$ minutes	t @ f = 0.9 f$_{eq}$ minutes
Ideal case			1143	3800
10^{-10}	10^{-10}	0.01	1280	> 2 days
10^{-10}	10^{-11}	0.1	1740	> 2 days
10^{-9}	10^{-10}		1740	
10^{-10}	10^{-12}	1	> 2 days	> 2 days
10^{-9}	10^{-11}			
10^{-8}	10^{-10}			
10^{-9}	10^{-12}	10	> 2 days	> 2 days
10^{-8}	10^{-11}			
10^{-7}	10^{-10}			
10^{-8}	10^{-12}	100	> 2 days	> 2 days
10^{-7}	10^{-11}			
10^{-7}	10^{-12}	1000	> 2 days	> 2 days

The time to reach $f = 0.5\,f_{eq}$ and $f = 0.9\,f_{eq}$ is given. It increases with the Damkohler number Da.

In all cases, no convection was added, and $k_f = 10^2$ L·mol^{-1}·s^{-1}; $k_r = 10^{-5}$ s^{-1}; $[T]_0 = 1$ pM.

Table 15: Hybridization time ($k_f = 10^2$ L·mol^{-1}·s^{-1}; $k_r = 10^{-3}$ s^{-1}; $[P]_{max}$ =1 pM)

[P]$_{max}$ moles·m^{-2}	D m^2·s^{-1}	Da No unit	t @ f = 0.5 f$_{eq}$ minutes	t @ f = 0.9 f$_{eq}$ minutes
Ideal case			12	38
10^{-10}	10^{-10}	0.01	14	61
10^{-10}	10^{-11}	0.1	15	71
10^{-9}	10^{-10}		17	94
10^{-10}	10^{-12}		17	119
10^{-9}	10^{-11}	1	28	390
10^{-8}	10^{-10}		66	365
10^{-9}	10^{-12}		103	2750
10^{-8}	10^{-11}	10	530	2140
10^{-7}	10^{-10}		620	2010
10^{-8}	10^{-12}	100	> 2 days	> 2 days
10^{-7}	10^{-11}			
10^{-7}	10^{-12}	1000	> 2 days	> 2 days

The time to reach $f = 0.5 f_{eq}$ and $f = 0.9 f_{eq}$ is given. It increases with the Damkohler number Da.

In all cases, no convection was added, and $k_f = 10^2$ L·mol^{-1}·s^{-1}; $k_r = 10^{-3}$ s^{-1}; $[T]_0$ =1 pM.

Table 16: Hybridization time ($k_f = 10^3$ L·mol⁻¹·s⁻¹; $k_r = 10^{-5}$ s⁻¹; $[T]_0 = 100$ pM)

$[P]_{max}$ moles·m⁻²	D m²·s⁻¹	Da No unit	t @ f = 0.5 f_{eq} minutes	t @ f = 0.9 f_{eq} minutes
Ideal case			105	349
10^{-10}	10^{-10}	0.1	158	580
10^{-10}	10^{-11}	1	401	1320
10^{-9}	10^{-10}		484	1350
10^{-10}	10^{-12}	10	2440	> 2 days
10^{-9}	10^{-11}		> 2 days	
10^{-8}	10^{-10}			
10^{-9}	10^{-12}	100	> 2 days	> 2 days
10^{-8}	10^{-11}			
10^{-7}	10^{-10}			
10^{-8}	10^{-12}	1000	> 2 days	> 2 days
10^{-7}	10^{-11}			
10^{-7}	10^{-12}	10000	> 2 days	> 2 days

The time to reach $f = 0.5\, f_{eq}$ and $f = 0.9\, f_{eq}$ is given. It increases with the Damkohler number Da.

In all cases, no convection was added, and $k_f = 10^3$ L·mol⁻¹·s⁻¹; $k_r = 10^{-5}$ s⁻¹; $[T]_0 = 100$ pM.

Table 17: Hybridization time ($k_f = 10^3$ L·mol^{-1}·s^{-1}; $k_r = 10^{-3}$ s^{-1}; $[T]_0 = 100$ pM)

$[P]_{max}$ moles·m^{-2}	D m^2·s^{-1}	Da No unit	t @ f = 0.5 f_{eq} minutes	t @ f = 0.9 f_{eq} minutes
Ideal case			11	35
10^{-10}	10^{-10}	0.1	15	81
10^{-10}	10^{-11}	1	24	315
10^{-9}	10^{-10}		59	290
10^{-10}	10^{-12}		82	2320
10^{-9}	10^{-11}	10	459	1890
10^{-8}	10^{-10}		540	1780
10^{-9}	10^{-12}			
10^{-8}	10^{-11}	100	> 2 days	> 2 days
10^{-7}	10^{-10}			
10^{-8}	10^{-12}	1000	> 2 days	> 2 days
10^{-7}	10^{-11}			
10^{-7}	10^{-12}	10000	> 2 days	> 2 days

The time to reach $f = 0.5\,f_{eq}$ and $f = 0.9\,f_{eq}$ is given. It increases with the Damkohler number Da.

In all cases, no convection was added, and $k_f = 10^3$ L·mol^{-1}·s^{-1}; $k_r = 10^{-3}$ s^{-1}; $[T]_0 = 100$ pM.

Table 18: Hybridization time ($k_f = 10^3$ L·mol^{-1}·s^{-1}; $k_r = 10^{-5}$ s^{-1}; $[T]_0 = 1$ pM)

$[P]_{max}$ moles·m^{-2}	D m^2·s^{-1}	Da No unit	t @ f = 0.5 f_{eq} minutes	t @ f = 0.9 f_{eq} minutes
Ideal case			1050	3489
10^{-10}	10^{-10}	0.1	1600	> 2 days
10^{-10}	10^{-11}	1	> 2 days	> 2 days
10^{-9}	10^{-10}			
10^{-10}	10^{-12}	10	> 2 days	> 2 days
10^{-9}	10^{-11}			
10^{-8}	10^{-10}			
10^{-9}	10^{-12}	100	> 2 days	> 2 days
10^{-8}	10^{-11}			
10^{-7}	10^{-10}			
10^{-8}	10^{-12}	1000	> 2 days	> 2 days
10^{-7}	10^{-11}			
10^{-7}	10^{-12}	10000	> 2 days	> 2 days

The time to reach $f = 0.5 f_{eq}$ and $f = 0.9 f_{eq}$ is given. It increases with the Damkohler number Da.

In all cases, no convection was added, and $k_f = 10^3$ L·mol^{-1}·s^{-1}; $k_r = 10^{-5}$ s^{-1}; $[T]_0 = 1$ pM.

Table 19: Hybridization time ($k_f = 10^3$ L·mol^{-1}·s^{-1}; $k_r = 10^{-3}$ s^{-1}; $[T]_0$=1 pM)

[P]$_{max}$ moles·m^{-2}	D m^2·s^{-1}	Da No unit	t @ f = 0.5 f$_{eq}$ minutes	t @ f = 0.9 f$_{eq}$ minutes
Ideal case			12	38
10^{-10}	10^{-10}	0.1	17	94
10^{-10}	10^{-11}	1	28	390
10^{-9}	10^{-10}		66	364
10^{-10}	10^{-12}		103	2740
10^{-9}	10^{-11}	10	530	2140
10^{-8}	10^{-10}		610	2000
10^{-9}	10^{-12}			
10^{-8}	10^{-11}	100	> 2 days	> 2 days
10^{-7}	10^{-10}			
10^{-8}	10^{-12}	1000	> 2 days	> 2 days
10^{-7}	10^{-11}			
10^{-7}	10^{-12}	10000	> 2 days	> 2 days

The time to reach $f = 0.5 f_{eq}$ and $f = 0.9 f_{eq}$ is given. It increases with the Damkohler number Da. In all cases, no convection was added, and $k_f = 10^3$ L·mol^{-1}·s^{-1}; $k_r = 10^{-3}$ s^{-1}; $[T]_0$ =1 pM.

Let us first examine the eight ideal cases. The kinetics is governed by the time constant

$$\tau = \frac{1}{k_f [T]_0 + k_r}$$

. When the dissociation rate constant k_r is set to its higher value (10^{-3} s^{-1}), it dominates over the term $k_f [T]_0$ and the equilibrium is reached quickly. Tables 13, 15, 17 and 19 show that $f = 0.9 f_{eq}$ is reached in less than 40 minutes. When the dissociation rate constant k_r is set to its lower value (10^{-5} s^{-1}), it compares with the term $k_f [T]_0$. In this case, the time necessary to reach equilibrium depends also on $k_f [T]_0$, but in general, we observe in tables 12, 14, 16 and 18 that the time to reach equilibrium is significantly higher, sometimes going above two days (tables 14 and 18).

The presence of a diffusion limitation can be deduced by comparing the time to reach $f = 0.5 f_{eq}$ and $f = 0.9 f_{eq}$ to the time calculated in the ideal case. In all cases, the kinetics is slower than the kinetics of the ideal case, which proves the validity of the computer simulations. Clearly, as the Damkohler number increases, the kinetics becomes slower than in the ideal case. Generally, for a Damkohler number lower or equal to 1, the kinetics is still comparable to the ideal case. For values equal or higher than 10, the diffusion limitation becomes strong and the time to reach $f = 0.5 f_{eq}$ or $f = 0.9 f_{eq}$ is more than 10 times higher than the calculated time for the ideal case. These trends can be visualized by plotting $\dfrac{f}{f_{eq}}$ in function of time. The curves corresponding to the parameters used in table 13 have been plotted on six graphs (figures 3 to 6), each of them corresponding to a different value of the Damkohler number. Similar curves can be obtained with the cases presented in tables 12 to 19. When Da is equal to 0.1 (figure 3), the hybridization curves are not very different from the ideal case, so hybridization is not completely diffusion limited. When Da is equal or higher than 1 (figures 4 to 6), the hybridization curves become significantly lower than in the ideal case, which means that the process is diffusion limited. When Da takes higher values (figure 6), the diffusion limitation becomes very strong, and the kinetics are completely different from the ideal case.

Figure 3. Hybridization curves for $Da = 0.1$ ($k_f = 10^2$ L·mol^{-1}·s^{-1}, $k_r = 10^{-3}$ s^{-1}, $[T]_0 =$ 100 pM)
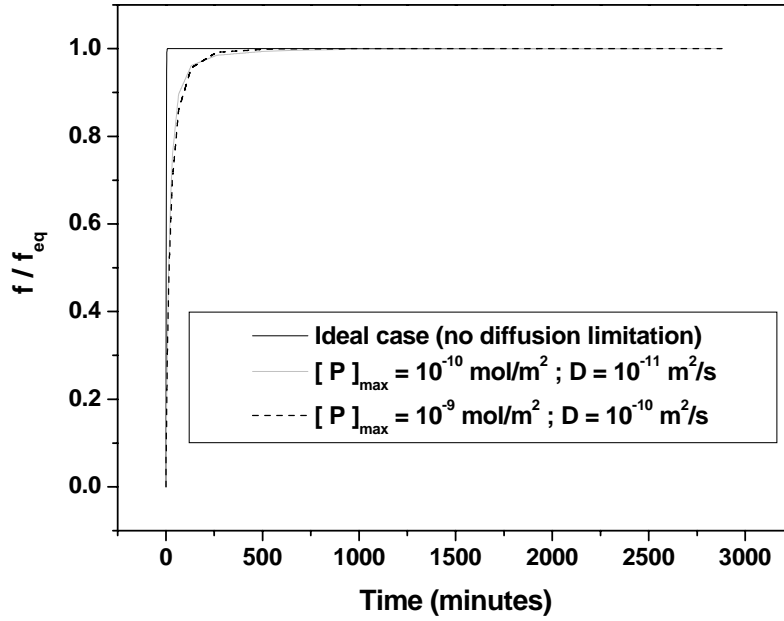
Figure 4. Hybridization curves for $Da = 1$ ($k_f = 10^2$ L·mol^{-1}·s^{-1}, $k_r = 10^{-3}$ s^{-1}, $[T]_0 = 100$ pM)
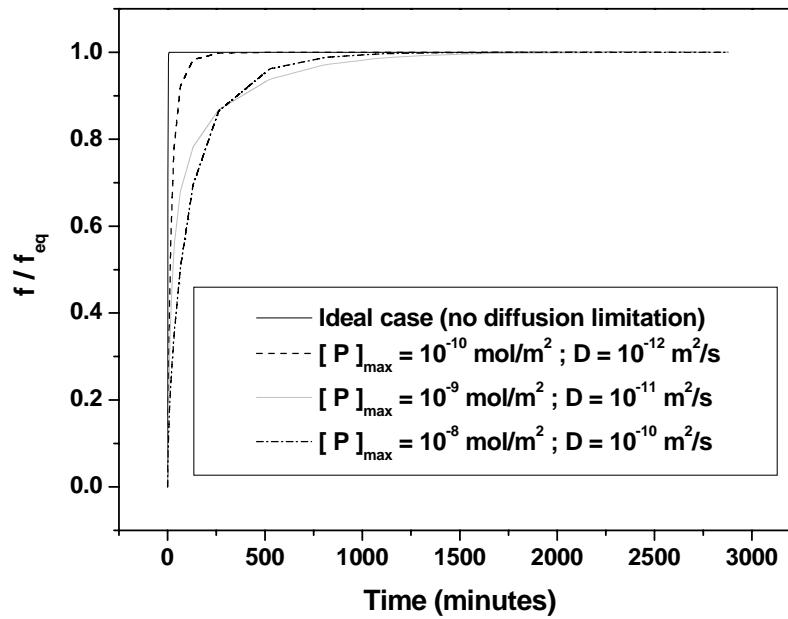
Figure 5. Hybridization curves for $Da = 10$ ($k_f = 10^2$ **L·mol^{-1}·s^{-1}**, $k_r = 10^{-3}$ **s^{-1}**, $[T]_0 =$ **100 pM**)
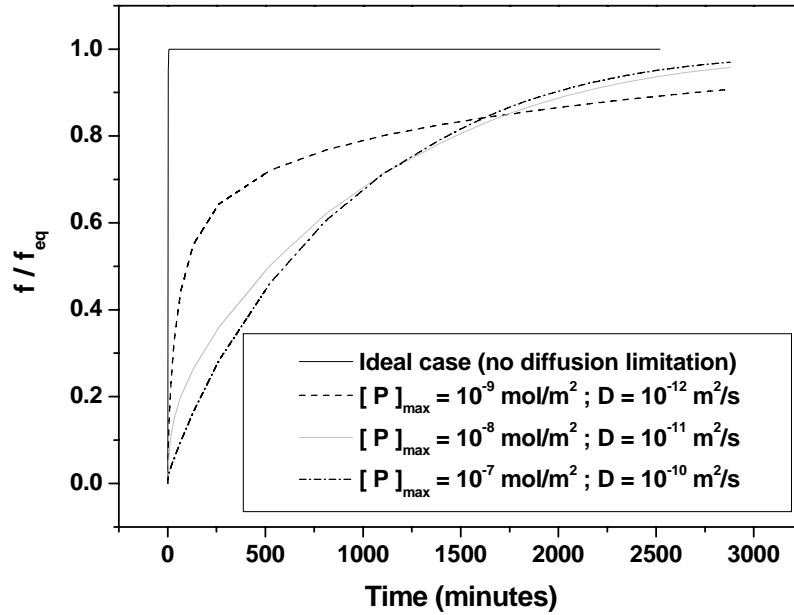
Figure 6. Hybridization curves for $Da = 100$ ($k_f = 10^2$ L·mol^{-1}·s^{-1}, $k_r = 10^{-3}$ s^{-1}, $[T]_0 =$ 100 pM)
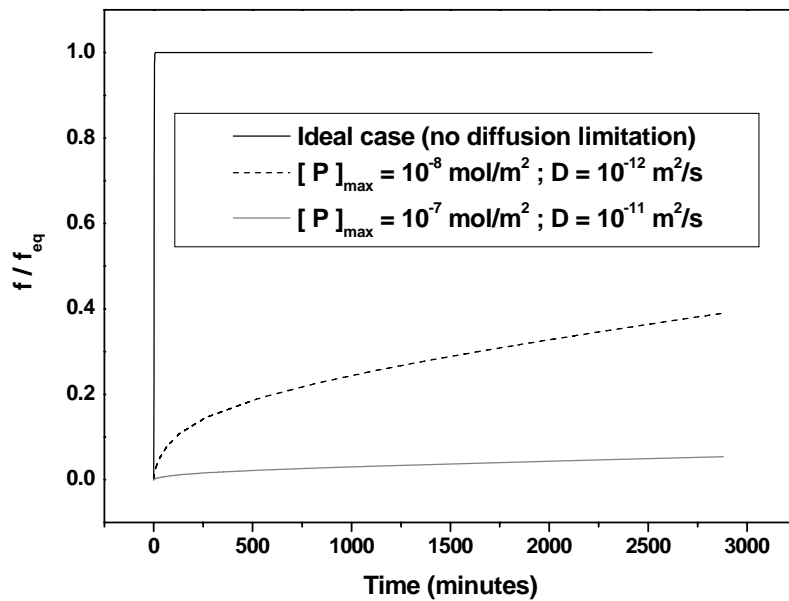
The occurrence of a diffusion limitation can also be observed by the formation of a diffusion barrier in the chamber. When the process is diffusion limited, the DNA supply is lower than the demand from the hybridization reaction. This results in the formation of a depletion zone above the sensing zone. The DNA bulk concentration along a horizontal line distant from the bottom wall by 1 micrometer is presented on figure 7. We can see that the DNA concentration is lower than $[T]_0$ above the sensing zone located between 400 and 600 µm. For a Da number lower than one, the concentration is still close to $[T]_0$. For higher values of the Damkohler number, the DNA concentration in the depletion becomes much lower than $[T]_0$. The DNA concentration in the whole chamber can be seen on figures 8 and 9. Figure 8 was obtained under the same conditions as the curve Da = 100 on figure 7. Figure 9 was obtained under the same conditions as the curve Da = 0.1 on figure 7. As expected, we can observe a depletion zone close to the sensing zone. This zone is bigger when Da = 100 (figure 8, the surface is not flat at all) than when Da = 0.1 (figure 9, the surface is almost flat).

Figure 7 : Depletion zone at t = 30 minutes, without convection
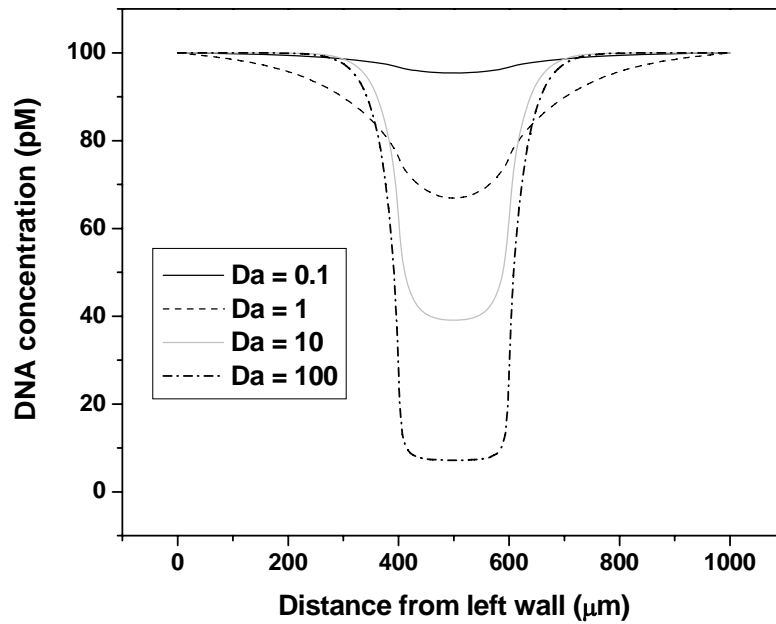
The DNA concenctation in the bulk at a height of 1mm above the sensing zone is plotted. All curves were obtained with $[T]_0$ = 100 pM; $k_f = 10^2$ L·mol^{-1}·s^{-1} , $k_r = 10^{-3}$ s^{-1}

Da= 0.1 ($[P]_{max}$ =10^{-10} moles·m^{-2}; $D = 10^{-11}$ m^2·s^{-1}); Da= 1 ($[P]_{max}$ =10^{-9} moles·m^{-2}; $D = 10^{-11}$ m^2·s^{-1})

Da=10 ($[P]_{max}$ =10^{-9} moles·m^{-2}; $D = 10^{-12}$ m^2·s^{-1}); Da=100 ($[P]_{max}$ =10^{-8} moles·m^{-2}; $D = 10^{-12}$ m^2·s^{-1})

Figure 8: Depletion zone at t=30minutes, Da=100, t = 30 minutes
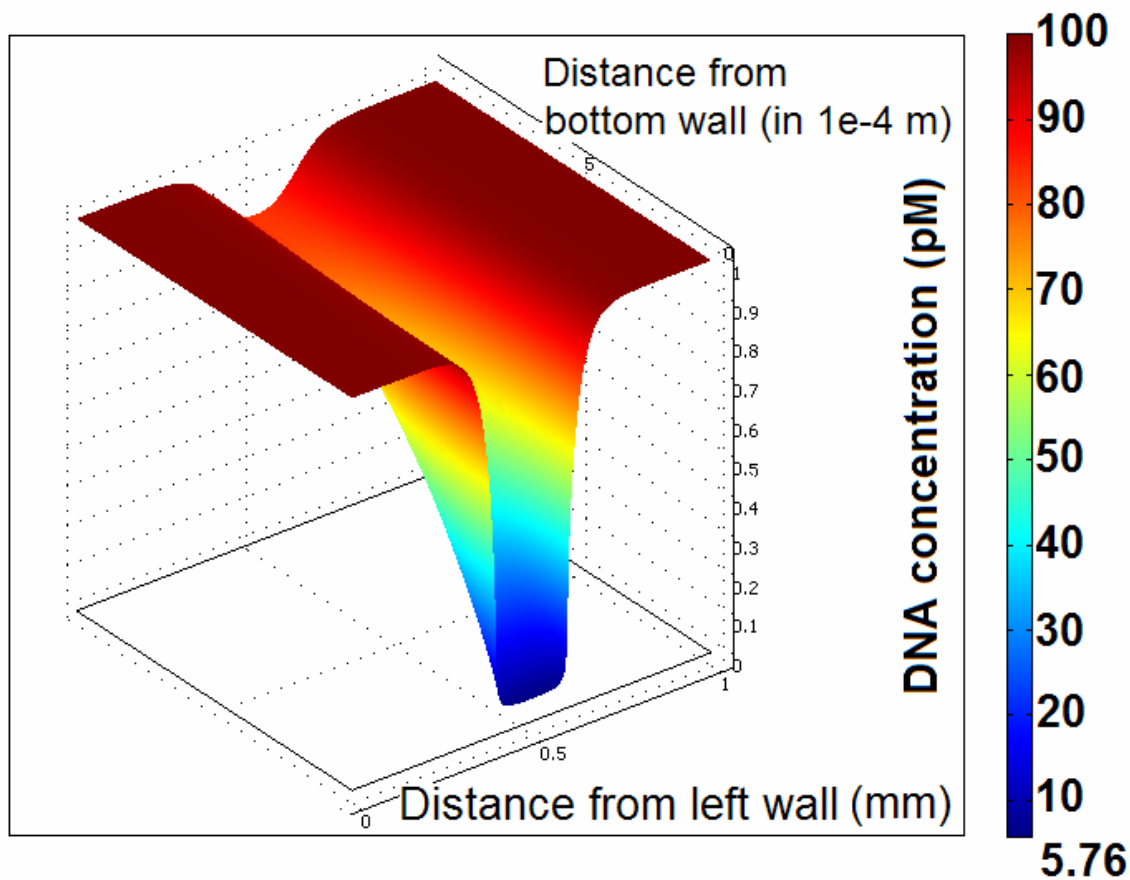
The DNA concentration in the bulk is plotted. Parameters used: $[T]_0 = 100$ pM; $k_f = 10^2$ L·mol⁻¹·s⁻¹ , $k_r = 10^{-3}$ s⁻¹, $[P]_{max} = 10^{-8}$ moles·m⁻² , $D = 10^{-12}$ m²·s⁻¹) so that Da = 100.

Figure 9: Depletion zone at t=30minutes, Da=0.1, t = 30 minutes
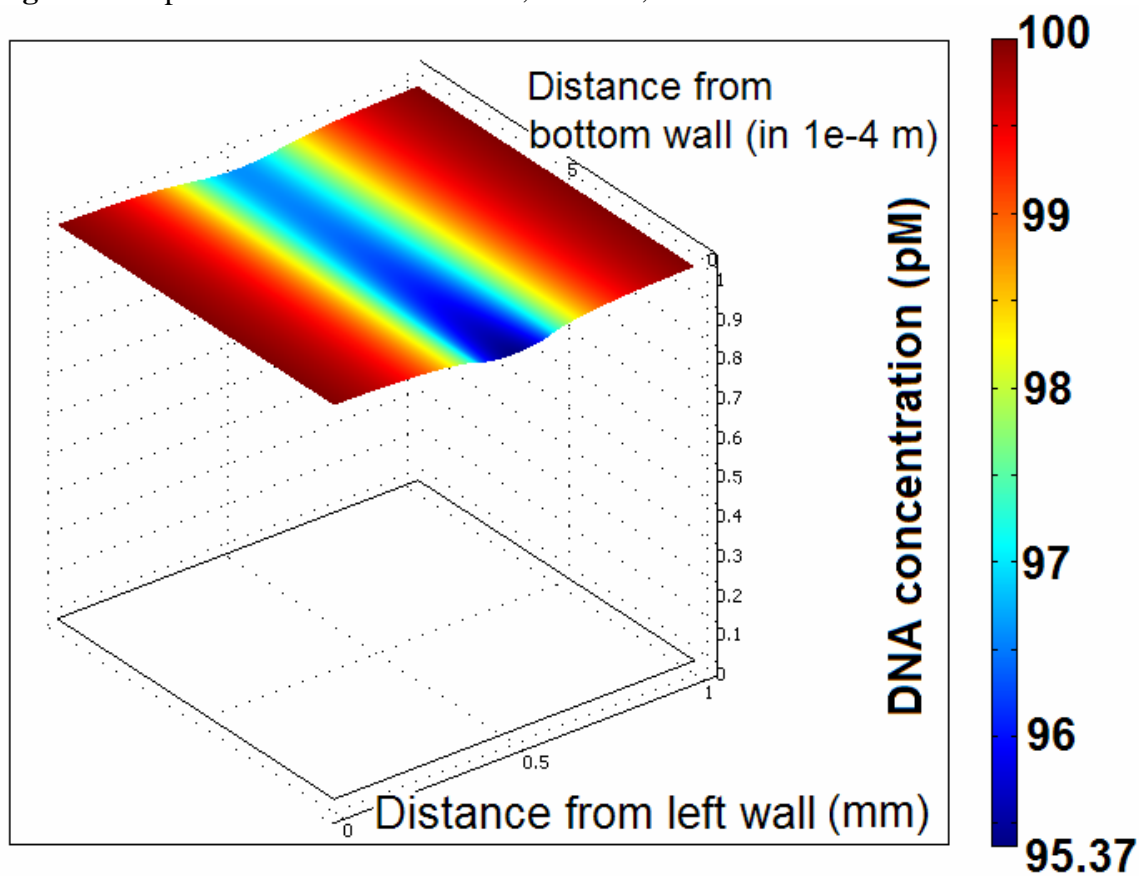
The DNA concentration in the bulk is plotted. All curves were obtained with $[T]_0 = 100$ pM; $k_f = 10^2$ L·mol^{-1}·s^{-1}, $k_r = 10^{-3}$ s^{-1}, $[P]_{max} = 10^{-10}$ moles·m^{-2}, $D = 10^{-11}$ m^2·s^{-1} so that Da = 0.1

This part shows that the Da - number is a good criterion to predict if hybridization is reaction limited or diffusion limited. When the Da - number is equal or higher than 1, the kinetics become significantly different from the ideal case. In tables 20 to 23, the Da - number has been calculated for different values spanning the range observed in DNA arrays. We can see that in many cases (highlighted in bold font), the Da - number will take values equal or higher than 1. It suggests that the diffusion limitation occurs in DNA arrays, and that it is logical to establish a strategy to overcome it. The introduction of DNA convective transport could be a way to enhance the kinetics by preventing the formation of a depletion zone. This possibility is studied in the next section.

Table 20: Damkohler number in DNA array ($[P]_{max} = 10^{-10}$ mol·m^{-2}; $h = 100$ µm)

		Target diffusion coefficient (m^2·s^{-1})		
		10^{-12}	10^{-11}	10^{-10}
k_f	10^2	**1**	0.1	0.01
(m^3·mol^{-1}·s^{-1})	10^3	**10**	**1**	**0.1**

In the cases highlighted with bold font, it is expected that hybridization will be diffusion limited.

Table 21: Damkohler number in DNA array ($[P]_{max} = 10^{-9}$ mol·m^{-2}; $h = 100$ µm)

		Target diffusion coefficient (m^2·s^{-1})		
		10^{-12}	10^{-11}	10^{-10}
k_f	10^2	**10**	**1**	0.1
(m^3·mol^{-1}·s^{-1})	10^3	**100**	**10**	**1**

In the cases highlighted with bold font, it is expected that hybridization will be diffusion limited.

Table 22: Damkohler number in DNA array ($[P]_{max} = 10^{-8}$ mol·m^{-2}; $h = 100$ μm)

		Target diffusion coefficient (m^2·s^{-1})		
		10^{-12}	10^{-11}	10^{-10}
k_f	10^2	**100**	**10**	1
(m^3·mol^{-1}·s^{-1})	10^3	**1000**	**100**	**10**

In the cases highlighted with bold font, it is expected that hybridization will be diffusion limited.

Table 23: Damkohler number in DNA array ($[P]_{max} = 10^{-7}$ mol·m^{-2}; $h = 100$ μm)

		Target diffusion coefficient (m^2·s^{-1})		
		10^{-12}	10^{-11}	10^{-10}
k_f	10^2	**1000**	**100**	**10**
(m^3·mol^{-1}·s^{-1})	10^3	**10000**	**1000**	**100**

In the cases highlighted with bold font, it is expected that hybridization will be diffusion limited.

3.4 Influence of DNA convective transport

In this section, convective transport of DNA was added. The hybridization times are given in tables 24 to 31.

Table 24: Hybridization time ($k_f = 10^2$ L·mol^{-1}·s^{-1}; $k_r = 10^{-5}$ s^{-1}; $[T]_0$ =100 pM)

[P]$_{max}$	D	Da	t @ f = 0.9 f$_{eq}$ no convection	t @ f = 0.9 f$_{eq}$ v = 10μm/s	t @ f = 0.9 f$_{eq}$ v = 100μm/s
moles·m^{-2}	m^2·s^{-1}	No unit	minutes	minutes	minutes
Ideal case			1919	1919	1919
10^{-10}	10^{-10}	0.01	2140	2090	2080
10^{-10}	10^{-11}	0.1	2710	2100	2090
10^{-9}	10^{-10}		2650	2120	2100
10^{-10}	10^{-12}	1	> 2 days	2120	2100
10^{-9}	10^{-11}			2210	2120
10^{-8}	10^{-10}			2500	2210
10^{-9}	10^{-12}	10	> 2 days	2490	2210
10^{-8}	10^{-11}			> 2 days	2490
10^{-7}	10^{-10}				> 2 days
10^{-8}	10^{-12}	100	> 2 days	> 2 days	> 2 days
10^{-7}	10^{-11}				
10^{-7}	10^{-12}	1000	> 2 days	> 2 days	> 2 days

The time to reach $f = 0.9 f_{eq}$ decreases as convection is added. It increases with the Damkohler number Da. In all cases $k_f = 10^2$ L·mol^{-1}·s^{-1}; $k_r = 10^{-5}$ s^{-1}; $[T]_0$ =100 pM.

Table 25: Hybridization time ($k_f = 10^2$ L·mol^{-1}·s^{-1}; $k_r = 10^{-3}$ s^{-1}; $[T]_0$ =100 pM)

$[P]_{max}$ moles·m^{-2}	D m^2·s^{-1}	Da No unit	t @ f = 0.9 f$_{eq}$ no convection minutes	t @ f = 0.9 f$_{eq}$ v = 10µm/s minutes	t @ f = 0.9 f$_{eq}$ v = 100µm/s minutes
Ideal case			38	38	38
10^{-10}	10^{-10}	0.01	49	47	44
10^{-10}	10^{-11}	0.1	62	47	47
10^{-9}	10^{-10}		74	48	47
10^{-10}	10^{-12}		89	48	47
10^{-9}	10^{-11}	1	297	51	48
10^{-8}	10^{-10}		258	58	51
10^{-9}	10^{-12}		2710	58	51
10^{-8}	10^{-11}	10	2106	82	58
10^{-7}	10^{-10}		2010	175	82
10^{-8}	10^{-12}	100	> 2 days	227	82
10^{-7}	10^{-11}			441	186
10^{-7}	10^{-12}	1000	> 2 days	1331	438

The time to reach $f = 0.9\, f_{eq}$ decreases as convection is added. It increases with the Damkohler number Da. In all cases $k_f = 10^2$ L·mol^{-1}·s^{-1}; $k_r = 10^{-3}$ s^{-1}; $[T]_0$ =100 pM.

Table 26: Hybridization time ($k_f = 10^2$ L·mol^{-1}·s^{-1}; $k_r = 10^{-5}$ s^{-1}; $[T]_0 = 1$ pM)

[P]$_{max}$ moles·m^{-2}	D m^2·s^{-1}	Da No unit	t @ f = 0.9 f$_{eq}$ no convection minutes	t @ f = 0.9 f$_{eq}$ v = 10μm/s minutes	t @ f = 0.9 f$_{eq}$ v = 100μm/s minutes
Ideal case			3800	3800	3800
10^{-10}	10^{-10}	0.01	> 2 days	> 2 days	> 2 days
10^{-10}	10^{-11}	0.1	> 2 days	> 2 days	> 2 days
10^{-9}	10^{-10}				
10^{-10}	10^{-12}	1	> 2 days	> 2 days	> 2 days
10^{-9}	10^{-11}				
10^{-8}	10^{-10}				
10^{-9}	10^{-12}	10	> 2 days	> 2 days	> 2 days
10^{-8}	10^{-11}				
10^{-7}	10^{-10}				
10^{-8}	10^{-12}	100	> 2 days	> 2 days	> 2 days
10^{-7}	10^{-11}				
10^{-7}	10^{-12}	1000	> 2 days	> 2 days	> 2 days

The time to reach $f = 0.9 f_{eq}$ decreases as convection is added. It increases with the Damkohler number

Da. In all cases $k_f = 10^2$ L·mol^{-1}·s^{-1}; $k_r = 10^{-5}$ s^{-1}; $[T]_0 = 1$ pM

Table 27: Hybridization time ($k_f = 10^2$ L·mol⁻¹·s⁻¹; $k_r = 10^{-3}$ s⁻¹; $[T]_0$ =1 pM)

$[P]_{max}$ moles·m⁻²	D m²·s⁻¹	Da No unit	t @ f = 0.9 f_{eq} no convection minutes	t @ f = 0.9 f_{eq} v = 10μm/s minutes	t @ f = 0.9 f_{eq} v = 100μm/s minutes
Ideal case			12	12	12
10^{-10}	10^{-10}	0.01	61	60	60
10^{-10}	10^{-11}	0.1	71	60	60
10^{-9}	10^{-10}		94	61	60
10^{-10}	10^{-12}	1	119	61	60
10^{-9}	10^{-11}		390	63	60
10^{-8}	10^{-10}		365	82	63
10^{-9}	10^{-12}	10	2750	81	63
10^{-8}	10^{-11}		2140	121	81
10^{-7}	10^{-10}		2010	252	121
10^{-8}	10^{-12}	100	> 2 days	249	121
10^{-7}	10^{-11}		> 2 days	660	249
10^{-7}	10^{-12}	1000	> 2 days	1530	650

The time to reach $f = 0.9\, f_{eq}$ decreases as convection is added. It increases with the Damkohler number Da. In all cases $k_f = 10^2$ L·mol⁻¹·s⁻¹; $k_r = 10^{-3}$ s⁻¹; $[T]_0$ =1 pM.

Table 28: Hybridization time ($k_f = 10^3$ L·mol⁻¹·s⁻¹; $k_r = 10^{-5}$ s⁻¹; $[T]_0$ =100 pM)

$[P]_{max}$ moles·m⁻²	D m²·s⁻¹	Da No unit	t @ f = 0.9 f_eq no convection minutes	t @ f = 0.9 f_eq v = 10µm/s minutes	t @ f = 0.9 f_eq v = 100µm/s minutes
Ideal case			349	349	349
10^{-10}	10^{-10}	0.1	580	520	520
10^{-10}	10^{-11}	1	1320	520	520
10^{-9}	10^{-10}		1350	550	520
10^{-10}	10^{-12}	10	> 2 days	540	520
10^{-9}	10^{-11}			720	540
10^{-8}	10^{-10}			1280	720
10^{-9}	10^{-12}	100	> 2 days	1280	720
10^{-8}	10^{-11}			2420	1280
10^{-7}	10^{-10}			> 2 days	> 2 days
10^{-8}	10^{-12}	1000	> 2 days	> 2 days	> 2 days
10^{-7}	10^{-11}				
10^{-7}	10^{-12}	10000	> 2 days	> 2 days	> 2 days

The time to reach $f = 0.9 f_{eq}$ decreases as convection is added. It increases with the Damkohler number

Da. In all cases $k_f = 10^3$ L·mol⁻¹·s⁻¹; $k_r = 10^{-5}$ s⁻¹; $[T]_0$ =100 pM.

Table 29: Hybridization time ($k_f = 10^3$ L·mol⁻¹·s⁻¹; $k_r = 10^{-3}$ s⁻¹; $[T]_0$ =100 pM)

$[P]_{max}$ moles·m⁻²	D m²·s⁻¹	Da No unit	t @ f = 0.9 f_{eq} no convection minutes	t @ f = 0.9 f_{eq} v = 10μm/s minutes	t @ f = 0.9 f_{eq} v = 100μm/s minutes
Ideal case			35	35	35
10^{-10}	10^{-10}	0.1	94	57	56
10^{-10}	10^{-11}	1	315	60	57
10^{-9}	10^{-10}		290	66	60
10^{-10}	10^{-12}	10	2320	66	66
10^{-9}	10^{-11}		1890	110	66
10^{-8}	10^{-10}		1780	228	110
10^{-9}	10^{-12}	100	> 2 days	660	224
10^{-8}	10^{-11}		> 2 days	494	148
10^{-7}	10^{-10}		> 2 days	1530	540
10^{-8}	10^{-12}	1000	> 2 days	1380	530
10^{-7}	10^{-11}		> 2 days	> 2 days	1380
10^{-7}	10^{-12}	10000	> 2 days	> 2 days	> 2 days

The time to reach $f = 0.9\, f_{eq}$ decreases as convection is added. It increases with the Damkohler number Da. In all cases $k_f = 10^3$ L·mol⁻¹·s⁻¹; $k_r = 10^{-3}$ s⁻¹; $[T]_0$ =100 pM.

Table 30: Hybridization time ($k_f = 10^3$ L·mol^{-1}·s^{-1}; $k_r = 10^{-5}$ s^{-1}; $[T]_0$ =1 pM)

$[P]_{max}$ moles·m^{-2}	D m^2·s^{-1}	Da No unit	t @ f = 0.9 f$_{eq}$ no convection minutes	t @ f = 0.9 f$_{eq}$ v = 100μm/s minutes	t @ f = 0.9 f$_{eq}$ v = 200μm/s minutes
Ideal case			3489	3489	3489
10^{-10}	10^{-10}	0.1	> 2 days	> 2 days	> 2 days
10^{-10}	10^{-11}	1	> 2 days	> 2 days	> 2 days
10^{-9}	10^{-10}				
10^{-10}	10^{-12}	10	> 2 days	> 2 days	> 2 days
10^{-9}	10^{-11}				
10^{-8}	10^{-10}				
10^{-9}	10^{-12}	100	> 2 days	> 2 days	> 2 days
10^{-8}	10^{-11}				
10^{-7}	10^{-10}				
10^{-8}	10^{-12}	1000	> 2 days	> 2 days	> 2 days
10^{-7}	10^{-11}				
10^{-7}	10^{-12}	10000	> 2 days	> 2 days	> 2 days

The time to reach $f = 0.9 f_{eq}$ decreases as convection is added. It increases with the Damkohler number Da. In all cases $k_f = 10^3$ L·mol^{-1}·s^{-1}; $k_r = 10^{-3}$ s^{-1}; $[T]_0$ =1 pM.

Table 31: Hybridization time ($k_f = 10^3$ L·mol⁻¹·s⁻¹; $k_r = 10^{-3}$ s⁻¹; $[T]_0 = 1$ pM)

$[P]_{max}$ moles·m⁻²	D m²·s⁻¹	Da No unit	t @ f = 0.9 f$_{eq}$ no convection minutes	t @ f = 0.9 f$_{eq}$ v = 10µm/s minutes	t @ f = 0.9 f$_{eq}$ v = 100µm/s minutes
Ideal case			38	38	38
10^{-10}	10^{-10}	0.1	94	61	60
10^{-10}	10^{-11}	1	390	63	61
10^{-9}	10^{-10}		364	82	63
10^{-10}	10^{-12}	10	2740	81	81
10^{-9}	10^{-11}		2140	121	66
10^{-8}	10^{-10}		2000	251	121
10^{-9}	10^{-12}	100	> 2 days	248	121
10^{-8}	10^{-11}			660	248
10^{-7}	10^{-10}			1530	660
10^{-8}	10^{-12}	1000	> 2 days	1530	650
10^{-7}	10^{-11}			> 2 days	1530
10^{-7}	10^{-12}	10000	> 2 days	> 2 days	> 2 days

The time to reach $f = 0.9 f_{eq}$ decreases as convection is added. It increases with the Damkohler number Da. In all cases $k_f = 10^3$ L·mol⁻¹·s⁻¹; $k_r = 10^{-3}$ s⁻¹; $[T]_0 = 1$ pM.

In all cases, the hybridization time is lower when convection is added compared to the case where DNA only moves by diffusion. Indeed, we can see on figures 10 to 13 that as convection is added, the concentration near the sensing zone becomes closer to $[T]_0$, and the concentration drop becomes more localized. This suggests that the depletion zone decreases as convection is added. We can also notice that the depletion zone is not symmetrical when convection is added. The flow goes from the left to the right, therefore the left edge of the sensing zone will see the DNA flux before the middle and the right edge, which induces the non symmetrical shape of the depletion zone.

For values of the Da - number lower than 1, the enhancement is small, the time to reach

$f = 0.9 f_{eq}$ is reduced by 30% maximum, and is still higher than the predicted time in the

ideal case without diffusion limitation. Indeed, as showed on figures 10 and 11, there will

always be a depletion zone above the sensing zone, even if it is very small when the

reaction is not diffusion limited. We can also observe that in these cases, a velocity of

100 μm/s does not seem to enhance the kinetics more than a velocity of 10 μm/s. It

suggests that when the reaction is already rather reaction limited, it is not necessary to

apply a strong convection enhance the kinetics.

Figure 10 : Depletion zone at t = 30 minutes, $v = 10 \, \mu m/s$
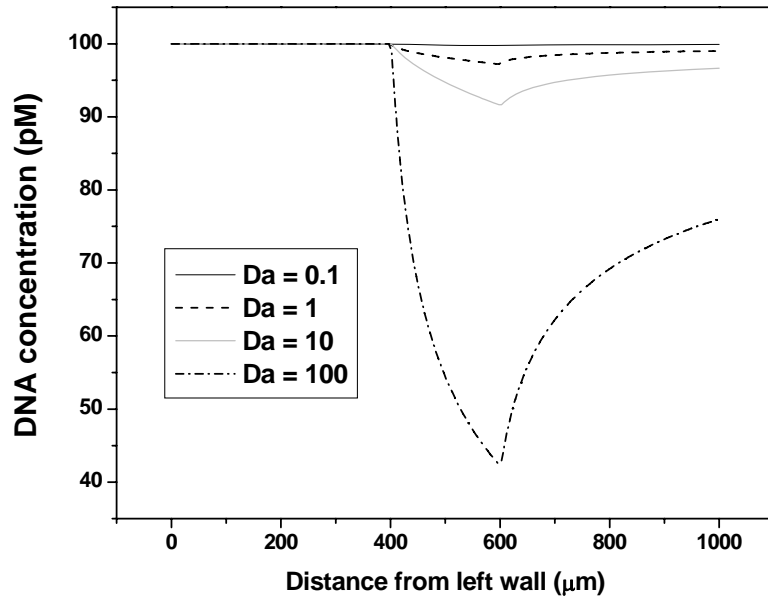
All curves obtained with $[T]_0 = 100$ pM; $k_f = 10^2$ L·mol^{-1}·s^{-1} , $k_r = 10^{-3}$ s^{-1}

Da= 0.1 ($[P]_{max} = 10^{-10}$ moles·m^{-2}; $D = 10^{-11}$ m^2·s^{-1}); Da= 1 ($[P]_{max} = 10^{-9}$ moles·m^{-2}; $D = 10^{-11}$ m^2·s^{-1})

Da=10 ($[P]_{max} = 10^{-9}$ moles·m^{-2}; $D = 10^{-12}$ m^2·s^{-1}); Da=10 ($[P]_{max} = 10^{-8}$ moles·m^{-2}; $D = 10^{-12}$ m^2·s^{-1})

Figure 11. Depletion zone at t = 30 minutes, $v = 100\,\mu m/s$
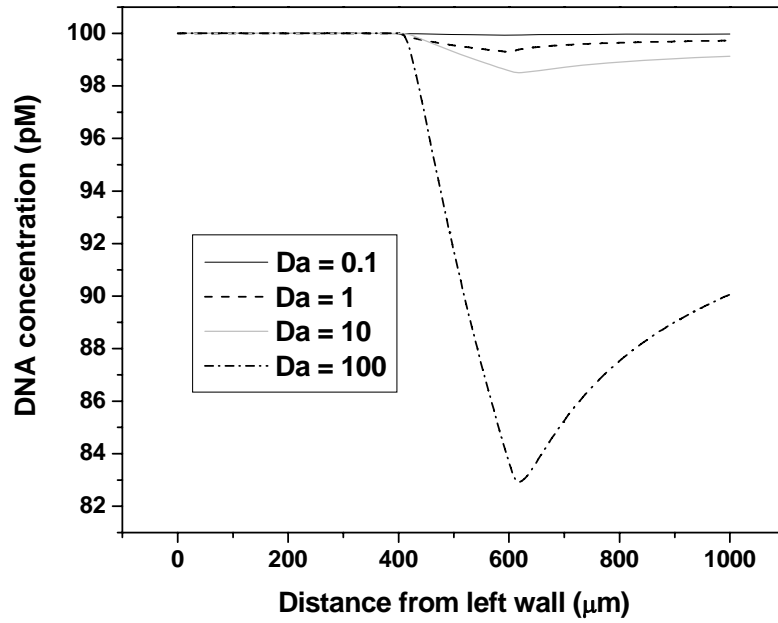
All curves obtained with $[T]_0 = 100$ pM; $k_f = 10^2$ L·mol^{-1}·s^{-1} , $k_r = 10^{-3}$ s^{-1}

Da= 0.1 ($[P]_{max} = 10^{-10}$ moles·m^{-2}; $D = 10^{-11}$ m^2·s^{-1}); Da= 1 ($[P]_{max} = 10^{-9}$ moles·m^{-2}; $D = 10^{-11}$ m^2·s^{-1})

Da=10 ($[P]_{max} = 10^{-9}$ moles·m^{-2}; $D = 10^{-12}$ m^2·s^{-1}); Da=100 ($[P]_{max} = 10^{-8}$ moles·m^{-2}; $D = 10^{-12}$ m^2·s^{-1})

Figure 12: Depletion zone at t = 30 minutes, $v = 10\ \mu m/s$, Da = 100
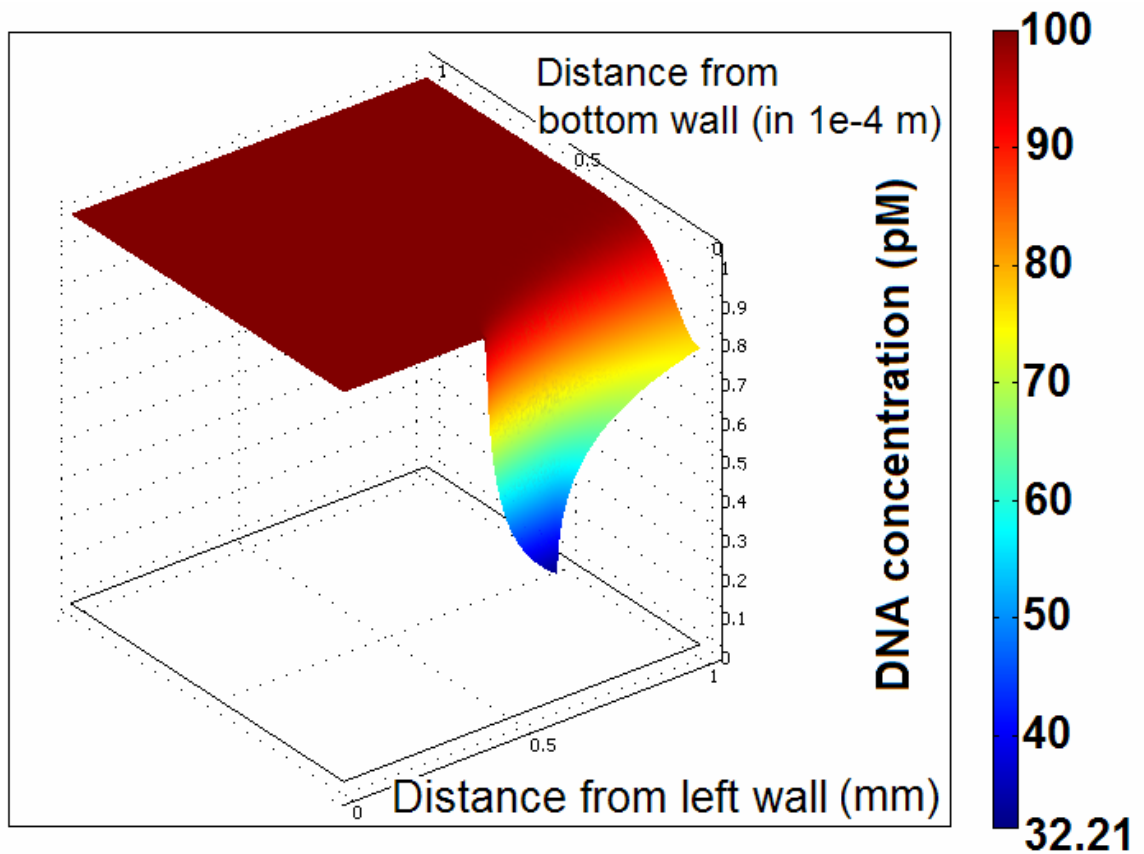
All curves obtained with $[T]_0 = 100$ pM; $k_f = 10^2$ L·mol^{-1}·s^{-1}, $k_r = 10^{-3}$ s^{-1}, $[P]_{max} = 10^{-8}$ moles·m^{-2}; $D = 10^{-12}$ m^2·s^{-1}, Da=100

Figure 13: Depletion zone at t = 30 minutes, $v = 10\,\mu m/s$, Da = 0.1
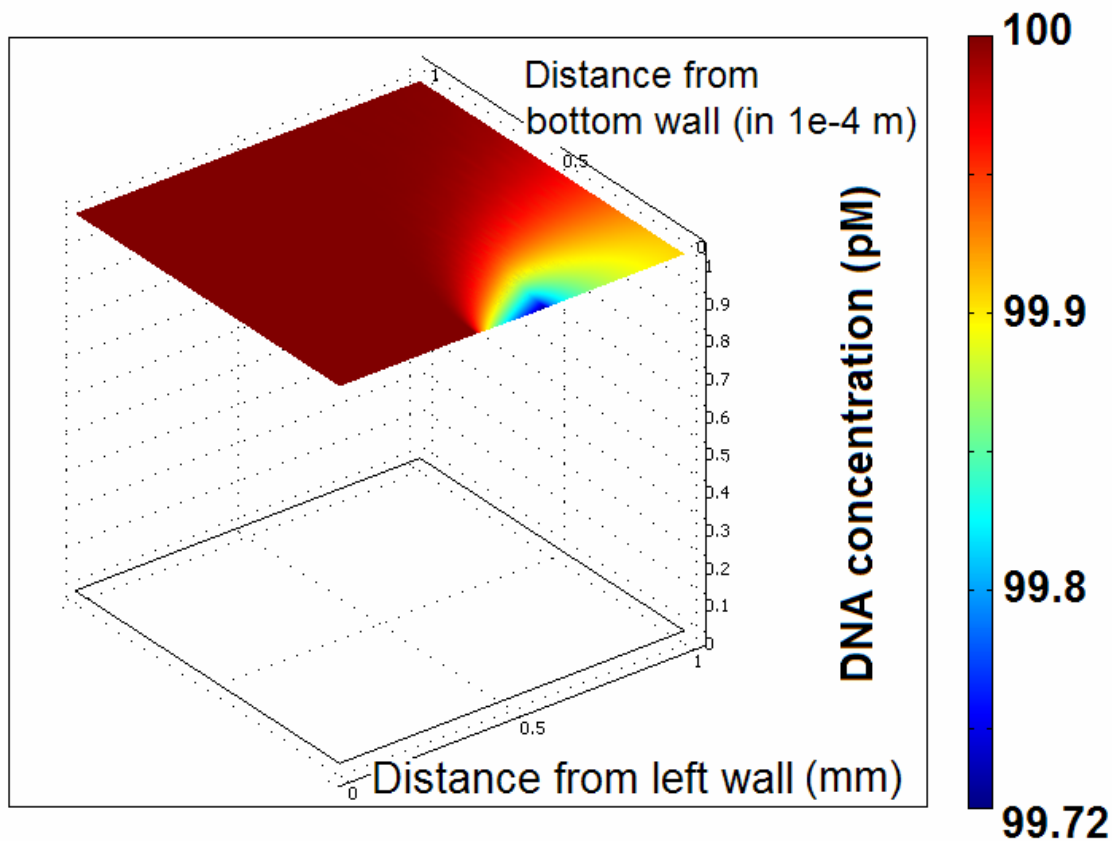
All curves obtained with $[T]_0 = 100$ pM; $k_f = 10^2$ L·mol^{-1}·s^{-1}, $k_r = 10^{-3}$ s^{-1}, $[P]_{max} = 10^{-10}$ moles·m^{-2}; $D = 10^{-11}$ m^2·s^{-1}, Da = 0.1

For a Da- number equal or higher than 1, the enhancement is important. The time to reach $f = 0.9\,f_{eq}$ increases between 20-fold to several hundred-fold. A velocity of 100 μm/s gives better results than a velocity of 10 μm/s, but a 10-fold increase of the velocity does not seem to enhance the kinetics much more. We have to consider these results with precaution. Our simulations do not take account of phenomena occurring at a molecular scale. When targets are longer than the probes, and when the probe density is high, the surface of the sensing zone can become crowded and phenomena such as probe-probe interaction or brush effects can occur[5], which affects the kinetics and the thermodynamics of hybridization. It has been observed that excessive convective transport could eventually hinder the kinetics. Vanderhoeven et al.[13] suggested that one of the steps involved in the hybridization process (collision between probe and target; formation of a binding nucleus, zippering reaction) could be affected by the convection. Nevertheless, convection should still be a good way to prevent the formation of a depletion zone and significantly enhance the kinetics.

3.4 Influence of non specific hybridization

An immobilized DNA probe can hybridize with a non complementary target, which is called "non specific hybridization" (see section 2.1.4). This phenomenon is not desired, since it leads to false results because of the non specific hybrids.

As reviewed in sections 2.1.4 and 2.6.3, the reaction rate of non specific hybridization is similar to the reaction rate of specific hybridization. Let us consider a specific hybridization reaction in presence of one non specific hybridization reaction:

$P + T_1 \Leftrightarrow H_1$ (specific)
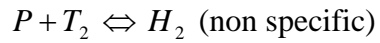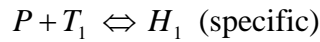
$P + T_2 \Leftrightarrow H_2$ (non specific)

The rate of formation of hybrids are:

$$\frac{\partial [H_1]}{\partial t} = k_f [P][T_1] - k_{r1} [H_1]$$

$$\frac{\partial [H_2]}{\partial t} = k_f [P][T_2] - k_{r2} [H_2]$$

Where $[T_1]$ and $[T_2]$ are the concentrations of specific and non specific target in the bulk. In the general case, since diffusion effects occur, $[T_1]$ and $[T_2]$ are not uniform and a depletion zone is formed near the sensing zone as shown in section 3.3. Therefore, in the general case, it is not possible to calculate $[H_1]$ and $[H_2]$ as a function of time.

The interaction, the "competition" between T_1 and T_2 for the free probes $[P]$ can be seen in the term:

$$[P] = [P]_{max} - [H_1] - [H_2]$$

So finally:

$$\frac{\partial [H_1]}{\partial t} = k_f \left([P]_{max} - [H_1] - [H_2] \right) [T_1] - k_{r1} [H_1]$$

$$\frac{\partial [H_2]}{\partial t} = k_f \left([P]_{max} - [H_1] - [H_2] \right) [T_2] - k_{r2} [H_2]$$

3.4.1 Occurrence of a "competition" between specific and non specific hybridization

The concentrations at equilibrium $[H_1]_{eq}$ and $[H_2]_{eq}$ can be calculated analytically by doing the assumption that targets are in excess compared to immobilized probes. Since the mixing affects how equilibrium is reached, but not its value, we can consider the ideal case where the solution is perfectly mixed to calculate $[H_1]_{eq}$ and $[H_2]_{eq}$. The values obtained will be valid even if in the cases where the chamber is not mixed; the only assumption is that targets are in excess. In the ideal case (perfect mixing), assuming that targets are in excess, the rate of formation of hybrids can be written:

$$\frac{\partial [H_1]}{\partial t} = k_f \left([P]_{max} - [H_1] - [H_2] \right) [T_1]_0 - k_{r1} [H_1]$$

$$\frac{\partial [H_2]}{\partial t} = k_f \left([P]_{max} - [H_1] - [H_2] \right) [T_2]_0 - k_{r2} [H_2]$$

Where $[T_1]_0$ and $[T_2]_0$ are the target concentration, which are uniform in space (perfect mixing) and constant in time (excess of targets).

At equilibrium:

$$\frac{\partial[H_1]}{\partial t} = k_f \left([P]_{max} - [H_1]_{eq} - [H_2]_{eq}\right)[T_1]_0 - k_{r1}[H_1]_{eq} = 0$$

$$\frac{\partial[H_2]}{\partial t} = k_f \left([P]_{max} - [H_1]_{eq} - [H_2]_{eq}\right)[T_2]_0 - k_{r2}[H_2]_{eq} = 0$$

This is just a linear system with two unknowns whose solution is:

$$[H_1]_{eq,both} = \frac{k_f k_{r2}[P]_{max}[T_1]_0}{k_f \left(k_{r1}[T_2]_0 + k_{r2}[T_1]_0\right) + k_{r1}k_{r2}}$$

$$[H_2]_{eq,both} = \frac{k_f k_{r1}[P]_{max}[T_2]_0}{k_f \left(k_{r1}[T_2]_0 + k_{r2}[T_1]_0\right) + k_{r1}k_{r2}}$$

The subscript "both" was inserted to show that these expressions correspond to the case where specific and non specific hybridization occur simultaneously. The expressions can be used to predict the number of hybridized probes.

Nevertheless, it is interesting to compare these expressions to what was obtained for single species hybridization (no simultaneous specific and non specific hybridization). It was calculated in section 3.3. If each reaction occurred independently we would have:

$$[H_1]_{eq,single} = \frac{[T_1]_0 [P]_{max}}{[T_1]_0 + \dfrac{k_{r1}}{k_f}}$$

$$[H_2]_{eq,single} = \frac{[T_2]_0 [P]_{max}}{[T_2]_0 + \dfrac{k_{r2}}{k_f}}$$

It can be easily seen that $[H_1]_{eq,single}$ and $[H_2]_{eq,single}$ are higher than $[H_1]_{eq,both}$ and $[H_2]_{eq,both}$ which seems logical. It was expected that the equilibrium concentrations will be lower when specific and non specific hybridization occur simultaneously.

Although we know $[H_1]_{eq,both}$ and $[H_2]_{eq,both}$, it is still useful to look at $[H_1]_{eq,\sin gle}$ and

$[H_2]_{eq,\sin gle}$ in order to predict if an interaction between specific and non specific targets

will occur. If the concentration of hybrids at equilibrium $[H_1]_{eq,\sin gle}$ and $[H_2]_{eq,\sin gle}$ are

much smaller than the initial concentration of free probes $[P]_{max}$, we can expect the

probes P to be in excess, and there will be no "competition" between T_1 and T_2. For

one single species, the fraction of hybridized probes at equilibrium is only a function of

$[T]_0$ and $\dfrac{k_r}{k_f}$. In table 32, the fraction of hybridized probes $\dfrac{[H]_{eq}}{[P]_{max}}$ at equilibrium is given

in function of $[T]_0$ and $\dfrac{k_r}{k_f}$. We can observe that the fraction of hybridized probes can

take values lower than 0.1, especially for lower DNA concentrations and higher values of

$\dfrac{k_r}{k_f}$.

Table 32: Fraction of hybridized probes at equilibrium

		Target concentration $[T]_0$ in pM			
		1	**10**	**100**	**1000**
k_r / k_f in mol/L	**10^{-9}**	0.5	0.91	0.99	0.999
	10^{-8}	0.1	0.5	0.91	0.99
	10^{-7}	0.01	0.1	0.5	0.91
	10^{-6}	0.001	0.01	0.1	0.5
	10^{-5}	0.0001	0.001	0.01	0.1

The fraction of hybridized probes $\dfrac{[H]_{eq}}{[P]_{max}}$ at equilibrium is given in function of $[T]_0$ and $\dfrac{k_r}{k_f}$.

First, the case of a low fraction of hybridized probes was studied. In order to check and illustrate this trend, the influence of non specific kinetics was studied with the following parameters: $k_f = 10^2$ L·mol^{-1}·s^{-1}, $k_{r1} = 10^{-3}$ s^{-1}, $k_{r2} = 10^{-2}$ s^{-1}, $[T_1]_0 = 1000$ pM, $[T_2]_0 = 1000$ pM, $[P]_{max} = 10^{-9}$ moles·m^{-2}, and a diffusion coefficient $D = 10^{-11}$ m^2·s^{-1}. This leads to $[H_1]_{eq,\sin gle} = 9.09 \cdot 10^{-11}$ moles·m^{-2} and $[H_2]_{eq,\sin gle}$ $9.90 \cdot 10^{-12}$ moles·m^{-2}, which are much lower than $[P]_{max}$. Simulations were performed using the geometry and methodology described in section 3.2. The result is plotted on figure 14.

We can compare hybridization in absence of "competition" (solid lines) and hybridization when specific and non specific targets are present (dashed lines). We can see that the difference is extremely small; the curves are almost identical, which means that the kinetics and the equilibrium are almost not affected by the non specific hybridization. It agrees with the trend we expected: the competition does not really occur if a small fraction of the probes is hybridized.

Figure 14: Influence of non specific hybridization
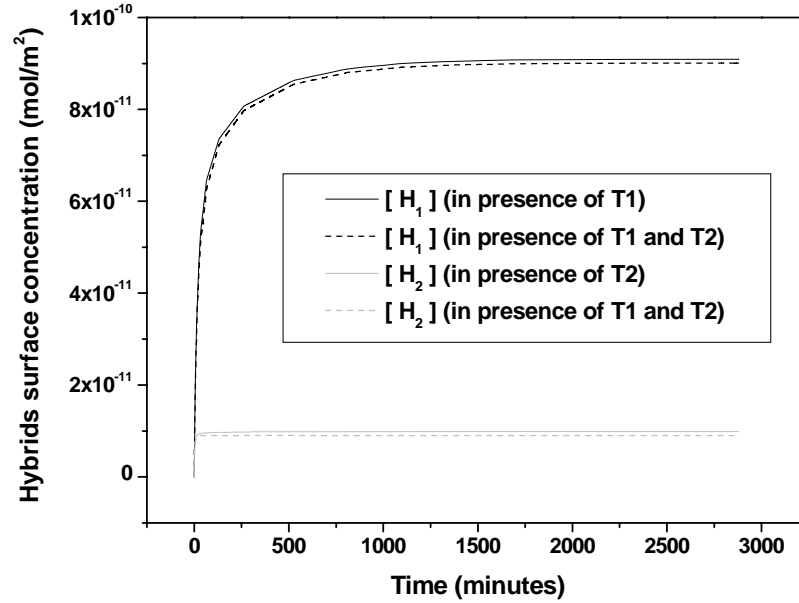
Parameters used: $k_f = 10^2$ L·mol^{-1}·s^{-1}, $k_{r1} = 10^{-3}$ s^{-1}, $k_{r2} = 10^{-2}$ s^{-1}, $[T_1]_0 = 1000$ pM, $[T_2]_0 = 1000$ pM, $[P]_{max} = 10^{-9}$ moles·m^{-2}, and a diffusion coefficient $D = 10^{-11}$ m^2·s^{-1}. Specific hybridization of target T1 is not affected by non specific hybridization of targets T2.

On the contrary, if $[H_1]_{eq,\sin gle}$ and $[H_2]_{eq,\sin gle}$ are high, we can expect a "competition"

between T_1 and T_2. Indeed, let us consider a case where $\dfrac{[H_1]_{eq,\sin gle}}{[P]_{max}} = 0.9$ and

$\dfrac{[H_2]_{eq,\sin gle}}{[P]_{max}} = 0.9$. Obviously, when specific hybridization and non specific hybridization

occur at the same time, the actual $\dfrac{[H_1]_{eq,both}}{[P]_{max}}$ and $\dfrac{[H_2]_{eq,both}}{[P]_{max}}$ will be lower than 0.9,

which means that the equilibrium is strongly modified. Such cases are studied in the next sections.

3.4.2 Kinetic differentiation

It can be anticipated that non specific hybridization reaches equilibrium faster than specific hybridization by looking at the characteristic time constant τ. In the ideal case, the expression of the fraction of hybridized probes as a function of time is:

$$[H] = \frac{[T]_0 [P]_{max}}{[T]_0 + \dfrac{k_r}{k_f}} \left[1 - \exp\left(-\frac{t}{\tau}\right) \right]$$

Where $\tau = \dfrac{1}{k_f [T]_0 + k_r}$

Non specific hybridization presents a higher reverse rate constant k_{r2} than specific hybridization with k_{r1}. In addition, as noticed by Dai et al.[29], if the concentration of mismatched target $[T_2]_0$ is higher than the concentration $[T_1]_0$ (no literature is available on that subject, but this case seems likely to arise), the time constant τ_2 for non specific hybridization will be lower than the time constant for specific hybridization τ_1. It means that equilibrium will be reached faster for non specific hybridization, and could therefore affect the kinetics of specific hybridization in a first phase of the overall hybridization process. Dai et al.[29] concluded that enough time should be given during the hybridization step, in order for specific hybridization to reach equilibrium, since it happens after non specific hybridization reaches equilibrium.

To verify this, we simulated several where the fraction of hybridized probes was not low, in order to observe the competition between specific and non specific target. The parameters used and the hybridization curves obtained are represented on figures 15 to 17. On each figure, a different combination of k_f, k_{r1}, k_{r2}, $\left[T_1\right]_0$ and $\left[T_2\right]_0$ is used and detailed in the text below. In these three cases, the competition between specific and non specific hybridization is clearly seen. The concentration of non specific hybrids as a function of time does not increase monotonically as it would if non specific hybridization was the only reaction occurring. Instead, in a first phase, the concentration of non specific hybrids increases quickly and reaches a maximum. In the case illustrated in figure 15, the concentration of non specific hybrids is even higher than the concentration of specific hybrids during this first phase. In a second phase, non specific hybrids are gradually replaced by specific hybrids until equilibrium is reached. This behavior was already studied by Dai et al.[29] who concluded that increasing the hybridization time will increase the hybridization specificity.

Figure 15: Influence of non specific hybridization
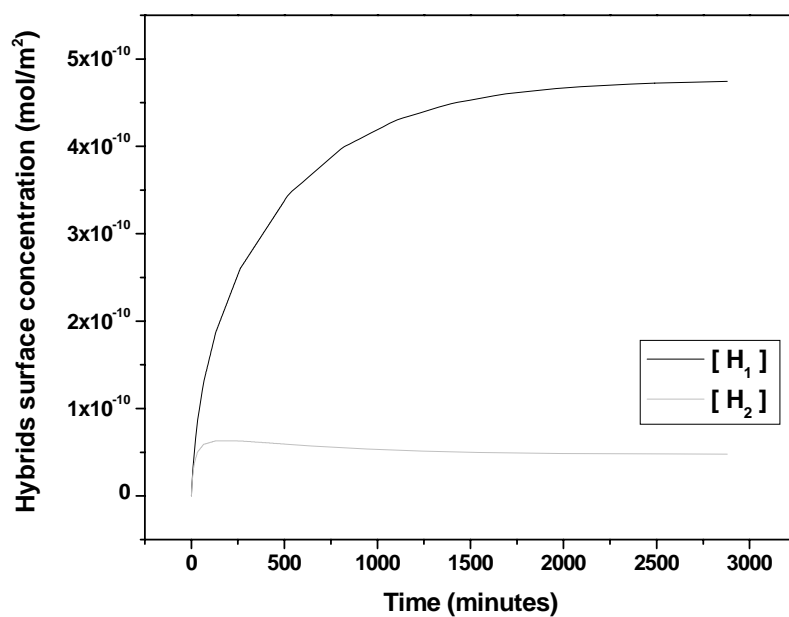
Parameters used: $k_f = 10^2$ L·mol^{-1}·s^{-1}, $k_{r1} = 10^{-4}$ s^{-1}, $k_{r2} = 10^{-3}$ s^{-1}, $[T_1]_0 = 1000$ pM, $[T_2]_0 = 1000$ pM, $[P]_{max} = 10^{-9}$ moles·m^{-2}, and a diffusion coefficient $D = 10^{-11}$ m^2·s^{-1}. Both targets T_1 and T_2 are present simultaneously in the medium.

Figure 16: Influence of non specific hybridization
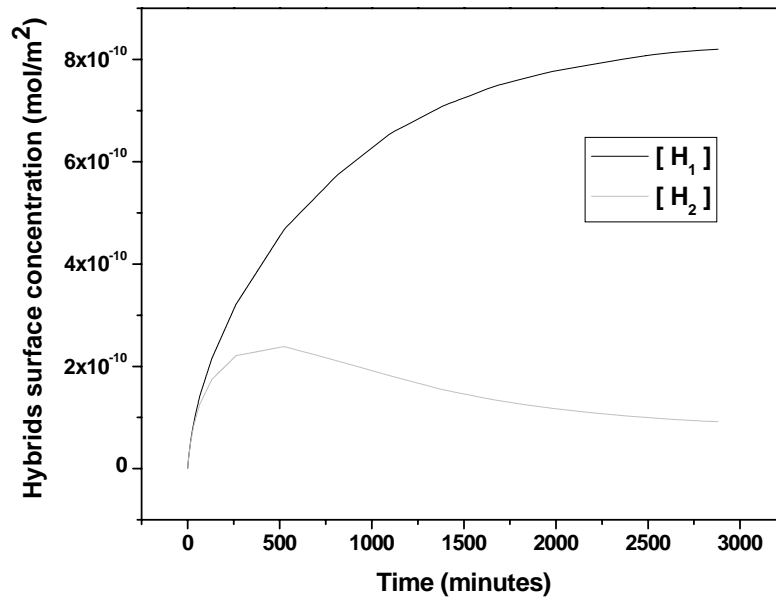
Parameters used: $k_f = 10^2$ L·mol^{-1}·s^{-1}, $k_{r1} = 10^{-5}$ s^{-1}, $k_{r2} = 10^{-4}$ s^{-1}, $[T_1]_0 = 1000$ pM, $[T_2]_0 = 1000$ pM, $[P]_{max} = 10^{-9}$ moles·m^{-2}, and a diffusion coefficient $D = 10^{-11}$ m^2·s^{-1}. Both targets T_1 and T_2 are present simultaneously in the medium.

Figure 17: Influence of non specific hybridization
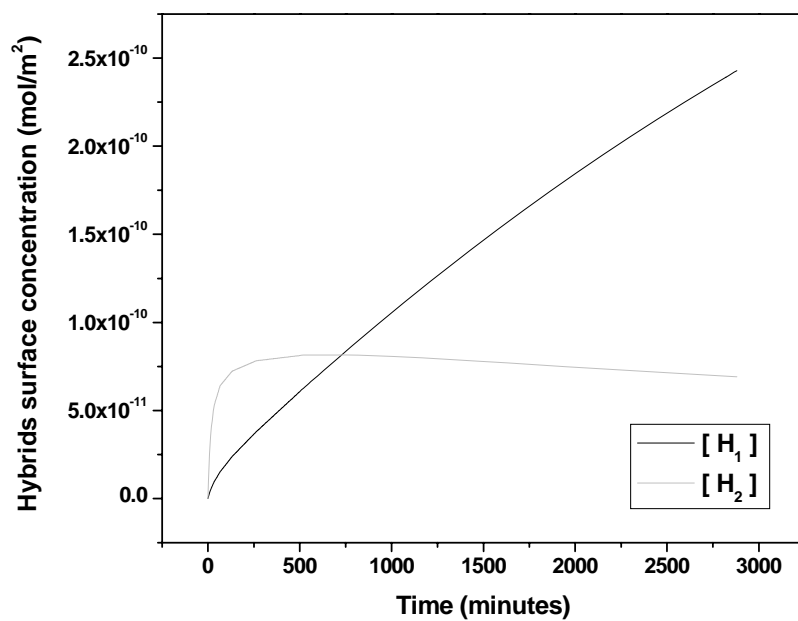
Parameters used: $k_f = 10^2$ L·mol^{-1}·s^{-1}, $k_{r1} = 10^{-5}$ s^{-1}, $k_{r2} = 10^{-3}$ s^{-1}, $[T_1]_0 = 100$ pM, $[T_2]_0 = 1000$ pM, $[P]_{max} = 10^{-9}$ moles·m^{-2}, and a diffusion coefficient $D = 10^{-11}$ m^2·s^{-1}. Both targets T_1 and T_2 are present simultaneously in the medium.

3.4.3 Influence of convection

In this section, the interaction between specific and non specific hybridization is studied in presence of convective transport. The conditions used in figures 15 to 17 were repeated, with an additional DNA velocity of 10 $\mu m \cdot s^{-1}$. Results obtained with and without convection are plotted in figures 18 to 20.

DNA hybridization being diffusion limited in the cases illustrated in figures 18 to 20, it is not surprising to see that the kinetics of specific and non specific hybridization are both enhanced. The non specific hybridization still presents two phases: an initial increase followed by a decrease as equilibrium is reached. When convection is added, the first phase is shorter and the maximum value reached by the concentration of non specific hybrids is slightly higher. However, overall, adding convection is beneficial. Clearly, equilibrium is reached faster, and the ratio between specific and non specific hybrids is better throughout the process before equilibrium is obtained (figures 21 to 23).

Figure 18: Influence of non specific hybridization and convection
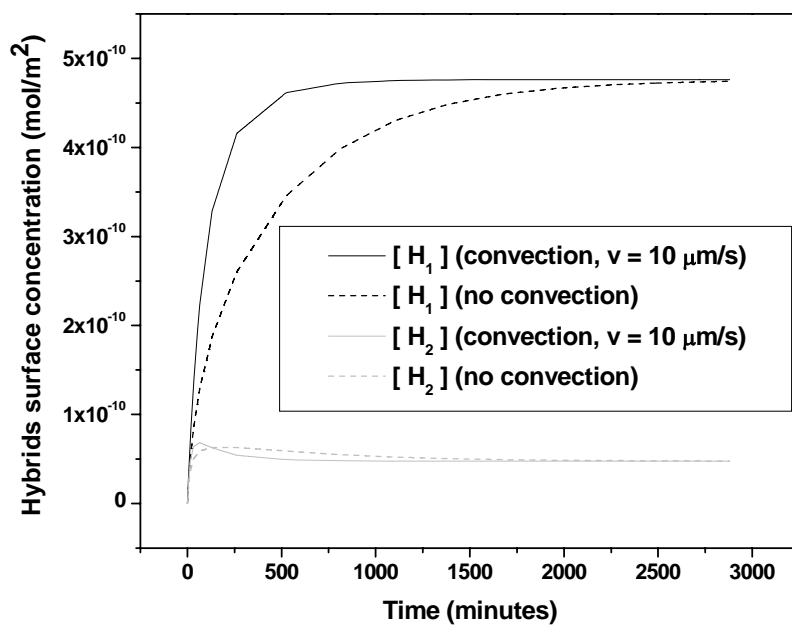
Parameters used: $k_f = 10^2$ L·mol^{-1}·s^{-1}, $k_{r1} = 10^{-4}$ s^{-1}, $k_{r2} = 10^{-3}$ s^{-1}, $\left[T_1\right]_0 = 1000$ pM, $\left[T_2\right]_0 = 1000$ pM, $\left[P\right]_{max} = 10^{-9}$ moles·m^{-2}, and a diffusion coefficient $D = 10^{-11}$ m^2·s^{-1}.

Figure 19: Influence of non specific hybridization and convection
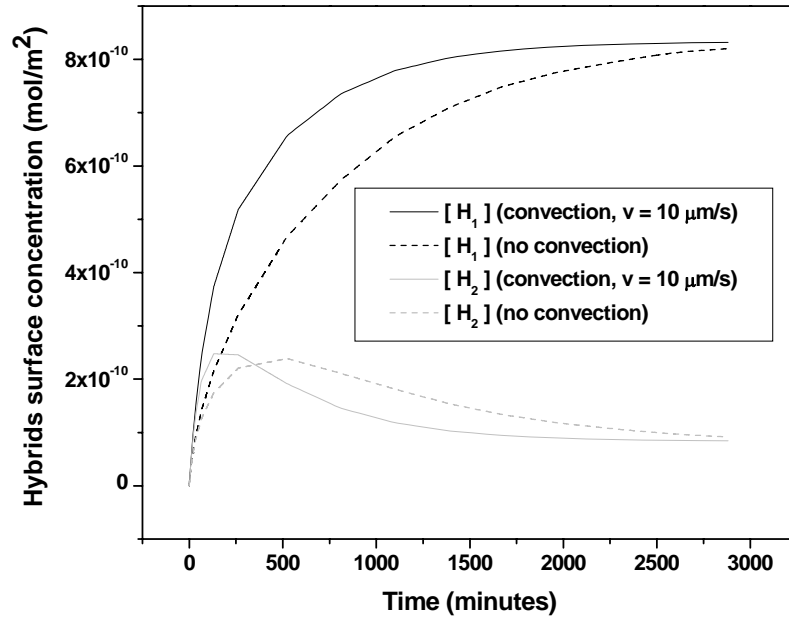
Parameters used: $k_f = 10^2$ L·mol^{-1}·s^{-1}, $k_{r1} = 10^{-5}$ s^{-1}, $k_{r2} = 10^{-4}$ s^{-1}, $[T_1]_0 = 1000$ pM, $[T_2]_0 = 1000$ pM, $[P]_{max} = 10^{-9}$ moles·m^{-2}, and a diffusion coefficient $D = 10^{-11}$ m^2·s^{-1}.

Figure 20: Influence of non specific hybridization and convection
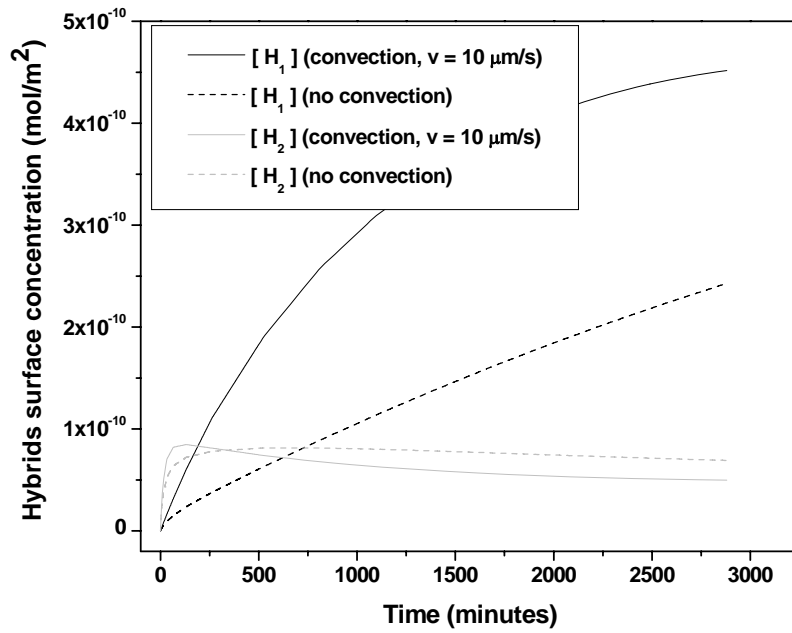
Parameters used: $k_f = 10^2$ L·mol^{-1}·s^{-1}, $k_{r1} = 10^{-5}$ s^{-1}, $k_{r2} = 10^{-3}$ s^{-1}, $\left[T_1\right]_0 = 100$ pM, $\left[T_2\right]_0 = 1000$ pM, $\left[P\right]_{max} = 10^{-9}$ moles·m^{-2}, and a diffusion coefficient $D = 10^{-11}$ m^2·s^{-1}.

Figure 21: Influence of non specific hybridization and convection - ratio specific / non specific hybrids
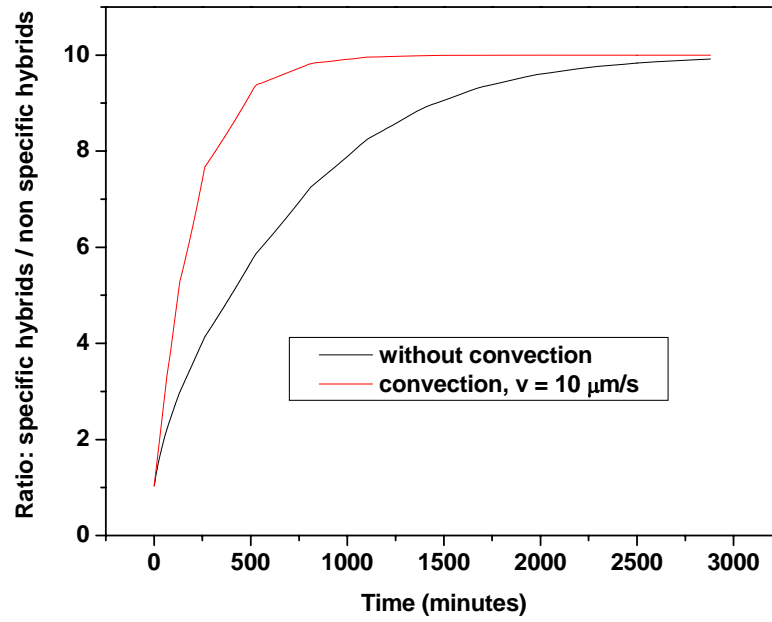
Parameters used (same as figure 14): $k_f = 10^2$ L·mol^{-1}·s^{-1}, $k_{r1} = 10^{-4}$ s^{-1}, $k_{r2} = 10^{-3}$ s^{-1}, $[T_1]_0 = 1000$ pM, $[T_2]_0 = 1000$ pM, $[P]_{max} = 10^{-9}$ moles·m^{-2}, and a diffusion coefficient $D = 10^{-11}$ m^2·s^{-1}.

Figure 22: Influence of non specific hybridization and convection - ratio specific / non specific hybrids
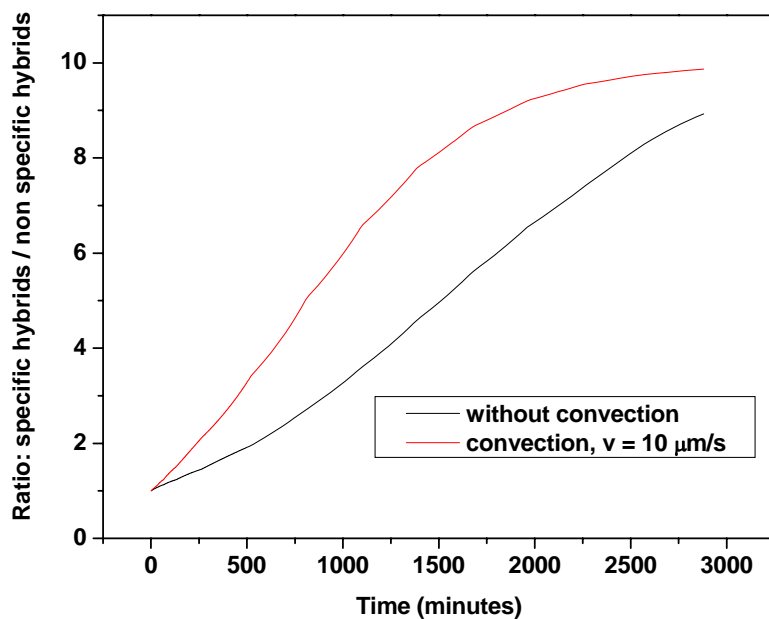
Parameters used (same as figure 15): $k_f = 10^2$ L·mol^{-1}·s^{-1}, $k_{r1} = 10^{-5}$ s^{-1}, $k_{r2} = 10^{-4}$ s^{-1}, $\left[T_1\right]_0 = 1000$ pM, $\left[T_2\right]_0 = 1000$ pM, $\left[P\right]_{max} = 10^{-9}$ moles·m^{-2}, and a diffusion coefficient $D = 10^{-11}$ m^2·s^{-1}.

Figure 23: Influence of non specific hybridization and convection - ratio specific / non specific hybrids
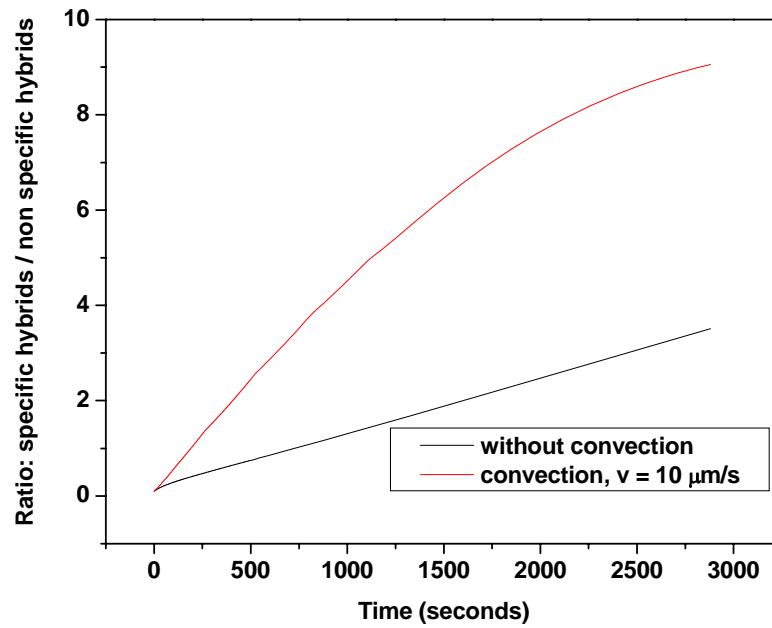
Parameters used (same as figure 16): $k_f = 10^2$ L·mol⁻¹·s⁻¹, $k_{r1} = 10^{-5}$ s⁻¹, $k_{r2} = 10^{-3}$ s⁻¹, $[T_1]_0 = 100$ pM, $[T_2]_0 = 1000$ pM, $[P]_{max} = 10^{-9}$ moles·m⁻², and a diffusion coefficient $D = 10^{-11}$ m²·s⁻¹.

Chapter 4. Actuation by superposition of a DC and an AC field

4.1 Theoretical background: harmonic AC electrical fields

This section introduces the basics about harmonic AC (alternating current) electrical fields (section 4.1.1) and the tools used to describe them (section 4.1.2). It is necessary to know and understand these tools to derive forces induced by harmonic AC fields (section 4.1.3).

4.1.1 Observation of harmonic AC electrical fields

Case 1: AC harmonic field with constant phase

First, let us consider the simplest case. Two electrodes are placed in a microchamber (figure 24). All the walls of the chamber are electrically insulated except the electrodes B1 and B2, where an AC potential is applied as summarized in table 33.

Figure 24: Case 1 – Chamber geometry
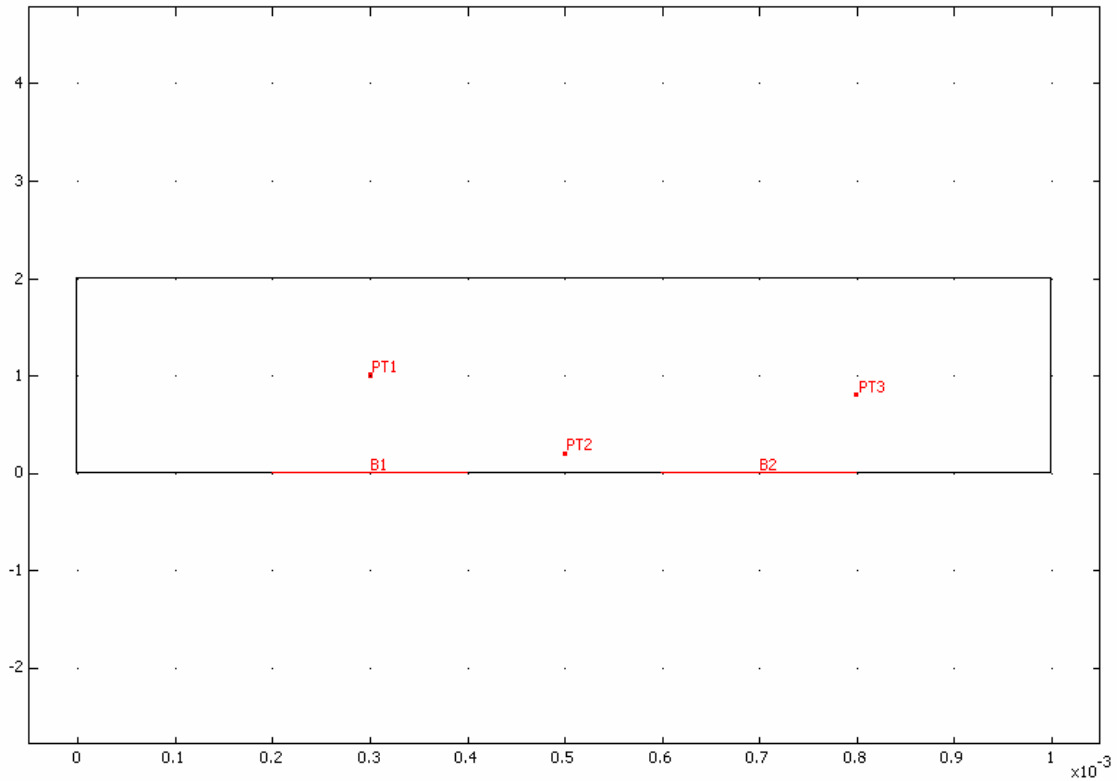
Geometry of the chamber simulated in case 1: two electrodes (B1 and B2) are placed at the bottom of the chamber. Chamber dimensions: length = 1 mm, height = 200 μm.

Table 33: Potential applied to the electrodes

Electrode	Phase	Potential
B1	0°	$V_0 \cos(\omega t)$
B2	180°	$V_0 \cos(\omega t + \pi)$

An AC electrical field is induced in the chamber. The period of the oscillations was chosen to be 1 second, and the amplitude V_0 was set to 10 V. The field varies with the position in space, and in addition, it varies with time. This can be seen by plotting the horizontal component of the electrical field as a function of time for different points in

the chamber. Three different points (see their location on figure 24) were considered (figure 25).

Figure 25: Case 1 - Electrical field (x-component) at different points
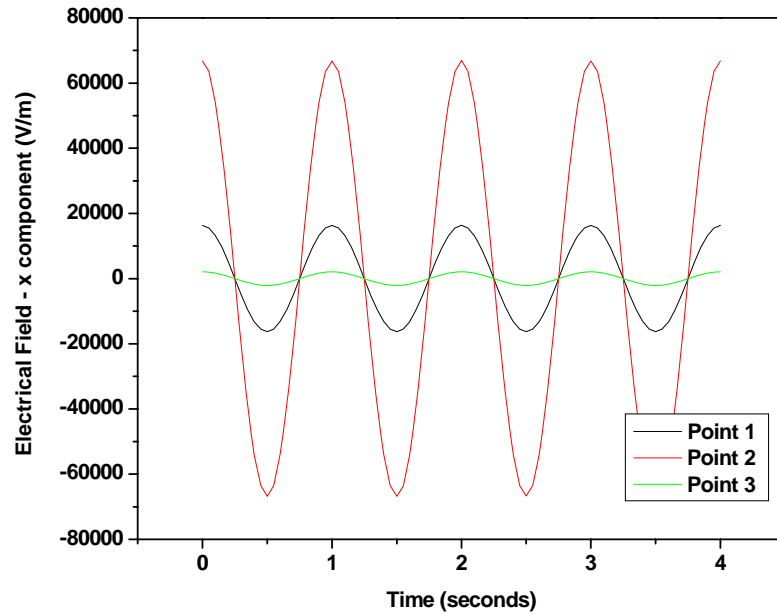
We can see that at every point in the chamber, the field presents sinusoidal oscillations around zero with the same frequency (equal to the frequency of the applied voltage): this is a harmonic field. At all points, the electrical field reaches its maximum and minimum at the same times: the phase is the same everywhere in the chamber. The same observations can be made with the vertical component of the electrical field (figure 26).

Figure 26: Case 1 - Electrical field (y-component) at different points
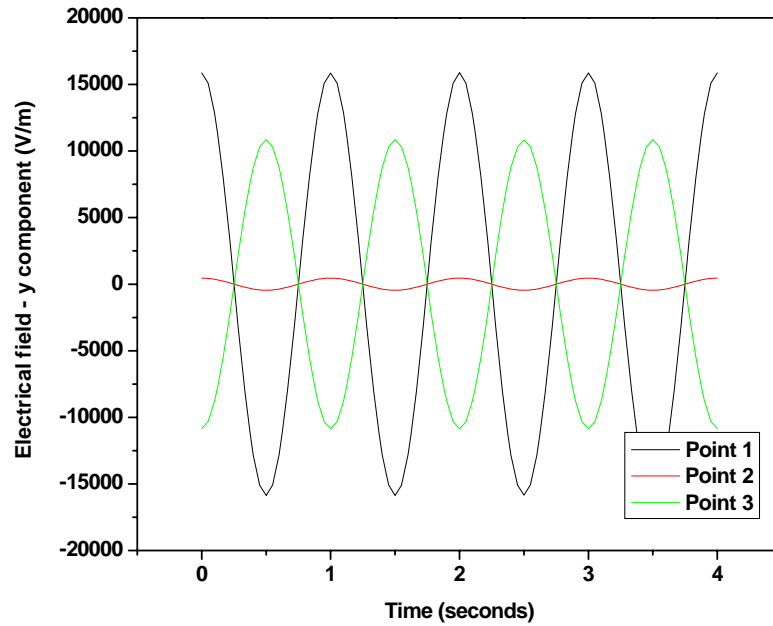
Case 2: AC harmonic field with space dependent phase

In this case, four electrodes are placed in the chamber (figure 27). Each one has a different phase, as shown in table 34.

Figure 27: Case 2 – Chamber geometry
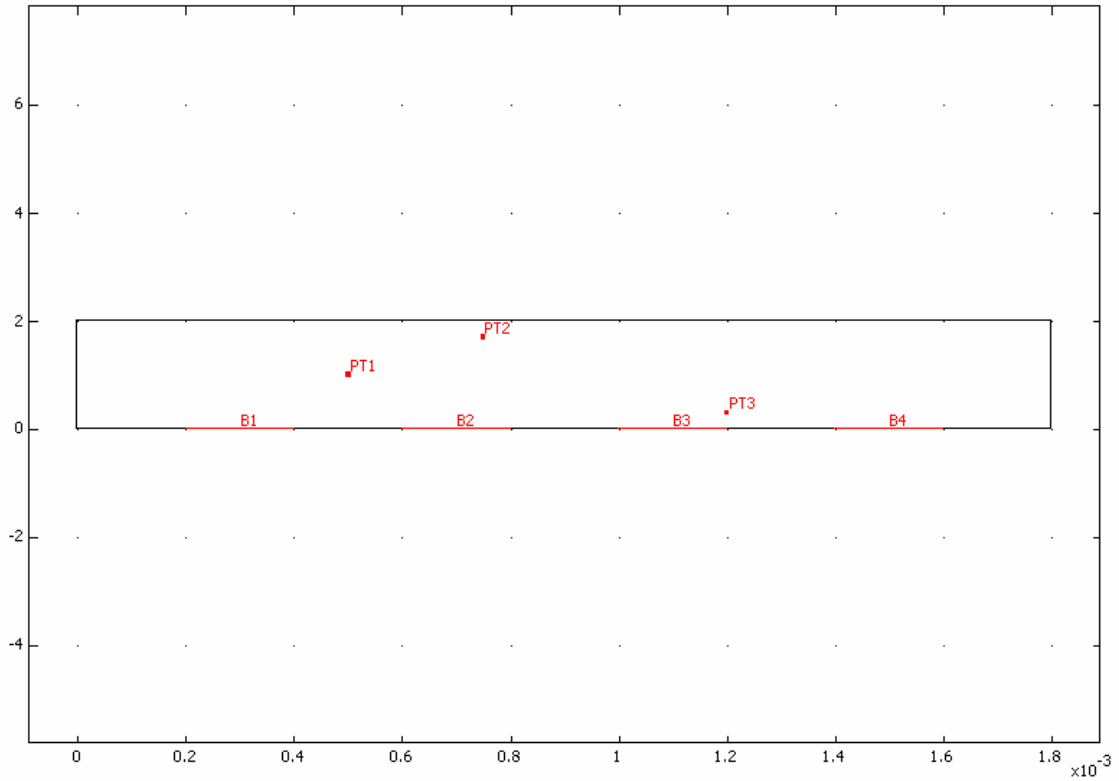
Geometry of the chamber simulated in case 2: four electrodes (B1 to B4) are placed at the bottom of the chamber. Chamber dimensions: length = 1 mm, height = 200 μm.

Table 34: Potential applied to the electrodes

Electrode	Phase	Potential
B1	0°	$V_0 \cos (\omega t)$
B2	90°	$V_0 \cos (\omega t + \pi/2)$
B3	180°	$V_0 \cos (\omega t+ \pi)$
B4	270°	$V_0 \cos (\omega t + 3\pi/2)$

Like in the previous case, the field varies with the position in space and time. In addition, we can see in figures 28 and 29 that the phase is not the same at different positions in the chamber.

Figure 28: Case 2 - Electrical field (x-component) at different points
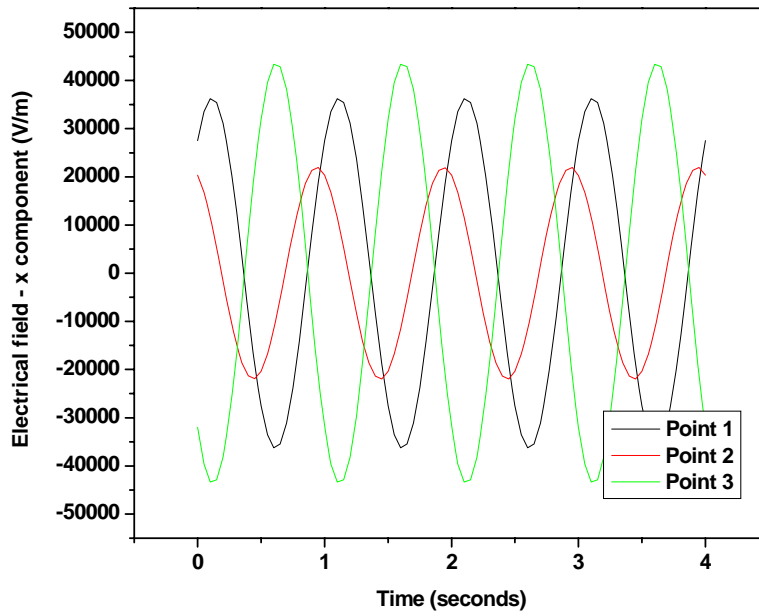
Figure 29: Case 2 - Electrical field (y-component) at different points
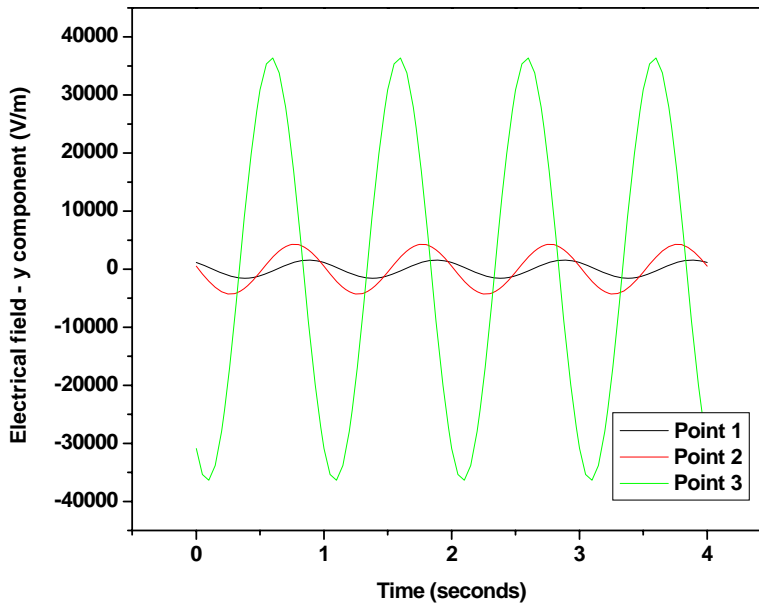
Conclusion

In the general case, if oscillating harmonic potentials are applied in a chamber, the resulting electrical field can be written:

$$\vec{E}(t,x,y) = E_{0,X}(x,y)\cos(\omega t + \varphi_X(x,y))\vec{u}_X + E_{0,Y}(x,y)\cos(\omega t + \varphi_Y(x,y))\vec{u}_Y$$

E_X and E_Y are the scalar amplitude of the electrical field in the x and y directions respectively. They are functions of the coordinates in space x and y. The pulsation of the oscillation ω is the same in all directions. The phase φ_X and φ_Y in each direction is a function of the coordinates in space x and y. The unit vectors in the x and y directions are $\vec{u}_X$ and $\vec{u}_Y$.

4.1.2 Phasor notation

The phasor notation is commonly used to describe AC phenomena. We have seen in the previous section that the electrical field could be written:

$$\vec{E}(t,x,y) = E_X(t,x,y)\vec{u}_X + E_Y(t,x,y)\vec{u}_Y$$

$$\vec{E}(t,x,y) = E_{0,X}(x,y)\cos(\omega t + \varphi_X(x,y))\vec{u}_X + E_{0,Y}(x,y)\cos(\omega t + \varphi_Y(x,y))\vec{u}_Y$$

It can be rewritten as:

$$\vec{E}(t,x,y) = \text{Re}\{\tilde{E}(x,y)e^{j\omega t}\} = \frac{1}{2}\text{Re}\{\tilde{E}(x,y)e^{j\omega t} + \tilde{E}^*(x,y)e^{-j\omega t}\}$$

Where j is the imaginary unit ($j^2 = -1$) and the asterisk * indicates the complex conjugate. $\tilde{E}(x, y)$ is the phasor electric field:

$$\tilde{E}(x, y) = E_{0,X}(x, y)e^{j\varphi_X(x,y)}\vec{u}_X + E_{0,Y}(x, y)e^{j\varphi_Y(x,y)}\vec{u}_Y$$

$\tilde{E}(x, y)$ is a complex whose amplitude and phase are the amplitude and initial phase of the electrical field. In other words, the phasor contains all the information about the field at different positions (amplitude, phase). The instantaneous complex electrical field $\underline{\vec{E}}(t, x, y)$ is obtained by multiplying the phasor $\tilde{E}(x, y)$ by the time-dependence factor $e^{j\omega t}$:

$$\underline{\vec{E}}(t, x, y) = \tilde{E}(x, y)e^{j\omega t}$$

The instantaneous electrical field $\vec{E}(t, x, y)$ is the real part of the complex electrical field:

$$\vec{E}(t, x, y) = \text{Re}\{\underline{\vec{E}}(t, x, y)\} = \text{Re}\{\tilde{E}(x, y)e^{j\omega t}\}$$

4.1.3 The dielectrophoretic force derived

The DEP force arises on polarizable particles in a non uniform electric field (direct current DC or alternating current AC). When placed in an electrical field, a polarizable particle acquires a dipole moment $\vec{p}$. In a DC field, the resulting force on the particle is:

$$\vec{F}_{DEP} = (\vec{p} \cdot \nabla)\vec{E}$$

This is a very well known basic result, therefore I am not going to derive here. Although it is also a well known result, it is more interesting to derive the expression of the force in

123

an AC field. Indeed, the detailed derivation is not given in the literature, and it is a good exercise before trying to derive more complex things with the same tools.

If a harmonic electrical potential is applied to the system (like the two cases studied in section 4.1.1), the electrical field $\vec{E}$ will present harmonic oscillations and can be described by a phasor:

$$\vec{E}(t,x,y) = \mathrm{Re}\left[\widetilde{E}(x,y)e^{j\omega t}\right]$$

In a DC field, the dipole moment of a spherical particle is proportional to the electrical field: $\vec{p} = \upsilon\alpha\vec{E}$, where υ is the volume of the particle and α the polarisability of the particle. In an AC field, there is a similar relation between the complex dipole moment , $\underline{\vec{p}}$, the volume υ, the complex polarisability $\widetilde{\alpha}$ and the complex electrical field $\underline{\vec{E}}$:

$$\underline{\vec{p}} = \upsilon\widetilde{\alpha}\,\underline{\vec{E}}$$

The polarisability $\widetilde{\alpha}$ is a complex number (but not a phasor, the ~ is there to show it is not a real number) because in an AC field, $\vec{p}$ and $\vec{E}$ do no align instantaneously, some relaxation times are involved. The dipole moment can be expressed in terms of phasor:

$$\widetilde{p} = \upsilon\widetilde{\alpha}\,\widetilde{E}$$

So the instantaneous value of the dipole moment and the electrical field are:

$$\vec{p}(t,x,y) = p_X(t,x,y)\vec{u}_X + p_Y(t,x,y)\vec{u}_Y = \frac{1}{2}\left(\widetilde{p}\,e^{j\omega t} + \widetilde{p}^{*}e^{-j\omega t}\right)$$

$$\vec{E}(t,x,y) = E_X(t,x,y)\vec{u}_X + E_Y(t,x,y)\vec{u}_Y = \frac{1}{2}\left(\widetilde{E}\,e^{j\omega t} + \widetilde{E}^{*}e^{-j\omega t}\right)$$

In a DC field, the resulting force on the particle is: $\vec{F}_{DEP} = (\vec{p} \cdot \nabla)\vec{E}$. In a harmonic AC field, this force is going to vary with time with a frequency similar to the frequency of the electrical field, which is very high in the devices used in microfluidics (from kilohertz to megahertz). Thus, the time average value of the force is used by researchers. This is what we are going to calculate here. Since we are dealing with vectors, we can examine the x component only, the others will be analogous:

$$F_{DEP,X} = p_X \frac{\partial E_X}{\partial x} + p_Y \frac{\partial E_X}{\partial y}$$

Let us expand the two terms $p_X \dfrac{\partial E_X}{\partial x}$ and $p_Y \dfrac{\partial E_X}{\partial y}$:

$$p_X \frac{\partial E_X}{\partial x} = \frac{1}{2}\left(\tilde{p}_X\ e^{j\omega t} + \tilde{p}_X^* e^{-j\omega t}\right)\frac{1}{2}\frac{\partial\left(\tilde{E}_X\ e^{j\omega t} + \tilde{E}_X^* e^{-j\omega t}\right)}{\partial x}$$

$$p_Y \frac{\partial E_X}{\partial y} = \frac{1}{2}\left(\tilde{p}_Y\ e^{j\omega t} + \tilde{p}_Y^* e^{-j\omega t}\right)\frac{1}{2}\frac{\partial\left(\tilde{E}_X\ e^{j\omega t} + \tilde{E}_X^* e^{-j\omega t}\right)}{\partial y}$$

Where $\tilde{E}_X$, $\tilde{E}_Y$, $\tilde{p}_X$ and $\tilde{p}_Y$ are the scalar components of the corresponding phasors:

$$\tilde{E}(x, y) = \tilde{E}_X(x, y)\vec{u}_X + \tilde{E}_Y(x, y)\vec{u}_Y$$

$$\tilde{p}(x, y) = \tilde{p}(x, y)\vec{u}_X + \tilde{p}(x, y)\vec{u}_Y$$

After expansion and simplification we obtain (details are given in appendix):

$$p_X \frac{\partial E_X}{\partial x} = \frac{1}{4}\left[\tilde{p}_X\ e^{j2\omega t}\frac{\partial \tilde{E}_X}{\partial x} + \tilde{p}_X\frac{\partial \tilde{E}_X^*}{\partial x} + \tilde{p}_X^*\frac{\partial \tilde{E}_X}{\partial x} + \tilde{p}_X^* e^{-j2\omega t}\frac{\partial \tilde{E}_X^*}{\partial x}\right]$$

$$p_Y \frac{\partial E_X}{\partial y} = \frac{1}{4}\left[\tilde{p}_Y\ e^{j2\omega t}\frac{\partial \tilde{E}_X}{\partial y} + \tilde{p}_Y\frac{\partial \tilde{E}_X^*}{\partial y} + \tilde{p}_Y^*\frac{\partial \tilde{E}_X}{\partial y} + \tilde{p}_X^* e^{-j2\omega t}\frac{\partial \tilde{E}_X^*}{\partial y}\right]$$

The whole point is to take the time average value of these expressions. It can be shown (details are given in appendix) that:

- the terms $\tilde{p}_X \ e^{j2\omega t} \dfrac{\partial \tilde{E}_X}{\partial x}$, $\tilde{p}_X^* e^{-j2\omega t} \dfrac{\partial \tilde{E}_X^*}{\partial x}$, $\tilde{p}_Y \ e^{j2\omega t} \dfrac{\partial \tilde{E}_X}{\partial y}$, and $\tilde{p}_Y \ e^{j2\omega t} \dfrac{\partial \tilde{E}_X}{\partial y}$ have a time average value equal to zero.

- the terms $\tilde{p}_X \dfrac{\partial \tilde{E}_X^*}{\partial x}$ and $\tilde{p}_X^* \dfrac{\partial \tilde{E}_X}{\partial x}$ are complex conjugate.

- the terms $\tilde{p}_Y \dfrac{\partial \tilde{E}_X^*}{\partial y}$ and $\tilde{p}_Y^* \dfrac{\partial \tilde{E}_X}{\partial y}$ are complex conjugate

Therefore, simplifications can be made and the time average values of $p_X \dfrac{\partial E_X}{\partial x}$ and

$p_Y \dfrac{\partial E_X}{\partial x}$ can be obtained:

$$\left\langle p_X \frac{\partial E_X}{\partial x} \right\rangle = \frac{1}{2} \, \mathrm{Re} \left[\tilde{p}_X \frac{\partial \tilde{E}_X^*}{\partial x} \right]$$

$$\left\langle p_Y \frac{\partial E_X}{\partial x} \right\rangle = \frac{1}{2} \, \mathrm{Re} \left[\tilde{p}_Y \frac{\partial \tilde{E}_X^*}{\partial y} \right]$$

Finally, the time average value of the dielectrophoretic force is:

$$\left\langle F_{DEP,X} \right\rangle = \frac{1}{2} \, \mathrm{Re} \left[\tilde{p}_X \frac{\partial \tilde{E}_X^*}{\partial x} + \tilde{p}_Y \frac{\partial \tilde{E}_X^*}{\partial y} \right]$$

This is for the x component, but we can generalize:

$$\boxed{\left\langle F_{DEP} \right\rangle = \frac{1}{2} \, \mathrm{Re} \left[\left(\tilde{p} \cdot \nabla \right) \tilde{E}^* \right]}$$

This is the expression given in the reference textbook by Morgan and Green[43].

4.2 Combination of a harmonic AC field with a DC field

In this section, one example of AC + DC field is studied. However, a more thorough study should be done to draw more general and accurate conclusions.

4.2.1 Observation of the AC + DC field

A microfluidic chamber with two AC electrodes and two DC electrodes (see figure 30) is studied. The potential applied to each electrode is summarized in table 35. The value of the x component of the electrical field at different points is plotted as a function of time in figure 31.

Figure 30: AC + DC – Chamber geometry
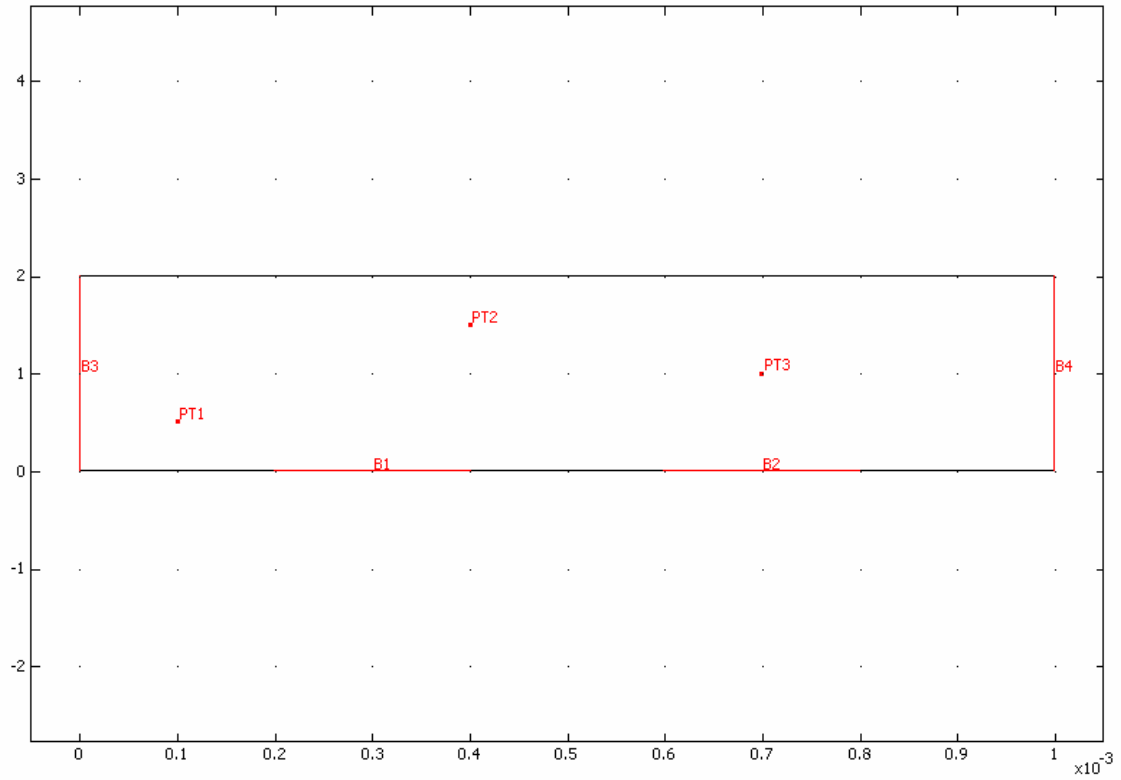
Geometry of the chamber: four electrodes (B1 to B4) are placed in the chamber. Chamber dimensions:

length = 1 mm, height = 200 μm.

Table 35: Potential applied to the electrodes

Electrode	Phase	Potential
B1	0°	$20 \cos(\omega t)$
B2	180°	$20 \cos(\omega t + \pi)$
B3	-	100 V
B4	-	200 V

The pulsation ω is chosen such that the period of the oscillations is 1 second.

Figure 31: AC + DC – x component of the electrical field at different points
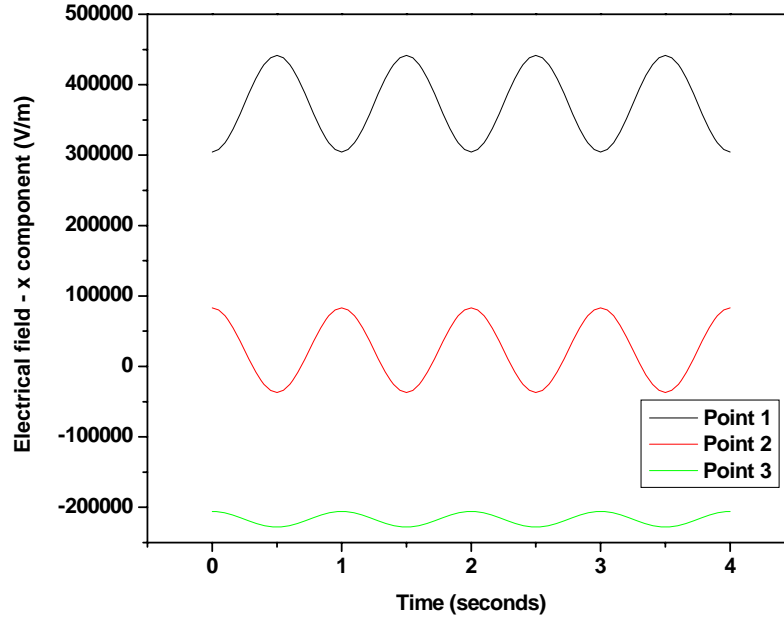
This example suggests that when a harmonic potential is applied to the chamber with an additional DC component, the resulting electrical field takes the form:

$$\vec{E}(t,x,y) = \vec{E}_M(x,y) + E_{0,X}\cos(\omega t + \varphi_X(x,y))\vec{u}_X + E_{0,Y}\cos(\omega t + \varphi_Y(x,y))\vec{u}_Y$$

$$\vec{E}(t,x,y) = \vec{E}_M(x,y) + \vec{E}_{osc}(x,y,t)$$

Where $\vec{E}_M(x,y)$ is a DC electrical field and $\vec{E}_{osc}(x,y,t)$ is an AC harmonic field.

Naturally, we wonder if we can intuitively predict $\vec{E}_M$ and $\vec{E}_{osc}$. For example, one could imagine that $\vec{E}_M$ could be equal to the electrical field that would be obtained if electrodes B3 and B4 were the only ones with an electrical potential (B1 and B2 would be insulated). Following the same logic, one could imagine that $\vec{E}_{osc}$ could be the field obtained when electrodes B1 and B2 are the only ones with an electrical potential. If B3

and B4 were switched on while B3 and B4 were switched off, the electrical field would

obviously be uniform, horizontal, with a value $E_{DC} = \dfrac{\Delta V}{length} = 10,000\ V/m$ in our case.

So we could expect the field to oscillate around 10,000 V at every point of the chamber,

with an amplitude that would depend on the position in the chamber. This is not what we

observe on figure 31, where $\vec{E}_M$ seems to be different at every point. We can look at the

field that would be obtained when B1 and B2 are on while B3 and B4 are off. We obtain

a harmonic field E_{AC} that oscillates with an amplitude that depends on the position, as

plotted on figure 32. If for each point (points 1, 2, and 3) we compare the amplitude of

the oscillations of the AC + DC field (figure 31) and to the amplitudes of the AC field

when the DC field is switched off (figure 32), we see that they are very different. This

results is not so surprising. The superposition principle allows to add the electrical

potential, but not the electrical fields, this is why we can not intuitively predict $\vec{E}_M$ and

$\vec{E}_{osc}$.

Figure 32: AC + DC – x component of the electrical field when the DC field is turned off
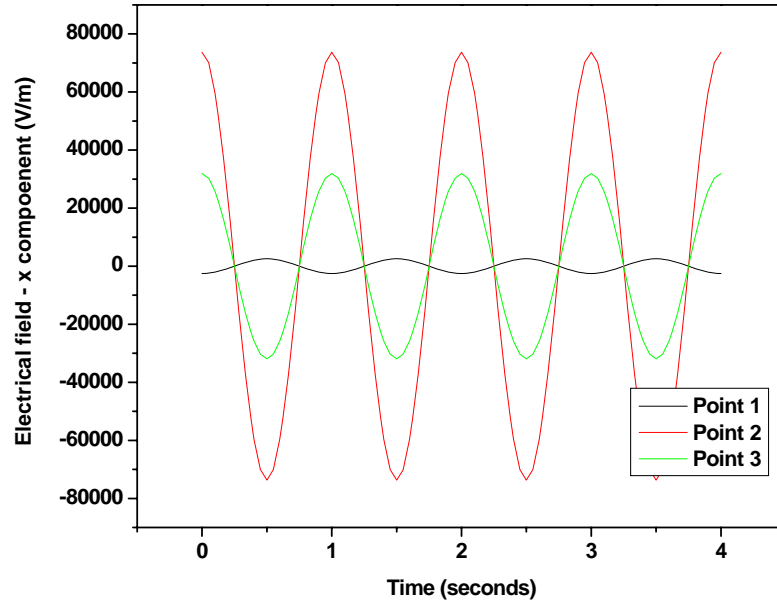
4.2.2 Derivation of the dielectrophoretic force in an AC + DC field

The derivation is similar to the one described in section 4.1.3. The instantaneous dielectrophoretic force is still $\vec{F}_{DEP} = \mathrm{Re}\left[\left(\underline{\vec{p}} \cdot \nabla\right)\underline{\vec{E}}\right]$, but in this section $\vec{p}$ and $\vec{E}$ will correspond to the observations made in section 4.2.1. So instead of having:

$$\vec{p}(t, x, y) = \frac{1}{2}\left(\tilde{p}\,e^{j\omega t} + \tilde{p}^{*}e^{-j\omega t}\right)$$

$$\vec{E}(t, x, y) = \frac{1}{2}\left(\tilde{E}\,e^{j\omega t} + \tilde{E}^{*}e^{-j\omega t}\right)$$

We will have:

$$\vec{p} = P_M + \frac{1}{2}\left(\tilde{p}\, e^{j\omega t} + \tilde{p}^*e^{-j\omega t}\right) \quad \text{(constant term + oscillating term)}$$

$$\vec{E} = \vec{E}_M + \frac{1}{2}\left(\tilde{E}\, e^{j\omega t} + \tilde{E}^*e^{-j\omega t}\right) \quad \text{(constant term + oscillating term)}$$

These two expressions can be plugged in the instantaneous force $\vec{F}_{DEP} = \left(\vec{p}\cdot\nabla\right)\vec{E}$. After expansion and simplifications, we obtain the time average value of the dielectrophoretic (all the derivations are in appendix):

$$\boxed{\left\langle F_{DEP}\right\rangle = \left(P_M\cdot\nabla\right)E_M + \frac{1}{2}\,\text{Re}\left[\left(\tilde{p}\ \cdot\nabla\right)\tilde{E}^*\right]}$$

The first term is equal to the dielectrophoretic force created by a constant E_M and the induced dipole moment P_M. The second term is equal to the dielectrophoretic force induced by a harmonic field equal to the oscillating part of the electrical field. To the best of our knowledge, this derivation and the calculation of the dielectrophoretic force in an AC + DC field have not been published in the literature. It would be interesting to compare the two terms $\left(P_M\cdot\nabla\right)E_M$ and $\frac{1}{2}\,\text{Re}\left[\left(\tilde{p}\ \cdot\nabla\right)\tilde{E}^*\right]$ and how they vary when the amplitude of the AC field or the DC potentials applied are changed. A priori, both would be affected by a change in the AC field, or by a change in the DC potential. This deserves a more exhaustive study.

4.2.4 Other expected effects

The dielectrophoretic force derived in section 4.2.2 arises on polarizable particles that can present an induced dipole moment. However, the AC + DC field can have more effects on the particle.

If the particle is charged (with a charge q for example), the Coulomb force ($q E_M$) will be exerted on the particle, leading to an additional electrophoretic force on the particle. It is not obvious that the electrophoretic force and the AC+DC dielectrophoretic force can be tuned independently: if the DC field is modified, the AC + DC field is also modified. This deserves a thorough study that could be done in a future work.

At lower frequencies of the AC field, AC electroosmosis and electrothermal could occur. AC electroosmosis in an AC + DC field is being studied by one research group[66].

At higher frequencies, AC electrothermal flow should occur. The analytical expression of the electrothermal flow in an AC+DC field has not been derived. The "driving force" of the electrothermal flow is the temperature gradients created by the field. Here again, a study should be done.

CONCLUSION

The general purpose of this thesis was to enhance the kinetics in DNA arrays. To achieve this goal, this problem was approached in a logical fashion.

First, in a preliminary study, we identified the parameters affecting the kinetics and determined that DNA is generally a diffusion limited process in the conditions seen in DNA arrays.

This encouraged us to investigate convection as a solution to overcome the diffusion limitation. The finite element method (with the software Comsol Multiphysics) was used to simulate the DNA transport coupled with the hybridization kinetics. It was found that even a small velocity (10 μm/s) allowed a significant enhancement of the hybridization rate. This result was expected as researchers are trying to enhance DNA hybridization experimentally by using convection. However, our work provides a sound study of the diffusion limitation and how it is overcome by convection, which was lacking in the literature. The beneficial effect of convection on the specificity of DNA hybridization was also demonstrated, which is a new result. Nevertheless, the authors remain aware of the limits of their simulation, since they can not take account of effects occurring at a molecular scale such as surface crowding.

In a last part of this work, inspired by the Nanogen approach (focusing of DNA on the sensing zones by application of a positive potential) we investigated the methods to act on particles. Indeed, the hybridization rate can be enhanced by improving the DNA

transport (convection previously studied) or by locally increasing the concentration of target DNA. AC and DC electrokinetics are well known means to act on particles, but the combination of an AC and a DC has almost not been studied. We derive the expression of the dielectrophoretic force in an AC+DC field, and discuss some possible implications. However, this part deserves a true thorough study that could be done in a future work.

APPENDICES

1. The dielectrophoretic force on a particle placed in a harmonic AC electrical field

In an AC harmonic field, the instantaneous value of the dipole moment and the electrical field are:

$$\vec{p}(t,x,y) = p_X(t,x,y)\,\vec{u}_X + p_Y(t,x,y)\,\vec{u}_Y = \frac{1}{2}\left(\tilde{p}\,e^{j\omega t} + \tilde{p}^*e^{-j\omega t}\right)$$

$$\vec{E}(t,x,y) = E_X(t,x,y)\,\vec{u}_X + E_Y(t,x,y)\,\vec{u}_Y = \frac{1}{2}\left(\tilde{E}\,e^{j\omega t} + \tilde{E}^*e^{-j\omega t}\right)$$

These two expressions can be plugged in the instantaneous force $\vec{F}_{DEP} = (\vec{p}\cdot\nabla)\vec{E}$:

$$F_{DEP,X} = p_X\frac{\partial E_X}{\partial x} + p_Y\frac{\partial E_X}{\partial y}$$

Let us separate the two terms $p_X\dfrac{\partial E_X}{\partial x}$ and $p_Y\dfrac{\partial E_X}{\partial y}$:

$$p_X\frac{\partial E_X}{\partial x} = \frac{1}{2}\left(\tilde{p}_X\,e^{j\omega t} + \tilde{p}_X^*e^{-j\omega t}\right)\frac{1}{2}\frac{\partial\left(\tilde{E}_X\,e^{j\omega t} + \tilde{E}_X^*e^{-j\omega t}\right)}{\partial x}$$

$$p_Y\frac{\partial E_X}{\partial y} = \frac{1}{2}\left(\tilde{p}_Y\,e^{j\omega t} + \tilde{p}_Y^*e^{-j\omega t}\right)\frac{1}{2}\frac{\partial\left(\tilde{E}_X\,e^{j\omega t} + \tilde{E}_X^*e^{-j\omega t}\right)}{\partial y}$$

Where $\tilde{E}_X$, $\tilde{E}_Y$, $\tilde{p}_X$ and $\tilde{p}_Y$ are the scalar components of the corresponding phasors:

$$\tilde{E}(x,y) = \tilde{E}_X(x,y)\vec{u}_X + \tilde{E}_Y(x,y)\vec{u}_Y = E_{0,X}\,e^{j\omega t+\varphi_X}\,\vec{u}_X + E_{0,Y}\,e^{j\omega t+\varphi_Y}\,\vec{u}_Y$$

$$\tilde{p}(x,y) = \tilde{p}(x,y)\vec{u}_X + \tilde{p}(x,y)\vec{u}_Y$$

After expansion and reduction we obtain:

$$p_X \frac{\partial E_X}{\partial x} = \frac{1}{4} \left[\tilde{p}_X \; e^{j\omega t} \frac{\partial \tilde{E}_X \; e^{j\omega t}}{\partial x} + \tilde{p}_X \; e^{j\omega t} \frac{\partial \tilde{E}_X^* \; e^{-j\omega t}}{\partial x} + \tilde{p}_X^* e^{-j\omega t} \frac{\partial \tilde{E}_X \; e^{j\omega t}}{\partial x} + \tilde{p}_X^* \; e^{-j\omega t} \frac{\partial \tilde{E}_X^* \; e^{-j\omega t}}{\partial x} \right]$$

$$p_Y \frac{\partial E_X}{\partial y} = \frac{1}{4} \left[\tilde{p}_Y \; e^{j\omega t} \frac{\partial \tilde{E}_X \; e^{j\omega t}}{\partial y} + \tilde{p}_Y \; e^{j\omega t} \frac{\partial \tilde{E}_X^* \; e^{-j\omega t}}{\partial y} + \tilde{p}_Y^* \; e^{-j\omega t} \frac{\partial \tilde{E}_X \; e^{j\omega t}}{\partial y} + \tilde{p}_Y^* \; e^{-j\omega t} \frac{\partial \tilde{E}_X^* \; e^{-j\omega t}}{\partial y} \right]$$

Which simplifies in:

$$p_X \frac{\partial E_X}{\partial x} = \frac{1}{4} \left[\tilde{p}_X \; e^{j2\omega t} \frac{\partial \tilde{E}_X}{\partial x} + \tilde{p}_X \frac{\partial \tilde{E}_X^*}{\partial x} + \tilde{p}_X^* \frac{\partial \tilde{E}_X}{\partial x} + \tilde{p}_X^* e^{-j2\omega t} \frac{\partial \tilde{E}_X^*}{\partial x} \right]$$

$$p_Y \frac{\partial E_X}{\partial y} = \frac{1}{4} \left[\tilde{p}_Y \; e^{j2\omega t} \frac{\partial \tilde{E}_X}{\partial y} + \tilde{p}_Y \frac{\partial \tilde{E}_X^*}{\partial y} + \tilde{p}_Y^* \frac{\partial \tilde{E}_X}{\partial y} + \tilde{p}_Y^* e^{-j2\omega t} \frac{\partial \tilde{E}_X^*}{\partial y} \right]$$

The whole point is to take the time average value of these expressions.

We are going to show that:

(a) the terms $\tilde{p}_X \; e^{j2\omega t} \dfrac{\partial \tilde{E}_X}{\partial x}$, $\tilde{p}_X^* e^{-j2\omega t} \dfrac{\partial \tilde{E}_X^*}{\partial x}$, $\tilde{p}_Y \; e^{j2\omega t} \dfrac{\partial \tilde{E}_X}{\partial y}$, and $\tilde{p}_Y \; e^{j2\omega t} \dfrac{\partial \tilde{E}_X}{\partial y}$ have a

time average value equal to zero.

(b) the terms $\tilde{p}_X \dfrac{\partial \tilde{E}_X^*}{\partial x}$ and $\tilde{p}_X^* \dfrac{\partial \tilde{E}_X}{\partial x}$ are complex conjugate.

(c) the terms $\tilde{p}_Y \dfrac{\partial \tilde{E}_X^*}{\partial y}$ and $\tilde{p}_Y^* \dfrac{\partial \tilde{E}_X}{\partial y}$ are complex conjugate

(a) So let us look at $\tilde{p}_X \; e^{j2\omega t} \dfrac{\partial \tilde{E}_X}{\partial x}$:

$$\tilde{p}_X \; e^{j2\omega t} \frac{\partial \tilde{E}_X}{\partial x} = \upsilon \tilde{\alpha} \tilde{E}_X \; e^{j2\omega t} \frac{\partial \tilde{E}_X}{\partial x}$$

$$\tilde{p}_X \; e^{j2\omega t} \frac{\partial \tilde{E}_X}{\partial x} = \upsilon \tilde{\alpha} E_{0,X} \; e^{j\varphi_X} \; e^{j2\omega t} \left(\frac{\partial E_{0,X}}{\partial x} e^{j\varphi_X} + j E_0 \frac{\partial \varphi_X}{\partial x} e^{j\varphi_X} \right)$$

137

$$\tilde{p}_X \, e^{j2\omega t} \frac{\partial \tilde{E}_X}{\partial x} = \upsilon \, \tilde{\alpha} \, E_{0,X} \frac{\partial E_{0,X}}{\partial x} e^{j2(\omega t + \varphi_X)} + j\upsilon \, \tilde{\alpha} \, E_{0,X}^2 \frac{\partial \varphi_X}{\partial x} e^{j2(\omega t + \varphi_X)}$$

Since υ, $\tilde{\alpha}$, E_0, $\frac{\partial E_{0,X}}{\partial x}$, $\frac{\partial \varphi_X}{\partial x}$ do not vary with time, and since the time average of $e^{j2(\omega t + \varphi_X)}$ is zero (it oscillates harmonically around zero), the time average of

$\tilde{p}_X \, e^{j2\omega t} \dfrac{\partial \tilde{E}_X}{\partial x}$ is zero.

(b) Let us compare $\tilde{p}_X \dfrac{\partial \tilde{E}_X^*}{\partial x}$ and $\tilde{p}_X^* \dfrac{\partial \tilde{E}_X}{\partial x}$:

First, $\tilde{p}_X \dfrac{\partial \tilde{E}_X^*}{\partial x}$:

$$\tilde{p}_X \frac{\partial \tilde{E}_X^*}{\partial x} = \upsilon \, \tilde{\alpha} \, \tilde{E}_X \frac{\partial \left(E_0 e^{-j\varphi_X} \right)}{\partial x}$$

$$\tilde{p}_X \frac{\partial \tilde{E}_X^*}{\partial x} = \upsilon \, \tilde{\alpha} \, E_0 e^{j\varphi_X} \frac{\partial \left(E_0 e^{-j\varphi_X} \right)}{\partial x}$$

$$\tilde{p}_X \frac{\partial \tilde{E}_X^*}{\partial x} = \upsilon \, \tilde{\alpha} \, E_0 e^{j\varphi_X} \left(\frac{\partial E_0}{\partial x} e^{-j\varphi_X} - E_0 \, j \frac{\partial \varphi_X}{\partial x} e^{-j\varphi_X} \right)$$

$$\tilde{p}_X \frac{\partial \tilde{E}_X^*}{\partial x} = \upsilon \, \tilde{\alpha} \, E_0 \frac{\partial E_0}{\partial x} - j\upsilon \, \tilde{\alpha} \, E_0^2 \frac{\partial \varphi_X}{\partial x}$$

Second, $\tilde{p}_X^* \dfrac{\partial \tilde{E}_X}{\partial x}$:

$$\tilde{p}_X^* \frac{\partial \tilde{E}_X}{\partial x} = \upsilon \, \tilde{\alpha}^* \, \tilde{E}_X^* \frac{\partial \left(E_0 e^{j\varphi_X} \right)}{\partial x}$$

$$\tilde{p}_X^* \frac{\partial \tilde{E}_X}{\partial x} = \upsilon \, \tilde{\alpha}^* \, E_0 e^{-j\varphi_X} \frac{\partial \left(E_0 e^{j\varphi_X} \right)}{\partial x}$$

$$\tilde{p}_X^* \, \frac{\partial \tilde{E}_X}{\partial x} = \upsilon \tilde{\alpha}^* \, E_0 e^{-j\varphi_X} \left(\frac{\partial E_0}{\partial x} e^{j\varphi_X} + E_0 j \frac{\partial \varphi_X}{\partial x} e^{j\varphi_X} \right)$$

$$\tilde{p}_X^* \, \frac{\partial \tilde{E}_X}{\partial x} = \upsilon \tilde{\alpha}^* \, E_0 \frac{\partial E_0}{\partial x} + j \upsilon \tilde{\alpha}^* \, E_0^2 \frac{\partial \varphi_X}{\partial x}$$

The complex conjugate of $\upsilon \tilde{\alpha}^* \, E_0 \dfrac{\partial E_0}{\partial x}$ is $\upsilon \tilde{\alpha} \, E_0 \dfrac{\partial E_0}{\partial x}$, because υ, E_0 and $\dfrac{\partial E_0}{\partial x}$ are real numbers. The conjugate of $\tilde{\alpha}^*$ is $\tilde{\alpha}$.

The complex conjugate of $j \upsilon \tilde{\alpha}^* \, E_0^2 \dfrac{\partial \varphi_X}{\partial x}$ is $- j \upsilon \tilde{\alpha} \, E_0^2 \dfrac{\partial \varphi_X}{\partial x}$, because υ, E_0 and $\dfrac{\partial \varphi}{\partial x}$ are real. The complex conjugate of j is $- j$.

So $\tilde{p}_X \, \dfrac{\partial \tilde{E}_X^*}{\partial x}$ and $\tilde{p}_X^* \, \dfrac{\partial \tilde{E}_X}{\partial x}$ are complex conjugate.

Therefore:

$$\mathrm{Re}\left[\tilde{p}_X \, \frac{\partial \tilde{E}_X^*}{\partial x} + \tilde{p}_X^* \, \frac{\partial \tilde{E}_X}{\partial x} \right] = 2 \, \mathrm{Re}\left[\tilde{p}_X \, \frac{\partial \tilde{E}_X^*}{\partial x} \right]$$

(c) Let us compare $\tilde{p}_Y \, \dfrac{\partial \tilde{E}_X^*}{\partial y}$ and $\tilde{p}_Y^* \, \dfrac{\partial \tilde{E}_X}{\partial y}$:

The approach is exactly similar to the one followed in (b). Eventually it is found that $\tilde{p}_Y \, \dfrac{\partial \tilde{E}_X^*}{\partial y}$ and $\tilde{p}_Y^* \, \dfrac{\partial \tilde{E}_X}{\partial y}$ are complex conjugates.

Therefore:

$$\mathrm{Re}\left[\tilde{p}_Y \, \frac{\partial \tilde{E}_X^*}{\partial y} + \tilde{p}_{y}^* \, \frac{\partial \tilde{E}_X}{\partial y} \right] = 2 \, \mathrm{Re}\left[\tilde{p}_Y \, \frac{\partial \tilde{E}_X^*}{\partial y} \right]$$

Finally:

$$\left\langle F_{DEP,X} \right\rangle = \frac{1}{4} \, \mathrm{Re}\left[\tilde{p}_X \, \frac{\partial \tilde{E}_X^*}{\partial x} + \tilde{p}_X^* \, \frac{\partial \tilde{E}_X}{\partial x} \right] + \frac{1}{4} \, \mathrm{Re}\left[\tilde{p}_Y \, \frac{\partial \tilde{E}_X^*}{\partial y} + \tilde{p}_Y^* \, \frac{\partial \tilde{E}_X}{\partial y} \right]$$

$$\left\langle F_{DEP,X} \right\rangle = \frac{1}{2} \, \mathrm{Re}\left[\tilde{p}_X \, \frac{\partial \tilde{E}_X^*}{\partial x} + \tilde{p}_Y \, \frac{\partial \tilde{E}_x^*}{\partial y} \right]$$

This is for the x component, but we can generalize:

$$\left\langle F_{DEP} \right\rangle = \frac{1}{2} \, \mathrm{Re} \left[\left(\tilde{p} \cdot \nabla \right) E^* \right]$$

2. The dielectrophoretic force on a particle placed in a shifted AC electrical field (AC + DC field)

The DC + AC field will lead to a field that will not oscillate around 0. It looks like the sum of a constant field + an oscillating part.

The derivation explained in appendix 1 has to be done with a different starting point.

$$\vec{p}(t,x,y) = p_X(t,x,y)\,\vec{u}_X + p_Y(t,x,y)\,\vec{u}_Y = \frac{1}{2}\left(\tilde{p}\,e^{j\omega t} + \tilde{p}^*e^{-j\omega t}\right)$$

$$\vec{E}(t,x,y) = E_X(t,x,y)\,\vec{u}_X + E_Y(t,x,y)\,\vec{u}_Y = \frac{1}{2}\left(\tilde{E}\,e^{j\omega t} + \tilde{E}^*e^{-j\omega t}\right)$$

Will be replaced by:

$$\vec{p} = \vec{P}_M + \frac{1}{2}\left(\tilde{p}\,e^{j\omega t} + \tilde{p}^*e^{-j\omega t}\right) \quad \text{(constant term + oscillating term)}$$

$$\vec{E} = \vec{E}_M + \frac{1}{2}\left(\tilde{E}\,e^{j\omega t} + \tilde{E}^*e^{-j\omega t}\right) \quad \text{(constant term + oscillating term)}$$

$$F_{DEP,X} = p_X\frac{\partial E_X}{\partial x} + p_Y\frac{\partial E_X}{\partial y}$$

$$p_X\frac{\partial E_X}{\partial x} = \left(P_M + \frac{1}{2}\left(\tilde{p}_X\,e^{j\omega t} + \tilde{p}_X^*\,e^{-j\omega t}\right)\right)\left(\frac{\partial E_M}{\partial x} + \frac{1}{2}\frac{\partial\left(\tilde{E}_X\,e^{j\omega t} + \tilde{E}_X^*\,e^{-j\omega t}\right)}{\partial x}\right)$$

$$p_Y\frac{\partial E_X}{\partial y} = \left(P_M + \frac{1}{2}\left(\tilde{p}_Y\,e^{j\omega t} + \tilde{p}_Y^*\,e^{-j\omega t}\right)\right)\left(\frac{\partial E_M}{\partial y} + \frac{1}{2}\frac{\partial\left(\tilde{E}_X\,e^{j\omega t} + \tilde{E}_X^*\,e^{-j\omega t}\right)}{\partial y}\right)$$

After development:

$$p_X\frac{\partial E_X}{\partial x} = A + B$$

$$p_Y\frac{\partial E_X}{\partial y} = C + D$$

Where

$$A = \frac{1}{4}\left[\tilde{p}_X\ e^{j\omega t}\frac{\partial \tilde{E}_X\ e^{j\omega t}}{\partial x} + \tilde{p}_X\ e^{j\omega t}\frac{\partial \tilde{E}_X^*\ e^{-j\omega t}}{\partial x} + \tilde{p}_X^*e^{-j\omega t}\frac{\partial \tilde{E}_X\ e^{j\omega t}}{\partial x} + \tilde{p}_X^*e^{-j\omega t}\frac{\partial \tilde{E}_X^*\ e^{-j\omega t}}{\partial x}\right]$$

$$B = P_M\frac{\partial E_M}{\partial x} + \frac{1}{2}P_M\frac{\partial\left(\tilde{E}_x\ e^{j\omega t} + \tilde{E}_x^*e^{-j\omega t}\right)}{\partial x} + \frac{1}{2}\frac{\partial E_M}{\partial x}\left(\tilde{p}_X\ e^{j\omega t} + \tilde{p}_X^*\ e^{-j\omega t}\right)$$

$$C = \frac{1}{4}\left[\tilde{p}_Y\ e^{j\omega t}\frac{\partial \tilde{E}_X\ e^{j\omega t}}{\partial y} + \tilde{p}_Y\ e^{j\omega t}\frac{\partial \tilde{E}_X^*\ e^{-j\omega t}}{\partial y} + \tilde{p}_Y^*e^{-j\omega t}\frac{\partial \tilde{E}_X\ e^{j\omega t}}{\partial y} + \tilde{p}_Y^*e^{-j\omega t}\frac{\partial \tilde{E}_X^*\ e^{-j\omega t}}{\partial y}\right]$$

$$D = P_M\frac{\partial E_M}{\partial y} + \frac{1}{2}P_M\frac{\partial\left(\tilde{E}_X\ e^{j\omega t} + \tilde{E}_X^*e^{-j\omega t}\right)}{\partial y} + \frac{1}{2}\frac{\partial E_M}{\partial y}\left(\tilde{p}_Y\ e^{j\omega t} + \tilde{p}_Y^*\ e^{-j\omega t}\right)$$

Terms A and C have been studied in the previous case (appendix 1, harmonic field), and

will produce a time average force $\left\langle F_{A+C}\right\rangle = \frac{1}{2}\ \mathrm{Re}\left[\left(\tilde{p}\ \cdot\nabla\right)E^*\right].$

Now, let us look at the different terms in B:

(a) $P_M\frac{\partial E_M}{\partial x}$

This term is real, and constant with time.

(b) $\frac{1}{2}P_M\frac{\partial\left(\tilde{E}_X\ e^{j\omega t} + \tilde{E}_X^*e^{-j\omega t}\right)}{\partial x}$

This term needs to be further developed:

$$\frac{1}{2}P_M \frac{\partial\left(\tilde{E}_X\, e^{j\omega t} + \tilde{E}_X^* e^{-j\omega t}\right)}{\partial x} = \frac{1}{2}P_M \frac{\partial \tilde{E}_X e^{j\omega t}}{\partial x} + \frac{1}{2}P_M \frac{\partial \tilde{E}_X^* e^{-j\omega t}}{\partial x}$$

$$= \frac{1}{2}P_M\ e^{j\omega t} \frac{\partial E_{0,X}\, e^{j\varphi_X}}{\partial x} + \frac{1}{2}P_M e^{j\omega t} \frac{\partial E_{0,X}\, e^{-j\varphi_X}}{\partial x}$$

$$= \frac{1}{2}P_M e^{j\omega t} \frac{\partial E_{0,X}}{\partial x}\, e^{j\varphi_X} + \frac{1}{2}P_M e^{j\omega t} E_{0,X} \frac{\partial e^{j\varphi_X}}{\partial x} + \frac{1}{2}P_M e^{j\omega t} \frac{\partial E_{0,X}}{\partial x}\, e^{-j\varphi_X} + \frac{1}{2}P_M e^{j\omega t} E_{0,X} \frac{\partial e^{-j\varphi_X}}{\partial x}$$

$$= \frac{1}{2}P_M e^{j(\omega t+\varphi_X)} \frac{\partial E_{0,X}}{\partial x} + \frac{1}{2}P_M E_{0,X} e^{j\omega t} j\frac{\partial \varphi_X}{\partial x} e^{j\varphi_X} + \frac{1}{2}P_M e^{j(\omega t-\varphi_X)} \frac{\partial E_{0,X}}{\partial x} - \frac{1}{2}P_M E_{0,X} e^{j\omega t} j\frac{\partial \varphi_X}{\partial x} e^{-j\varphi_X}$$

$$= \frac{1}{2}P_M e^{j(\omega t+\varphi_X)} \frac{\partial E_{0,X}}{\partial x} + \frac{1}{2}P_M E_{0,X} e^{j\omega t} j\frac{\partial \varphi_X}{\partial x} e^{j\varphi_X} + \frac{1}{2}P_M e^{j(\omega t-\varphi_X)} \frac{\partial E_{0,X}}{\partial x} - \frac{1}{2}P_M E_{0,X} e^{j(\omega t-\varphi_X)} j\frac{\partial \varphi_X}{\partial x}$$

The terms P_M, $E_{0,X}$, j, $\dfrac{\partial \varphi_X}{\partial x}$, $\dfrac{\partial E_{0,X}}{\partial x}$ are constant with respect to time. The time average value of the terms $e^{j(\omega t+\varphi_X)}$ and $e^{j(\omega t-\varphi_X)}$ is zero (harmonic oscillations around zero). Therefore, the time average value of the whole expression is zero.

(c) $\dfrac{1}{2}\dfrac{\partial E_M}{\partial x}\left(\tilde{p}_X\, e^{j\omega t} + \tilde{p}_X^* e^{-j\omega t}\right)$

This term also needs to be developed:

$$\frac{1}{2}\frac{\partial E_M}{\partial x}\left(\tilde{p}_X\, e^{j\omega t} + \tilde{p}_X^* e^{-j\omega t}\right) = \frac{1}{2}\frac{\partial E_M}{\partial x}\left(\upsilon\tilde{\alpha}\, E_0 e^{j\varphi_X} e^{j\omega t} + \upsilon\tilde{\alpha}^*\, E_0 e^{-j\varphi_X} e^{j\omega t}\right)$$

143

$$\frac{1}{2}\frac{\partial E_M}{\partial x}\left(\tilde{p}_X \, e^{j\omega t} + \tilde{p}_{Xx}^* e^{-j\omega t}\right) = \frac{1}{2}\frac{\partial E_M}{\partial x}\left(\upsilon\tilde{\alpha}\,E_0 e^{j(\omega t+\varphi_X)} + \upsilon\tilde{\alpha}^*\,E_{0,X} e^{j(\omega t-\varphi_X)}\right)$$

The terms υ, $\tilde{\alpha}$, $E_{0,X}$ and $\dfrac{\partial E_M}{\partial x}$ are constant with respect to time. The time average

value of the terms $e^{j(\omega t+\varphi_X)}$ and $e^{j(\omega t-\varphi_X)}$ is zero (harmonic oscillations around zero).

Therefore, the time average value of the whole expression is zero.

Let us take look at the terms in D. Following an approach similar to the one followed to

study the different terms in B, we find:

(a) $P_M \dfrac{\partial E_M}{\partial x}$

This term is real, and constant with time.

(b) $\dfrac{1}{2} P_M \dfrac{\partial\left(\tilde{E}_X \, e^{j\omega t} + \tilde{E}_X^* e^{-j\omega t}\right)}{\partial y}$

After development, reduction and analysis, this term has a zero time average value.

(c) $\dfrac{1}{2}\dfrac{\partial E_M}{\partial y}\left(\tilde{p}_X \, e^{j\omega t} + \tilde{p}_X^* e^{-j\omega t}\right)$

After development, reduction and analysis, this term also has a zero time average value.

Finally, by adding A, B, C and D, the expression of the dielectrophoretic force in a field

that presents sinusoidal oscillations around a non zero value is:

$$\boxed{\left\langle F_{DEP}\right\rangle = \left(P_M \cdot\nabla\right)E_M + \frac{1}{2}\,\mathrm{Re}\left[\left(\tilde{p}\,\cdot\nabla\right)\tilde{E}^*\right]}$$

REFERENCES

1.   Freeman, W., Fundamentals of DNA Hybridization Arrays for Gene Expression Analysis. *BioTechniques* **2000,** 29, 1042-1055.

2.   Stoughton, R. B., Applications of DNA Microarrays in Biology. *Annu. Rev. Biochem.* **2005,** 74, 53-82.

3.   http://www.affymetrix.com.

4.   Affymetrix,   GeneChip   Expression   Analysis.   Technical   manual. *http://www.affymetrix.com/support/technical/manuals* **2004**.

5.   Halperin, A., Brush Effects on DNA Chips: Thermodynamics, Kinetics, and Design Guidelines. *Biophysical Journal* **2005,** 89, 796-811.

6.   Rubinstein, M., *Polymer Physics*. Oxford, 2003.

7.   Peterson, A., Kinetic Control of Hybridization in Surface Immobilized DNA Monolayer Films. *Journal of the American Chemical Society* **2000,** 122, 7837-7838.

8.   Washizu, M., Electrostatic Manipulation of DNA in Microfabricated Structures. *Proceedings of IEE* **1989,** 2, 1978-1984.

9.   Germishuizen, W. A., Dielectric manipulation of surface-bound DNA. *IEE Proc.-Nanobiotechnol.* **2003,** 150, (2).

10.   Rouzina, I., Force-Induced Melting of the DNA Double Helix 1. Thermodynamic Analysis. *Biophysical Journal* **2001,** 80 882–893.

11.   Dewarrat, F., Orientation and Positioning of DNA Molecules with an Electric Field Technique. *Single Molecules* **2002,** 3, (4), 189-193.

12.   Naef, F., Solving the riddle of the bright mismatches: Labeling and effective binding in oligonucleotide arrays. *Physical Review* **2003,** 68, (011906).

13.   Vanderhoeven, J., DNA Microarray Enhancement Using a Continuously and Discontinuously Rotating Microchamber. *Analytical Chemistry* **2005,** 77, 4474-4480.

14.   Chetverin, A. B., Oligonucleotide Arrays: New Concepts and Possibilities. *Nature Bio/Technology* **1994,** 12, 1093-1099

15.   Eggers, M., A Microchip for Quantitative Detection of Molecules Utilizing Luminescent and Radioisotop Reporter Groups *BioTechniques* **1994,** 17, (3), 516-525.

16.   Lamture, J. B., Direct detection of nucleic acid hybridization on the surface of a charge coupled device. *Nucleic Acids Research* **1994,** 22, (11), 2121-2125.

17.   Maskos, U., A study of oligonucleotide reassociation using large arrays of oligonucleotides synthesised on a glass support. *Nucleic Acids Research* **1993,** 21, (20), 4663-4669.

18.   Pease, A. C., Light-Generated Oligonucleotide Arrays for Rapid DNA Sequence Analysis. *Proc. Natl. Acad. Sci. USA* **1994,** 91, 5022-5026.

19.   Southern, E. M., Arrays of complementary oligonucleotides for analysing the hybridisation behaviour of nucleic acids *Nucleic Acids Research* **1994,** 22, (8), 1368-1373.

20.   Chan, V., Adsorption and Surface Diffusion of DNA Oligonucleotides at Liquid/Solid Interfaces. *Langmuir* **1997,** 13, 320-329.

21.   Chan, V., The Biophysics of DNA Hybridization with Immobilized Oligonucleotide Probes. *Biophysical Journal* **1995,** 69, 2243-2255.

22.   Erickson, D., Modeling of DNA Hybridization Kinetics for Spatially Resolved Biochips. *Analytical Biochemistry* **2003,** 317, 186-200.

23.   Wetmur, J. G., Kinetics of renaturation of DNA. *Journal of Molecular Biology* **1968,** 31 (3), 349-370

24.   Pappaert, K., Diffusion-reaction modelling of DNA hybridization kinetics on biochips. *Chemical Engineering Science* **2003,** 58, 4921-4930.

25.   Pappaert, K., A dimensionless number analysis of the hybridization process in diffusion- and convection-driven DNA microarray systems. *Journal of Biotechnology* **2006,** 123, 381-396.

26.   Levicky, R., Physicochemical perspetives on DNA microarray and biosensor technologies. *TRENDS in Biotechnology* **2005,** 23, (3).

27.   Peterson, A., Hybridization of Mismatched or Partially Matched DNA at surfaces. *Journal of the American Chemical Society* **2002,** 124, 14601-14607.

28.   Forman, J. E., Thermodynamics of duplex formation and mismatch discrimination on photolithographically synthesized oligonucleotide arrays. *ACS Symp. Ser* **1998**, 206-228.

29.   Dai, H., Use of hybridization kinetics for differentiating specific from non-specific binding to oligonucleotide microarrays. *Nucleic Acids Research* **2002,** 30, (16 e86).

30.   Okahata, Y., Kinetic Measurements of DNA Hybridization on an Oligonucleotide-Immobilized 27-MHz Quartz Crystal Microbalance. *Analytical Chemistry* **1998,** 70, 1288-1296.

31.   Bishop, J., Competitive displacement of DNA during Surface Hybridization. *Biophysical Journal: Biophysical letters* **2007**.

32.   Bishop, J., A competitive Kinetic Model of Nucleic Acid Surface Hybridization in the Presence of Point Mutants. *Biophysical Journal* **2006,** 90, 831-840.

33.   Zhang, Y., Competitive Hybridization Kinetics Reveals Unexpected Behavior Patterns. *Biophysical Journal* **2005,** 89, 2950-2959.

34.   Halperin, A., On the hybridization isotherms of DNA microarrays: the Langmuir model and its extensions. *Journal of Physics: Condensed Matter* **2006,** 18, S463-S490.

35.   Halperin, A., Sensitivity, Specificity, and the Hybridization Isotherms of DNA Chips. *Biophysical Journal* **2004,** 86, 718-730.

36.   Nguyen, N., MEMS-Micropumps: A Review. *Journal of Fluids Engineering* **2002,** 124, 384-392.

37.   Laser, D. J., A review of micropumps. *Journal of Micromechanics and Microengineering* **2004,** 14, R35-R64.

38.   Nguyen, N. T., Micromixers-a review. *Journal of Microengineering* **2005,** 15, R1-R16.

39.   Lin, Y., Ultrafast Microfluidic Mixer and Freeze-Quenching Device. *Analytical Chemistry* **2003,** 75, 5381-5386.

40.   Wang, H., Numerical investigation of mixing in microchannels with patterned grooves. *Journal of Micromechanics and Microengineering* **2003,** 13, 801-808.

41.   Mengeaud, V., Mixing Processes in a Zigzag Microchannel: Finite Element Simulations and Optical Study. *Analytical Chemistry* **2002,** 16, 4279-4286.

42.   Liu, R. H., Passive mixing in a three-dimensional serpentine microchannel. *Journal of Microelecromechanical Systems* **2000,** 9, (2), 190-197.

43.   Morgan, H., *AC Electrokinetics: colloids and nanoparticles*. Research Studies Press Ltd: 2003.

44.   Sigurdson, M., Electrothermal stirring for heterogeneous immunoassays. *Lab on a Chip* **2005,** 5, 1366-1373.

45.   Zheng, L., Electronic manipulation of DNA and proteins for potential nano-bio circuit assembly. *Proc. of SPIE* **2003,** 5331, 126-135.

46.   Tuukkanen, S., Trapping of 27 bp - 8 kbp DNA and immobilization of thiol-modified DNA using dielectrophoresis. *submitted to Condensed Matter* **2007**.

47.   Tsukahara, S., Dielectrophoresis of microbioparticles in water with planar and capillary quadrupole electrodes. *IEE Proc.-Nanobiotechnol.* **2003,** 150, (2), 59-65.

48.   Chang, D. E., Separation of bioparticles using the travelling wave dielectrophoresis with multiple frequencies. *Proc. of the 42nd IEEE Conference on Decision and Control* **2003**, 6448-6453.

49.   Pethig, R., Enhancing Traveling-Wave Dielectrophoresis with Signal Superposition. *IEEE Engineering in Medecine and Biology Magazine* **2003**, 43-50.

50.   Aldaeus, F., Superpositioned dielectrophoresis for enhanced trapping efficiency. *Electrophoresis* **2005,** 26, 4252-4259.

51.   Zhang, Y. T., Experimental Study of Two-frequency Dielectrophoresis Effects on a Linear Electrode Array. *27th Annual Internal Conference of the IEE-EMBS* **2005**, 1020-1023.

52.   Toegl, A., Enhancing Results of Microarray Hybridizations Through Microagitation *Journal of Biomolecular Techniques* **2003,** 14, 197-204.

53.   Liu, R. H., Hybridization Enhancement Using Cavitation Microstreaming *Analytical Chemistry* **2003,** 75, (8), 1911-1917.

54.   Pappaert, K., Enhancement of DNA micro-array analysis using a shear-driven micro-channel flow system. *Journal of Chromatography A* **2003,** 1014, 1-9.

55.   Das, S., Modeling of coupled momentum, heat and solute transport during DNA hybridization in a microchannel in the presence of electro-osmotic effects and axial pressure gradients. *Microfluid Nanofluid* **2006,** 2, 37-49.

56.   http://www.nanogen.com.

57.   Kassegne, S. K., Numerical modeling of transport and accumulation of DNA on electronically active biochips. *Sensors and Actuators B* **2003,** 94, 81-98.

58.   Garcia de la Torre, J., Hydrodynamic properties of a double-helical model for DNA. *Biophysical Journal* **1994,** 66, 1573-1579.

59.   Ferrari, M., Scatteing and Diffusion of Mononucleosomal DNA: Effects of Counterion Valence and Salt and DNA Concentration. *Macromolecules* **1992,** 25, 5266-5276.

60.   Gosnell, D. L., Measurement of Diffusion Coefficients of DNA in Agarose Gel. *Macromolecules* **1993,** 26, 1304-1308.

61.   Liu, M.-K., Separation and Measurement of Diffusion Coefficients of Linear and Circular DNAs by Flow Field-Flow Fractionation. *Macromolecules* **1993,** 26, 3576-3588.

62.   Strassburger, J., Diffusion of DNA at very low concentration. *Biopolymers* **1971,** 10, (2), 263-273.

63.   Gadgil, C., A diffusion-reaction model for DNA microarray assays. *Journal of Biotechnology* **2004,** 114, 31-45.

64.   Heule, M., Sequential DNA hybridisation assays by fast micromixing. *Lab Chip* **2004,** 4, 506-511.

65.   Henry, M. R., Real-Time Measurements of DNA Hybridization on Microparticles with Fluorescence Resonance Energy Transfer. *Analytical Biochemistry* **1999,** 276, 204-214.

66.   Wu, J., Biased AC Electro-Osmosis for On-Chip Bioparticle Processi. *IEEE TRANSACTIONS ON NANOTECHNOLOGY* **2006,** 5, (2), 84-89.